EVALUATE THE USE OF ELLIPTICAL FINNED TUBES IN HEAT EXCHANGER DESIGN AND PERFORMANCE.

'THE STRUCTURAL CHARACTERISTICS OF FINNED TUBES'

by

XOLILE L. SIZANI

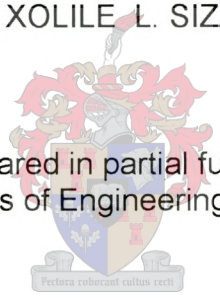

This thesis is prepared in partial fulfilment of the requirement for the degree of Masters of Engineering at the University of Stellenbosch.

Thesis supervisor : Mr. E. Terblanche

Department of Mechanical Engineering
University of Stellenbosch
March 2000

DECLARATION:

I, Xolile L. Sizani, hereby declare that the work contained in this thesis is my own original work and was not previously, in its entirety or in part, submitted at any other university for a degree.

ABSTRACT

This report describes the Experimental and Numerical Investigations conducted, during the determination of the structural mechanics of elliptical tubes, viz. the F- and the A-tubes. This report is requested in an endeavour to assist Sasol, who is currently busy developing and updating specifications on Air Cooled Heat Exchangers.

The objectives of this report therefore are to : (1) determine the strength and the effectiveness of the tube-to-tube-sheet joints. (2) determine the allowable pressure limits on the tubes and (3) investigate the effects of thermal load and vibration on the tube bundle. A series of experiments were conducted to meet these objectives. From a Shear Load experiment it was found that the maximum allowable axial load on the F- and the A-tube is 14.55 kN and 20. 86 kN respectively. Fin Plates were found to have little effect on the bending strength of the tube, whilst they have significant effect on the resistance to volumetric expansion of the tube. In fact the more fins per unit length the greater the resistance to volumetric expansion of the tube. These conclusions were drawn from Bending and Pressure Load experiments respectively and supported by FEM analysis of the tube using NASTRAN.

When the design pressure limit given by the manufacturer (GEA Air Cooled Systems), were tested using FEM analysis, it was found that they cause no significant deformation and failure of the tubes. Thermal stresses on the tube bundle greatly affect the first tube in the first row (row closest to the flanges) of the tube bundle and it is recommended that provision for thermal expansion be made to reduce these stresses. To reduce vibrations induced by the fan, it is recommended that the natural frequency of the tube bundle must not equal the number of blades (N) times the angular frequency (ω) of the fan, or multiples thereof, of each mode of vibration.

OPSOMMING

Hierdie tesis beskrywe die Numeriese en Eksperimentele ondersoeke na die sterkte van elliptiese verkoelingsbuise, naamlik die F- en A- tipes. Hierdie werk sal Sasol, wat huidiglik besig is met die opgradering, van spesifikasies vir lugverkoelde hitteuitruilers van nut wees.

Die doelwitte van hierdie tesis is om: (1) die sterkte en effektiwiteit van die buis laste was die buis and die buisplaat verdind, te ondersoek, (2) die toelaatbare druklimiete, sowel as (3) die effek wat hitte en vibrasie op 'n buisbundel het, te ondersoek. 'n Reeks eksperimente is uitgevoer om hierdie doelwitte te bevredig. 'n Skuifbelastingseksperiment het aangedui dat die toelaatbare krag wat op 'n F- en A-buis respektiewelik aangewend kan word 14.55 kN en 20.86 kN is. Die ondersoek het aangetoon dat vinne geen noemenswaardige effek op die buigsterkte van die buise gehad het nie, maar dat dit 'n aansienlike verstywingseffek teen volumetriese verandering as gevolg van interne druk, gehad het. Hierdie gevolgtrekkings is bereik deur die Druk- en Buigtoetse wat numeries bevestig is met die NASTRAN eindige element analise (EEA) pakket.

EEA het aangetoon dat die druklimiete voorgeskryf deur die buisvervaardiger (GEA Air Cooled Systems) nie noemenswaardige vervorming van die buise tot gevolg gehad het nie. Termiese belastings het 'n groot invloed op die eerste buise (die rye naaste aan die flense) van 'n buisbundel. Die invoeging van uitsettingslaste word aanbeveel om die spannings hier te verminder. Om vibrasie van die buisbundel te verhoed word aanbeveel dat die resonansfrekwensie van die buisbundel nie gelyk is aan die aantal lemme (N) vermenigvuldig met die rotasie frekwensie (ω) van die waaier vir elke vibrasiemode.

ACKNOWLEDGEMENTS

I would like to extend my greatest gratitude to the following people:

1) My sponsor, Sasol Limited, for their financial support throughout these years and for giving me an opportunity to be the best I can possible be. Without whom none of this would have been possible.

2) My supervisor, Mr E. Terblanche for his guidance and supervision.

3) Mr Van der Westhuizen, for his insight and assistance with FEM analysis

4) Mr F. Zietsman and Mr M. Siebritz for their assistance in the Structural laboratory.

Contents

NOMENCLATURE

A_{tc} - Internal flow area of the tube, $[m^2]$

d_e - Hydraulic diameter, $[m]$

E - Young's Modulus, $[N\,m^{-2}]$

fr_{test} - Joint Efficiency, $[-]$

I_{xx} - Moment of inertia in the y-z plane, $[m^4]$

$L_{\max}$ - Maximum allowable load, $[N]$

L_t - Tube length, $[m]$

L_{test} - Lowest axial load at which failure occurs, $[N]$

m_t - Mass of the tube, $[kg]$

N - Number of fan blades, $[-]$

n_t -.Number of tube rows, $[-]$

P_t - Plate thickness, $[m]$

P_w - Wetted perimeter of the tube, $[m]$

R_e - Reynold's number, $[-]$

Sa - ASME code's allowable tensile strength, $[Pa]$

St - Minimum tensile strength of the tube, $[Pa]$

Sy - Yield strength, $[Pa]$

V - Velocity of the fluid, $[ms^{-1}]$

Greek Symbols

γ_{xy} - Shear strain, $[m/m]$

ε_A -Strain along θ_A, $[m/m]$

$[-]$- Units are dimensionless

ε_{xx} - Normal strain, $\left[m/m\right]$

μ - Dynamic viscosity, $\left[kgm^{-1}s^{-1}\right]$

ρ - Density of the fluid, $\left[kgm^{-3}\right]$

$\sigma_{1,2}$ - Principal stress, $[Pa]$

σ_{xx} - Normal stress, $[Pa]$

τ_{xy} - Shear stress, $[Pa]$

ω - Angular speed of the fan, $\left[rads^{-1}\right]$

$[-]$ - Units are dimensionless

1. INTRODUCTION

SASOL is currently busy updating their specifications on Air- Cooled Heat Exchangers. In these specifications the use of elliptical finned tubes is allowed under special circumstances. A lot of these finned tubes are available in the market today, and to take advantage of this, SASOL would like to include them in their specifications as a design option.

In order to include elliptical finned tubes in these specifications, heat transfer performance, structural characteristic and the applicability of these tubes in the petrochemical industry are required. This thesis is about the acquisition of structural characteristic of these elliptical finned tubes so as to assist in developing and updating a SASOL Specification on Air-Cooled Heat Exchangers.

The department of Mechanical Engineering at the University of Stellenbosch has requested this report so as to determine the structural characteristics of these tubes. So, the main aims and objectives of this report are to:

1. determine the strength and the effectiveness of tube-to-tube-sheet joints.
2. determine the allowable pressure limits of the elliptical tubes.
3. look at the effects of thermal stress and structural dynamics of the tube bundle.

METHODS OF INVESTIGATION

Two methods were used in the determination of the information contained in this report viz.

1. Experimental and
2. Numerical Investigations.

Also, consultation with GEA Air-Cooled Systems has given more assistance in the compilation of the report. The literature on structural mechanics has also added valuable information on this subject.

LIMITATIONS OF INVESTIGATION

In the Numerical Investigation only the finite element program called NASTRAN was used. This finite element program limited the size of the models to a maximum of 5000 nodes. Only two types of tubes were tested viz.

1. F-tube with a 3.0 mm fin pitch and
2. A-tube with a 2.5 mm fin pitch and A-tube with a 4.3 mm fin pitch.

In the analysis of thermal and vibration effects of the tube bundle, the investigation was only limited to a typical tube bundle used in the Performance Evaluation of a Heat Exchanger at Stellenbosch University.

SCOPE OF THE REPORT

This report begins by outlining the experimental methods and procedures used in the Shear Load experiment. Subsequently the results of this experiment are discussed. Then, the Bending Load experiment is conducted and the effects of the fin plates on the resistance of the tube to bending is investigated. The distribution of the stress on the tube-sheet plate is given consideration. The Pressure Load experiment then follows with the results tabled and discussed. Based on the findings the conclusions on the Experimental Investigations are drawn.

Using the information obtained from the Experimental Investigations, finite element models are made. The findings on the Experimental Investigations about the effects of fin plates on the strength of fin tubes are tested by FEM, and the results are compared and discussed. The maximum design pressure limits given by the manufacturer are tested for validity and the findings of this investigation are discussed and the necessary conclusions are drawn. The thermal and vibration effects on the tube bundle are investigated and based on the results obtained conclusions are drawn. Finally based on all the conclusions that are drawn from the Experimental and Numerical Investigations, recommendations are made.

2. VIBRATION ON AIR-COOLED HEAT EXCHANGER

One cause of failure in heat exchangers early in their life is vibration. This vibration can be as a result of adjacent structural vibration and / or flow induced vibration, with the latter being the prime suspect in most failures.

2.1 FLOW INDUCED VIBRATION

As mentioned above, flow induced vibration accounts for most of the failure in heat exchangers. This occurs when the vortex shedding frequency, f_s, generated by the fluid flowing around the structure is approximately equal to the tube's natural frequency, f_{tn}. At this point the tubes begin to vibrate in resonance. Failure of these tubes will occur at points of high stress concentration e.g. at the point where the tube is clamped to the tube plate.

Understanding the interaction between fluid flow and theory of elasticity is essential in heat exchanger design.

2.1.1 VORTEX EXCITATION OF AN ELASTIC TUBE.

Here the phenomenon of vortex shedding is explained in greater detail. When a fluid flows past a bluff body, a pressure gradient is generated around the body. At the rear side of the body this pressure gradient becomes adverse resulting in the separation and breaking of the fluid. This separation results in the formation of a broad pulsating wake in the rear surface as seen in figure 2.1 (a) below.

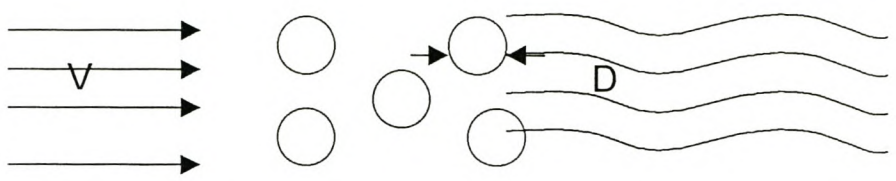

(a)

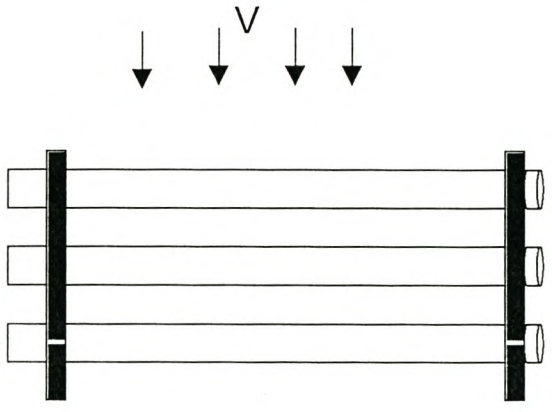

(b)

Figure 2.1. Illustration of typical installation

A pair of vortices are shed alternatively from the upper and the lower side of the tubes. This is called the Karman vortex streets. These streets are highly pronounced at Re_D>35, **[1WH].** A dimensionless Strouhal number is defined as:

$$S = {}^{f_s D}\!/_{V} = 0.2 \qquad \text{for } 100<Re_D<10^5 \qquad (2.1.1)$$

where:

D = Diameter of the tube $[m]$

f_s = Vortex shedding frequency $[Hz]$

V = Fluid velocity $[ms^{-1}]$

S = Strouhal number

The vortex shedding process is also characterised by a correlation length (L_C) above which the shedding of vortex is not coherent, uniform and varies over the span of the tube**[2GE]**.

2.1.2 VIBRATION RESPONSE OF THE TUBE TO EXCITATION

In the analysis of the tube's response to excitation one can treat the tube as if it is rigidly clamped at each end as seen in figure 2.1 (b). This treatment helps in the determination of the tube's natural frequency, which must not be surpassed to ensure non-destructive vibration. Using basic equations of strength of materials, the natural frequency of the tube as seen in figure 2.1 (b) is:

$$f_{tn} = C_n \sqrt{\frac{gEI}{Wl^4}} \qquad (2.1.2)$$

where:

C_n = 3.58, 9.82 (for the first and second mode of frequency respectively)

W = weight of the tube and its contents per unit length $\left[Nm^{-1} \right]$

At low fluid velocity there is no tube response to excitation, because the vortex shedding frequency is below the tube's first modal frequency. As the fluid velocity increases the tube begins to vibrate vigorously. At this point the tube's vibration and vortex dynamics are working together to feed energy from the fluid to the tube and this occurs over the so called the 'lock-in-range'.

The peak response in the lock-in-range occurs when the frequency is equal to the fluid-structural resonant frequency, and the results of this vibration can be detrimental to the structure of the heat exchanger. Tests conducted, have

shown that in the lock-in-range the Strouhal number decrease from 2 to 0.14 with a value of 1.7 at the peak response **[2GE]**. The response of the tube to flow induced excitation is shown in figure 2.2 below.

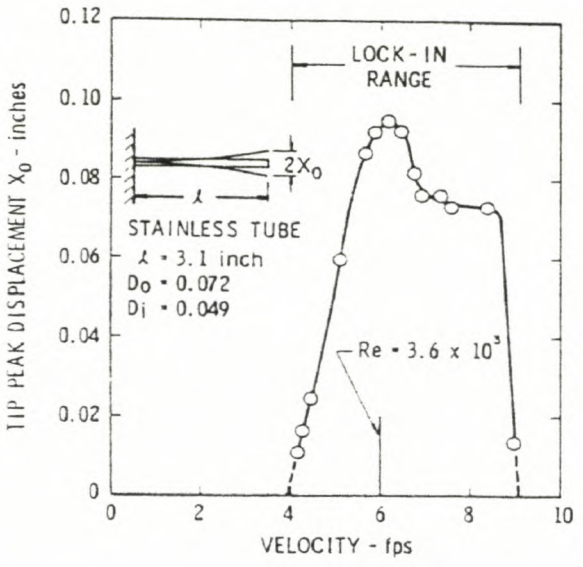

Figure 2.2. Tube's response to induced excitation. (Courtesy of ASME's technical committee on Unfired Heat Exchangers)

2.1.3 FLOW INDUCED VIBRATION EXPERIMENTS

During the conduction of flow induced experiments the engineer wants to determine the following:

- range of vortex shedding frequencies that may occur.
- modes of tube's vibration that can be excited in this range.
- the excitation forces that are exerted on the tube.
- stresses for each mode on the tube, and apply corrective measures.

2.1.4 EXPERIMENTAL PROCEDURE

1. The designer calculates the natural frequency of the tube for each mode using equation. 2.1.2.
2. Using $S = {f_s D}/{V}$ determine the flow velocity V . In a study conducted by Chen **[3NE]** et al it was shown that the use of S=0.2 result in significant errors.
3. Once the velocity at peak response is obtained a $\pm$ 40 % of this value gives an approximate lock-in-range **[2GE]**.
4. To determine the forces induced by flow the following equation is used.

$$F_L = 0.5 \times \rho V^2 (LD) C_L \qquad (2.1.4a)$$

where:

ρ = fluid density $\left[kgm^{-3}\right]$

L = tube length $\left[m\right]$

C_L = lift coefficient

F_L = amplitude of the oscillating force $\left[N\right]$

Because of the complex nature of determining a reliable C_L value, ($C_L = C_L(R_e, L/D, x_o/D, f/f_s)$), Geralch and Dodge **[3GE]** developed a reliable way of determining F_L . Their analysis is summarised as follows.

The tube clamped on both ends and subjected to an excitation force is modelled as a mass ,damper, spring system.

$$m\ddot{x} + c\dot{x} + kx = F_o \sin(2\pi ft + \theta) \qquad (2.1.4b)$$

where:

θ = phase angle of the fluid force relative to the cylinder motion.

F_o = maximum amplitude of the forcing function.

Solving the equation 2.1.4b for $x = x_o \sin(2\pi f_s t)$, results in:

$$\left(k - 4\pi^2 f_s^2 m\right)x_o = F_o \cos\theta \qquad (2.1.4c)$$

$$\left(2\pi f_s C\right)x_o = F_o \sin\theta \qquad (2.1.4d)$$

where:

x_o = maximum displacement amplitude

Assuming that θ is 90°, equation 2.1.4d becomes:

$$\omega C x_o = F_o \qquad (2.1.4e)$$

where:

$\omega = 2\pi f_s$

Equating equation 2.1.4e with equation 2.1.4a results in:

$$\omega C x_o = 0.5\rho V^2 (LD) C_L \qquad (2.1.4f)$$

The above equation can be simplified to give:

$$x_o/D = 0.5\rho V^2 (LQ) C_e \qquad (2.1.4g)$$

where:

Q = amplification factor

C_e = effective force coefficient

The maximum response, x_o, can be obtained experimentally by applying a fluid with a given V. Equation 2.1.4g can also be expressed as :

$$x_o/D = 0.5\rho V^2 (LQ)\overline{C}_e \qquad (2.1.4h)$$

where:

$$\overline{C}_e = \left(\frac{V}{V_o}\right)^2 C_e$$

V_o = maximum velocity at maximum response

Since $\overline{C}_e$ is directly proportional to the amplitude of the tube's response, then the maximum value of C_e occurs at maximum response amplitude. The maximum force acting on the tube can be determined from equation 2.1.4h. The stress at the clamped ends is calculated from basic equations of strength of materials.

2.2 VIBRATION CAUSED BY ADJACENT STRUCTURE

Adjacent structures can also induce vibration of the tubes of the heat exchanger. This occurs when the adjacent structures e.g. fans, transmit an oscillating force to the structure on which these heat exchangers are mounted.

2.2.1 VIBRATION OF HEAT EXCHANGERS INDUCED BY FANS.

When fans are installed they are in good mechanical balance. As they continue to operate, corrosion, erosion and even the mere collection of dust on the impellers and blades results in the out-of-balance of the fan. In the event of such an out-of- balance occurring, some form of damping device must be provided to reduce the excitation force being transmitted to the structure supporting the heat exchanger.

2.2.2 MOUNTING OF THE FAN SUPPORT STRUCTURE ON SPRING DAMPERS.

A fairly simple solution of reducing vibration transmitted to the heat exchanger's support structure is by mounting the fan on spring supports. Due to the fact that springs can sometimes amplify rather than reduce the vibration force transmitted, a careful design is necessary.

2.2.3 AN ANALYSIS OF FAN INDUCED VIBRATION.

The relationship between the natural frequency of the static assembly on the spring mountings and the excitation force induced by the fan, determines the degree of vibration transmission. The vibration force transmitted is

$$k x_o = F\cos(\omega t) \qquad (2.2.3a)$$

where :

k = spring stiffness $\left[Nm^{-1}\right]$

x_o = response amplitude $\left[m\right]$

ω = frequency of excitation $\left[rads^{-1}\right]$

In most cases it is difficult to find the exact value of F. In such cases the transmissibility (T) is used. This is defined as the ratio of the force transmitted to the structure over the force applied.

$$T = \frac{1}{r^2} - 1 \qquad (2.2.3b)$$

$$r = \frac{f}{f_o} \qquad (2.2.3c)$$

where:

f = frequency of excitation $\left[Hz\right]$

f_o = natural frequency of vibration of the structure $[Hz]$

To design a spring mounted structure, it is necessary to ascertain the lowest frequency of forced vibration, f, which is usually the lowest frequency of rotation. This value is divided by r >2,5 to give the natural frequency of the spring **[4OS]**. The spring stiffness is given by:

$$k = (2\pi f_o)^2 m \qquad (2.2.3d)$$

where:

m = mass of the structure supported by the springs $[kg]$

It is also advantageous to place pads of rubber under these springs to prevent high frequency vibration forces that might not have been considered during the analysis.

2.2.4 VIBRATIONS INDUCED BY PUMP INSTABILITY AND SURGING

Vibration can also be induced by flow being pumped from one centrifugal pump to the other or low frequency pressure pulsation from the pump. For pumps running separately , vibration induced by pressure pulsation are relatively low. Pressure pulsation measured when two or more pumps are working together are very large and result in large vibration amplitudes **[5ER]**.

3. BASIC DESIGN PHILOSOPHY OF PRESSURE VESSELS AND STRESS CONCENTRATION FACTORS

The design pressure in Pressure Vessel Design is always specified by the purchaser **[6WA]**. This pressure dictates the thickness and the type of material to be used for the design of the pressure vessel. In the design of most engineering components, stress analysis is frequently used. This analysis gives the designer a yardstick to quantitatively analyse the effects of load and assess the possibility of failure in service. The thickness of the tube can be obtained from this basic stress relationship.

In standards of pressure vessels, basic thickness of the shell is derived from calculations based on simple methods of stress analysis and allowable design stress. As an example , the thickness of a long and thin cylindrical shell subjected to an internal pressure load as shown in figure 3.1 below can be determined from these calculations. The circumferential stress (σ_θ) and the axial stress (σ_x) of this pressure vessel can be determined from the balance of forces.

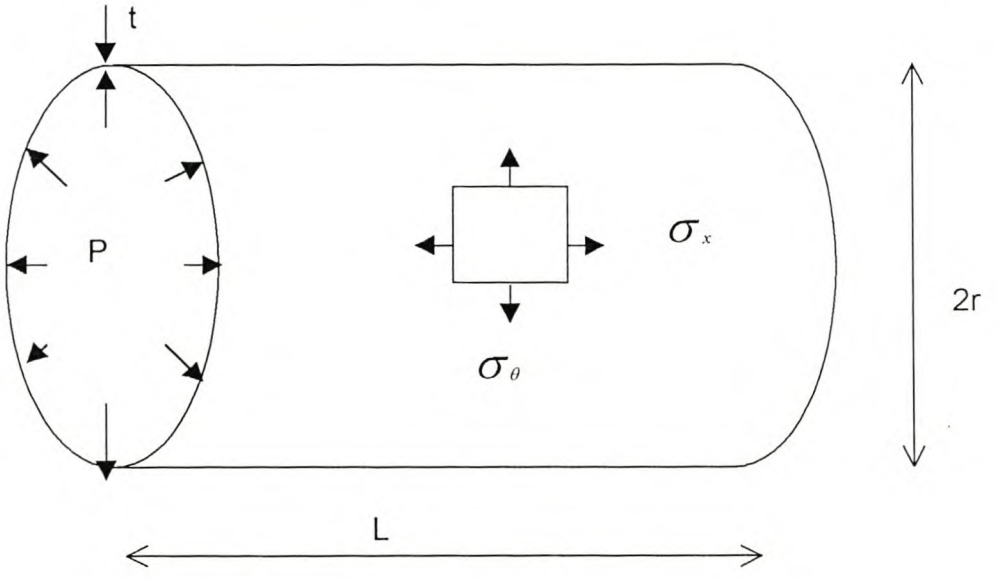

Figure 3.1. A sketch of a cylindrical shell.

Balancing forces in the radial direction results in:

$$2\sigma_\theta tL = p2rL \tag{3.1}$$

$$\sigma_\theta = \frac{pr}{t}$$

where:

L = length of the cylinder $[m]$

p = internal pressure $[Pa]$

t = wall thickness $[m]$

Similarly by balancing the longitudinal forces one obtains:

$$\sigma_x = \frac{pr}{2t} \tag{3.2}$$

The above formulae works fairly well for thin walled pressure vessels of $r \geq 10t$. Often pressure vessels have significant thickness and some standards take into consideration this effect. Lame's equation for thick cylinders are:

$$\sigma_\theta = p\left(\frac{1+\left(\frac{b}{r}\right)^2}{\left(\frac{b}{a}\right)^2 - 1}\right) \tag{3.3}$$

$$\sigma_r = p\left(\frac{1-\left(\frac{b}{r}\right)^2}{\left(\frac{b}{a}\right)^2 - 1}\right) \tag{3.3}$$

$$\sigma_r = \left(\frac{P}{\left(\frac{b}{a}\right)^2 - 1}\right) \tag{3.4}$$

where:

a = inner radius $[m]$

b = outer radius $[m]$

r = radius at any point between a and b $[m]$

For a moderately thick cylinder some standards use:

$$\sigma_\theta = \frac{pd_m}{2t} = \frac{p(D_i + t)}{2t} \qquad (3.5)$$

where :

D_i = internal diameter $[m]$

If the allowable circumferential stress is equated to that codes' allowable design stress **[7SP]**, then the thickness of the pressure vessel can be determined from:

$$t = \frac{pD_i}{2f - p} \qquad (3.6)$$

where:

f = allowable design stress $[Pa]$

3.1 THE STRESS CONCENTRATION FACTOR

In pressure vessels, localised stress occurs at transition between the thick and thin portions of the shell, and around the openings. The magnitude of the localised stress depends, amongst other things, on:

1. Physical properties of the material e.g. brittle or ductile, and
2. Type of loading.

To account for the effects of localised stress, the stress given by normal formulae must be multiplied by the theoretical stress concentration factor - K_t.

3.1.1 STRESS CONCENTRATION IN CIRCULAR HOLES

When a tube-sheet plate is subjected to a uniform tensile load, σ, and a circular hole of radius a, is drilled in it as shown in figure 3.1.1 below, then a high stress concentration occurs near the hole. The maximum value of the stress occurs on the edge of the hole that are perpendicular to the direction of the load.

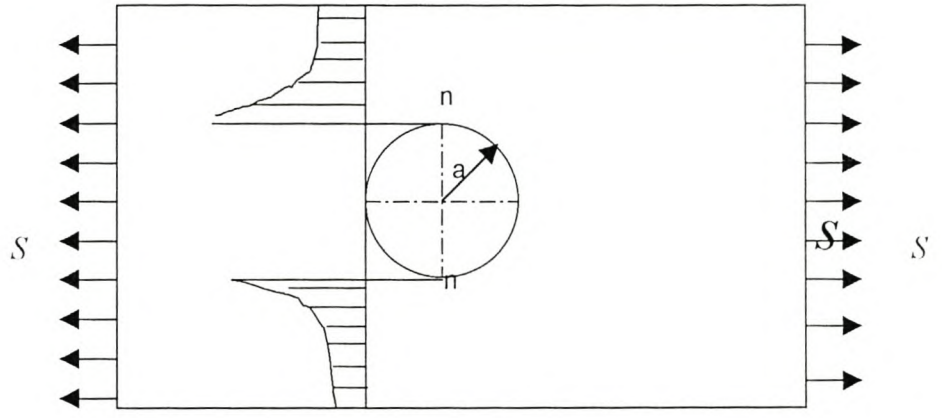

Figure 3.1.1. Variation in stress in a plate containing a circular hole and subjected to a uniform load.

The stress distribution on the plate around the hole on the diametrical section nn is given by:

$$\sigma K_t = \frac{S}{2}\left(2+\frac{a^2}{r^2}+3\frac{a^4}{r^4}\right) \qquad (3.1.1)$$

where:

S = Uniform stress acting in the plate $[Pa]$

a = radius of the hole $[m]$

r = radius at any point $[m]$

Timoshenko and Goodier **[8TI]** show a step by step derivation of the above equation 3.1.1.

3.1.2 STRESS CONCENTRATION IN ELLIPTICAL HOLES

In many applications elliptical openings are used in pressure vessel design. In the case where one has a tube-sheet plate subjected to a uniform load, with an elliptical hole, the stress concentration can be calculated. When the major axis of an ellipse lie perpendicular to the direction of the tensile load, (figure 3.1.2 (a)), the maximum stress occurs at the edges of the major axis. When the minor axis of an ellipse lie perpendicular to the direction of the tensile load (figure 3.1.2(b)), then the maximum stress occurs on the edge of the minor axis.

$$\sigma = S\left(1+2\frac{a}{b}\right) \qquad (3.1.2)$$

$$\sigma = S \qquad (3.1.3)$$

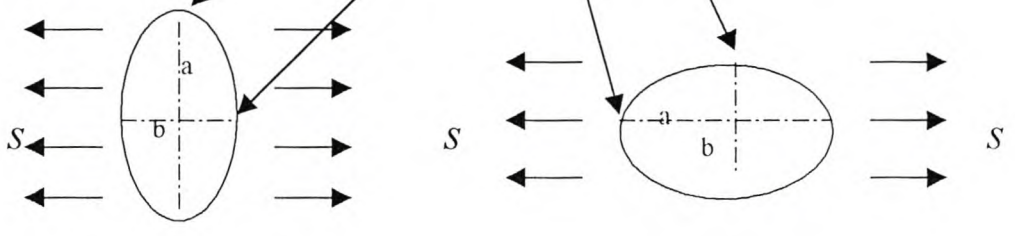

(a) (b)

Figure 3.1.2. Stress condition at the edge of an elliptical hole in a plate in tension.

From the above equations it is clear that the maximum stress increases with the increase in the ratio $\left(\frac{a}{b}\right)$. This shows that a narrow ellipse produces a high stress at the corners. This also results in cracks (at the edges) that are perpendicular to the direction of the tensile load, propagating faster. The spreading of these cracks can be halted by drilling holes at the end of the cracks **[9HA]**. The drilling of the hole results in the removal of the sharp corners that promote this condition.

4. MATERIAL SELECTION AND TUBE-TO-TUBE-SHEET JOINTS FOR HEAT EXCHANGERS.

To ensure the integrity and the durability of heat exchangers as pressure vessels one must consider an integral part of heat exchanger design : Mechanical design. This process ensures the safe operation of the exchanger unit with a primary objective of providing enclosures that are sufficiently strong and can completely prevent leaks of the fluid flowing through the system.

The material to be selected for the design of heat exchangers is selected on the basis of strength (it must be able to withstand operational temperatures and pressures) and must be compatible with the fluid (it must withstand the corrosive nature of the fluid).

4.1 PROPERTIES OF MATERIAL

The material selected for heat exchanger design are selected because of their

1. strength properties at certain temperatures
2. ability to resist corrosion
3. cost
4. availability
5. ease of cleaning

4.1.1 STRENGTH PROPERTIES

During the design of heat exchangers the designer must ensure that the material used operates within the elastic range. This ensures that when loads (thermal or mechanical) are removed, the tubes retain their original undeformed shape.

To allow for uncertainties in material properties, loading conditions and stress concentration, safety factors are used.

4.1.2 EFFECT OF TEMPERATURE ON MATERIAL PROPERTIES.

When materials are heated up, their yield strength and ultimate strength decrease.

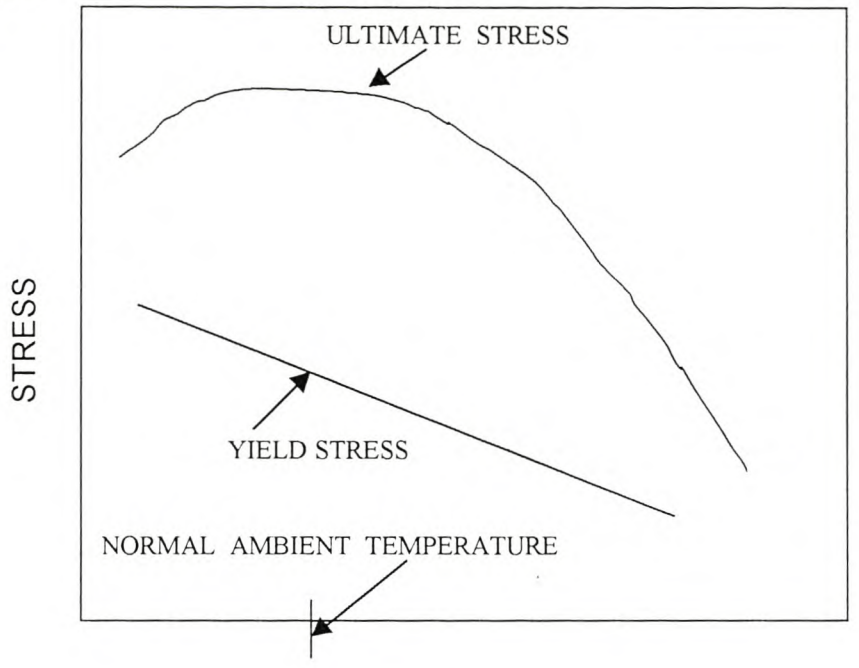

Figure 4.1.2. Effects of temperature on yield and ultimate strength.

Figure 4.1.2 shows that there is a linear relationship between the yield stress and temperature. The ultimate strength is less affected at low temperature but sharply decreases as temperature increases.

The ability of a material to creep at higher temperature is also increased. Creeping is the continuous deformation of a material when the load is kept constant.

Materials subjected to cyclic load (thermal cycles) fail under loads that are considerably less than their ultimate tensile strength. This process is called material fatigue. To determine the stress variation under which one can operate without causing the material to fail, one uses a S-N curve shown in figure 4.1.3 below.

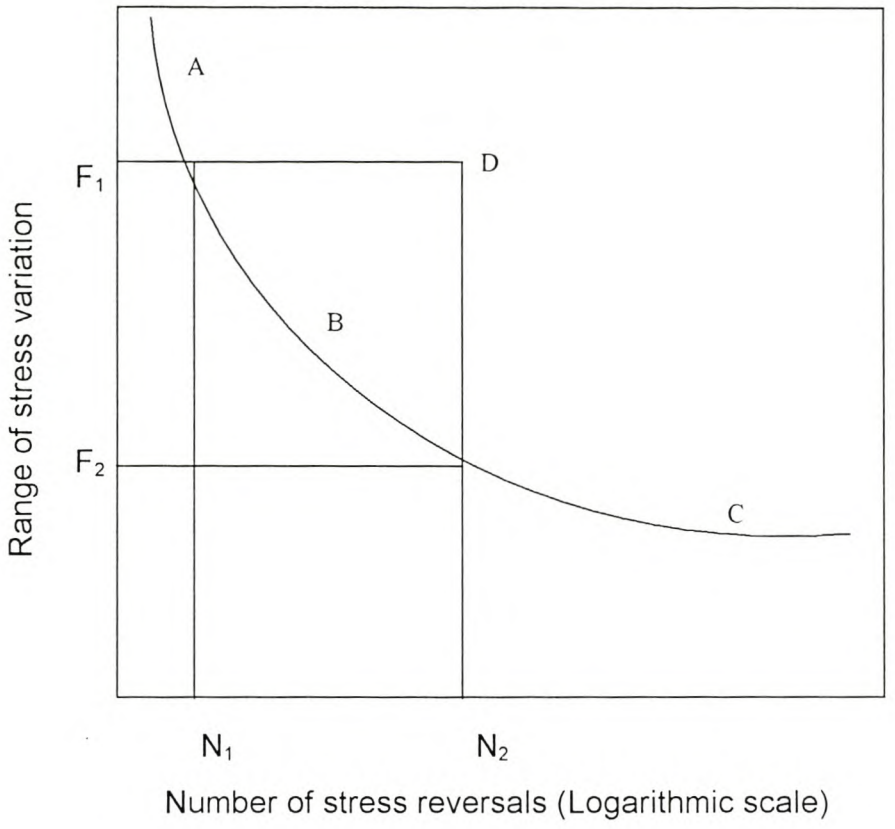

Figure 4.1.3. Fatigue strength curve.

Fatigue failure begins on small cracks or points of high stress concentration. Crack ends are themselves points of high stress concentration, and once a crack begins it will continue to grow until fracture occurs. In heat exchangers fatigue failure due to thermal cyclic strain is more common **[6WA],** and care must be taken in avoiding the onset of high stress levels due to temperature effects.

Another property highly influenced by temperature is the toughness of the metal. Toughness is the ability of the metal to resist crack propagation. Some metals become brittle at low temperatures, even though they are normally ductile at room temperature e.g. steel. A treatment of carbon steel with nickel (which is not brittle at low temperatures) can reduce the onset of ductile-brittle transformation.

Metals can be manipulated to produce properties that are not normally inherent in them. These properties can be obtained by, *inter alia* , heat treatment , cold working etc.

4.1.3 HEAT TREATMENT

The mechanical properties of a metal depend on the crystal structure of that metal. One can get a hard brittle structure (Martensite) by fast quenching a carbon steel that was heated. One can also get a soft ductile steel by slowly cooling the carbon steel. So by manipulating the crystal structure one can get any type of metallurgical structure. To obtain these structures one usually tempers, anneals, and / or normalises the metal.

During the manufacturing process, mechanical properties can be changed by cold working and forming, which the material undergoes during rolling, bending and pressing. The hardness that arises during cold working as a result of residual stresses can be eliminated by annealing or heating.

Surface hardness can also be increased by shot peening, a process that causes cold working of the metal close to the surface.

Another process that greatly affects the metallurgical properties of a metal is the welding process. The structural change is localised around the welded joints. In the weld itself the structure is completely different from the base metal, and can sometimes result in a brittle structure around the welded joints.

Preheating the joint to be welded, minimises the tendency for the formation of a hard and brittle joint, susceptible to crack propagation.

Another important property in the design of heat exchangers is the thermal coefficient. It is important because of high stress induced when tubes are

mechanically constrained. In some heat exchanger designs, stresses arising from thermal expansion of tubes are relieved by using flexible expansion joints or allowing the ends of the bundle to float **[6WA]**.

All the information presented above is of cardinal importance when it comes to the fabrication of tubes and tube-sheet. These tubes and tube-sheets provide the primary support for the tube in both radial and longitudinal directions.

4.2 TUBE-SHEET MATERIAL

Most tube-sheets are made from rolled plates or forged ingots. For small production volumes, tube-sheets may be cast. Also in small air conditioning units non-metallic materials and composites of thin metals coated with epoxy resin have been used. Sometimes high alloy and non-ferrous tube-sheets are parted from plates by powder burning , plasma arc cutting or machining. Thicker tube-sheets are machined from forgings.

Tube-sheets can also be made from a base metal (most often carbon steel) clad with another metal or metal alloy. This cladding process can be:

1. Fusion weld cladding
2. Roll cladding
3. Explosive cladding

4.3 TUBE-TO-TUBE-SHEET JOINTS

The reliability of the heat exchanger partly depends on the integrity of the tube-to-tube-sheet joints. More attention is given to these joints than the rest of the tube body because of their susceptibility to high stresses and consequently a likely site of failure.

Here more focus is given to the function and requirements of tube-to-tube-sheet joints and the methods used in the joining of tubes to tube-sheets.

4.3.1 FUNCTIONS AND REQUIREMENTS OF THE JOINTS

The main functions of the tube-to-tube-sheet joints are to:

1. seal the tube tightly to the tube-sheet.
2. create a firm contact between the tube and tube-sheet.
3. assist in the resistance of bending by the tube-sheet .
4. transfer forces from the tube-sheet to the tube when the tube-sheet is subjected to a pressure load.

In order to perform these functions the following requirements must be met:

1. The joints must remain tight and leak free.
2. The tube must remain in the tube hole under all loading conditions.
3. The joint must withstand thermal load.

4.3.2 TESTING TUBE-TO-TUBE-SHEET JOINTS

ASME code [SEC VIII D1 NMA APP A,1998] has set-up standards that one need to follow when testing the tightness and the strength of the joints.

Joint tightness test

The measure of how tight a joint is, is its resistance to leak. The following methods are used in joint tightness tests:

1. Visual observation of the tube ends during a hydrostatic pressure test
2. Bubble testing
3. Gas leak test
4. Helium mass-spectrometer detector probe testing sniffer
5. Halogen diode detector probe testing
6. Helium mass-spectrometer tracer-probe technique

7. Helium mass-spectrometer hood method

Yokell **[10YO]** explains how these methods work in great detail. The only quantitative measure acceptable by ASME code [SEC VIII D1 NMA APP A,1998], for the joint tightness test, is the helium hood method.

Joint strength test

Pullout or push-out (Shear Load) tests are used to measure the strength of the joint. These shear loads subject the specimen (tube) to an axial load until the tube or the joint fails. The reasons for conducting the Shear Load test are:

i) To determine the strength of a joint .

ii)To determine the joint efficiency, which will be used to determine the maximum allowable joint load.

To calculate the efficiency of the joint, ASME code [SEC VIII D1 NMA APP A,1998] sets out different formulas depending on the method used to create that joint. Joints are made in the following ways:

1. Stuffing the space between the tube and the tube hole with packing
2. Sealing the tube to the tube hole by means of an interference fit
3. Welding or brazing the tube to the tube-plate
4. Gluing the tube to the tube-sheet.

ASME code's Appendix A, Section VIII, Division 1 **[11AS]** specifies specimen preparation , testing procedures and acceptable standards for Shear Load tests.

4.3.3 METHODS OF MAKING TUBE-TO-TUBE-SHEET JOINTS

A brief explanation of the procedures on making tube-to-tube-sheet joints is undertaken here.

Packed joints

Figure 4.3.3 below shows a packed tube-to-tube-sheet joint. A hole large enough for the tube to slide in, is drilled in the tube-sheet. On the outer side of the tube, packing rings are inserted. Threads are made on the outer side of the tube-sheet and a threaded ferrule is used to squeeze the packing rings. The compression of the packing rings against the tubes determines the strength of the joint.

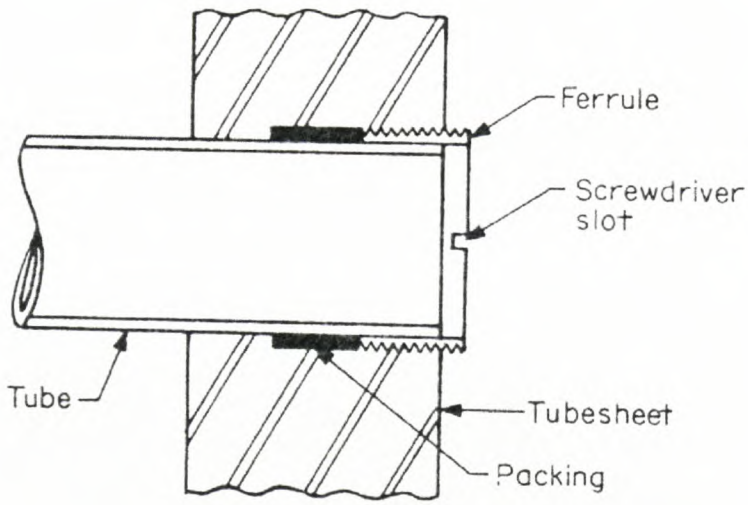

Figure 4.3.3. Packed tube-to-tube-sheet joints. (Courtesy of Chemical Engineering)

The advantages of using this type of joint are:

1. Ease of assembly and disassembly.
2. Allowable expansion of the tube in the tube-sheet.

While the disadvantages are :

1. The packing may dry out in service becoming stiff and hard.
2. The ferrule may freeze making it difficult for the replacement of the tube.

Interference fit joints by tube expansion

A hole is drilled in the tube-sheet, and the clearance fit that exist between the tube and the tube-sheet allows for the insertion of the tube in the hole. Applying

In expanding pressure in the tube, deforms it until it makes contact with the tube-sheet hole. When the expanding pressure is greater than the tube's yield strength, the deformation will be permanent and the residual stresses created at the tube-to-tube-sheet interface determines the strength of the joint. It is important to ensure that the tube's yield strength is less than that of the tube-sheet's yield strength. If that is not the case, when the expanding pressure reaches a value equal to the tube-plate's yield stress, the plate will yield and the hole will be enlarged.

Goodier and Schoessow **[12GO]** found that to obtain the strongest joint, the highest pressure used should not cause the tube to extrude i.e. the expanding pressure should not be greater than the yield strength of the tube. Some of the methods used to expand the tube are:

1. Roller expanding
2. Explosion expanding
3. Rubber expanding
4. Hydro-expanding
5. Hybrid expanding

Yokell **[10YO]** gives a detailed description of these methods.

Welded and brazed joints

These types of joints are used in cases where:

1. The operating temperatures are high.
2. There are cyclic stresses.
3. Joints are required to be very tight.

4. Tube expansion is not permissible.

Brazed joints are made by placing a braze metal between the tube and tube-sheet hole assembly and heating the braze metal until it melts. The braze metal will flow into the clearance space between the tube and the hole. The operating temperature of this joint is then dictated to, by the melting point of that braze metal.

Joints are also made by welding the tube to the tube-sheet. Fusion-welded joints are made by forming a molten pool consisting of the base metal (tube), filler metal, and some flux elements. Upon cooling the base metal and these elements form a complex solid solution that tightens the joint.

The welding process can be made by Oxy-fuel-gas(OFS), Electric Resistance welding (ERW), Electric Induction welding (EIW) and many more. In cases where the tube and the tube-sheet metal are not compatible with fusion welding, an explosive welded joint can be made.

5. NUMERICAL METHODS

In cases where analytical solutions to problems can not be easily found, numerical methods are used. Finite element methods is a numerical technique used to find approximate solutions in a wide range of engineering problems.

5.1 FINITE ELEMENT METHODS (FEM)

FEM is a useful tool in obtaining solutions to problems where the geometry is irregular or arbitrary. This is done by finding an approximate numerical solution . Here the governing equations are expressed in a piecewise form, and the solution region is analytically modelled or approximated by replacing it with an assemblage of elements. Since these elements can be put together in a variety of ways, FEM can be used to analyse the most complex geometry.

In FEM the unknown field variable(pressure; temperature; stress; displacement;...;etc.) is expressed in terms of approximate functions, and these functions are defined between nodal points within an element. The nodal value of the field variable and interpolation functions completely define the behaviour of the field variable throughout that element. The degree of accuracy of FEM depends on the size, number of elements and also the interpolation function used.

Due to the fact that FEM has an ability to formulate solutions for individual elements, complex problems are reduced to small manageable 'pieces'. Different methods are used to formulate individual properties of elements and Huebner **[13HU]** gives these methods in great detail. These methods are :

1. Direct approach
2. Variational approach
3. Weight residual approach
4. Energy balance approach

Many computer programs have been developed for FEM. These programs include:

1. ANSYS
2. ASK
3. BERDYNE
4. MARC
5. NASTRAN and many more

These programs can perform, *inter alia,* analysis from stress-strain analysis both under dynamic load and static loads to buckling analysis.

5.2 BENDING OF PLATES

Many structures contain sections that are made of thick or thin plates. Some of these structures, like straight beams, support transverse loads by the bending action. The magnitude of the normal stresses are given by these equations:

$$\sigma_Z = M_X \frac{Z}{I} \quad ; \quad \sigma_Y = M_Y \frac{Z}{I} \quad ; \quad \tau_{XY} = M_{XY} \frac{Z}{I} \qquad (5.2)$$

where:

M_X = Bending moment about the x-axis $[Nm]$

I = Section modulus or Moment of inertia $[m^4]$

As can be clearly seen normal stresses vary linearly with Z. In the analysis of plates in bending two theories are widely used, 1) Kirchoff, 2) Mindlin Theory **[14C0]**.

Kirchoff Theory

In Kirchoff's analysis of plate deformation, the assumption is that lines that are straight and normal to the mid-surface remain straight and normal after the

load has been applied. This assumption suggests that transverse shear deformation are zero. This is very true for thin plates. Therefore if one is analysing thin plates, Kirchoff's analysis would give good results. As a result, in the formulation of the stiffness matrix, using for example, the Variational approach, the strain energy is expressed as follows:

$$U = \int_V \tfrac{1}{2} \{\varepsilon\}^T \lfloor \mathrm{E} \rfloor \{\varepsilon\} dV \qquad (5.2\ a)$$

where :

$$\{\varepsilon\}^T = \lfloor -z\omega_{,xx} ; -z\omega_{,yy} ; -2\omega_{,xy} \rfloor$$

Here the strain energy is determined entirely by in-plane strain $(\varepsilon_x ; \varepsilon_y ; \gamma_{xy})$ and these strains are determined by a lateral displacement field $\omega = \omega(x, y)$.

Mindlin theory

Mindlin assumes that a line that was initially straight and normal to the mid-surface before loading, remains straight but not necessary normal to the mid-surface after the load has been applied. Here shear deformations are not zero. Mindlin 's theory is used to analysè thick plates and its elements account for bending and shear deformation. In formulating the stiffness matrix here, using the Variational approach, the strain energy is expressed as follows:

$$U = \tfrac{1}{2} \int_A \int_{-\frac{t}{2}}^{\frac{t}{2}} \{\varepsilon\}^T \lfloor \mathrm{E} \rfloor \{\varepsilon\} dz\, dA \qquad (5.2.b)$$

where :

$$\{\varepsilon\}^T = \lfloor \varepsilon_x , \varepsilon_y , \gamma_{xy} , \gamma_{yz} , \gamma_{zx} \rfloor$$

5.3 FEM IN VIBRATION AND DYNAMIC ANALYSIS

FEM can also be used in the analysis of vibration and dynamic effects on the structures. In cases where the frequency of the exciting force is greater than one third of the structure's lowest natural frequency of vibration, inertia forces become important. To account for the inertia and damping forces, a mass matrix $\lfloor M \rfloor$ and a damping matrix $\lfloor C \rfloor$ are defined. If one looks at the equilibrium of forces then, the inertia , damping and elastic force balance with the external force. Expressed mathematically this gives:

$$\lfloor M \rfloor \{\ddot{D}\} + \lfloor C \rfloor \{\dot{D}\} + \{R^{\text{int}}\} = \{R^{ext}\} \qquad (5.3)$$

where:

$$\{R^{\text{int}}\} = \lfloor K \rfloor \{D\}$$

The are two types of dynamic problems: 1) wave propagation problems and 2) structural dynamic problems. The former is concerned with the stress wave as a result of sudden impact. Whilst the latter is concerned with structural response to excitation. Two types of structural dynamic analysis are used viz.

1) NATURAL FREQUENCY OF VIBRATION ANALYSIS - where one wants to compare the natural frequency of a structure to frequency of the exciting force.
2) HISTORY- ANALYSIS – where one wants to know how the structure moves in time in response to the load. In time-history analysis two methods are used i.e. 1) Modal method, 2) Direct integration method.

5.3.1 MASS AND DAMPING MATRICES

The success of a finite element's vibrational analysis depends on the appropriate development of the following elemental matrices:

1. Stiffness matrix

2. Mass matrix
3. and Damping matrix

Mass Matrix

To account for inertia forces in dynamic analysis, a mass consistent matrix is developed from:

$$\lfloor M \rfloor = \int_{Ve} \rho \lfloor N \rfloor^T \lfloor N \rfloor dV \qquad (5.3.1a)$$

This mass matrix can be developed as consistent or lumped . Different schemes are used to develop lumped mass matrices and some of these schemes are:

1. Hinton, Rock and Zienkiewicz (HRZ) lumping scheme
2. and Optimal lumping scheme

Lumped mass matrices have an advantage of reduced solution time because of their diagonal nature and may lead to loss of upper bound convergence property of the computed spectrum **[15Gé].**

Damping Matrix

The ease of the solution of equation 5.3 depends on the actual damping mechanism used. Two methods that are used in the treatment of damping computational analysis are :1) Phenomenological and 2) Spectral methods. A popular Spectral damping scheme is Rayleigh or proportional damping where the damping matrix is expressed as the fraction of the mass and stiffness matrix.

$$\lfloor C \rfloor = \alpha \lfloor K \rfloor + \beta \lfloor M \rfloor \qquad (5.3.1b)$$

5.3.2 NATURAL FREQUENCY OF VIBRATION AND MODE SHAPES

When both the damping matrix and external forces are zero, equation 5.3 reduces to:

$$\lfloor K \rfloor \{D\} - \lambda \lfloor M \rfloor \{D\} = 0 \qquad (5.3.2a)$$

where:

$\lambda_i = \omega_i^2$

For a non-trivial solution the determinant of the above matrix must be zero, which when solved gives each λ_i (Eigenvalue).

$$\left| \lfloor K \rfloor - \lambda \lfloor M \rfloor \right| = 0 \qquad (5.3.2b)$$

Each eigenvalue when substituted in equation 5.3.2a gives an eigenvector $\{D\}$, and $\{D\}$ gives the mode shapes corresponding to each eigenvalue.

6. EXPERIMENTAL INVESTIGATION

The objective of these experiments are to obtain information about the structural mechanics of these elliptical finned tubes viz. A-tubes with a 4.3 mm and 2.5 mm fin pitch and F-tubes with a 3 mm fin pitch. To successfully quantify the structural characteristic of these elliptical finned tubes, the following experiments will have to be conducted.

1) Shear load test
2) Bending load test
3) Pressure load test

In the above experiments the tube-to-tube-sheet assembly will be subjected to static loads. The Shear Load experiment will be conducted to determine the efficiency of the weld. This information will then be used to determine the maximum allowable axial load that the welds and the tube should be subjected to, to avoid failure.

The Bending Load experiment will be conducted to determine the bending stress on the tube-sheet plates, and how that bending stress varies with the change in fin pitch.

The Pressure Load experiment will be conducted so as to see the distribution of stress in the tube-sheet plate. Also the effects of varying the fin pitch will be investigated.

The results obtained from these experiments will be compared with and used in a Finite Element Model of the tube-to-tube-sheet assembly.

6.1 SHEAR LOAD TEST

The main aim and objective of conducting this experiment is to determine the following:

i) The strength of the joints made by welding.

ii) The joint efficiency which will be used to quantify the maximum allowable joint load.

Specimen preparation

- The specimen consist of a tube joined to a test block that simulates the tube-sheet.
- This test block (BS 1501-151-430A) is of rectangular geometry (200 mm x 300 mm) and its thickness is 16 mm .
- The tube is welded on the geometric centre of the test block.
- To ensure consistency the tube is taken from the same heat treatment, and the procedure used to prepare the tube-to-tube-sheet joint during production is maintained.
- The length of the tube used for testing the joint is 150 mm.
- Figure A.1 in appendix A shows the apparatus used in the execution of the Shear Load experiment.

Experimental procedure

- The tube-to-tube-sheet assembly is placed on the tensile testing machine.
- The load cell and the displacement transducers are connected to the scanner as shown in figure A.1 of appendix A.
- The assembly is then loaded mechanically until failure occurs.
- The axial load (L_{test}) that causes failure to occur is recorded.
- A minimum of three specimens are to be tested to determine the joint efficiency (fr_{test}).

- From the three tests , a mean value of L_{test} is determined and the standard deviation (s) about the mean is also calculated.
- To calculate a value of fr_{test}, an L_{test} corresponding to approximately 2 times the standard deviation (s) is used.
- Different formulae to calculate the joint efficiency, fr_{test}, are used depending on the type or method used to make that joint **[11AS].**
- For welded joints

$$fr_{test} = \frac{L_{test}}{St \times A_t} \qquad (6.1a)$$

- For expanded joints

$$fr_{test} = \frac{L_{test}}{f_y \times f_e \times St \times A_t} \qquad (6.1b)$$

where:

L_{test} = lowest axial load at which failure occur $[N]$

St = minimum tensile strength of the tube $[Pa]$

A_t = cross sectional area $[m^2]$

L_X = length of the expanded portion of the tube $[m]$

d_o = outer diameter of the tube $[m]$

f_e = factor for the length of the expanded tube = $\frac{L_x}{d_o}$

f_e = 1 when the tube holes are grooved

f_y = factor for different material properties. This factor is the ratio of tube-sheet yield stress to tube yield stress or 1 whichever is smaller. These yield stresses are minimum values at particular temperatures.

- The calculated value of fr_{test} is then used to calculate the maximum allowable load ($L_{\max}$) that the joint can withstand under room temperature conditions.

- ASME code's Section VIII, Division 1 to Appendix A **[11AS]**, gives the basis for establishing the maximum allowable axial load for the joints.
- For welded joints

$$L_{\max} = A_t \times S_a \times fr_{test} \qquad (6.1c)$$

- For expanded joints

$$L_{\max} = A_t \times S_a \times f_y \times f_e \times fr_{test} \qquad (6.1d)$$

where:

$L_{\max}$ = maximum allowable load $[N]$

S_a = ASME code's allowable stress of a tube in tension at a given temperature $[Pa]$

6.1.1 ANALYSIS AND DISCUSSION OF RESULTS

1. The minimum axial load that causes the deformation of the A-tube at the tube-to tube-sheet interface is 98.33 kN, whilst an axial load of 59.25 kN causes the deformation of the F-tube. Figure B.1 and B.2 in appendix B shows graphically the Force vs. Displacement curve.

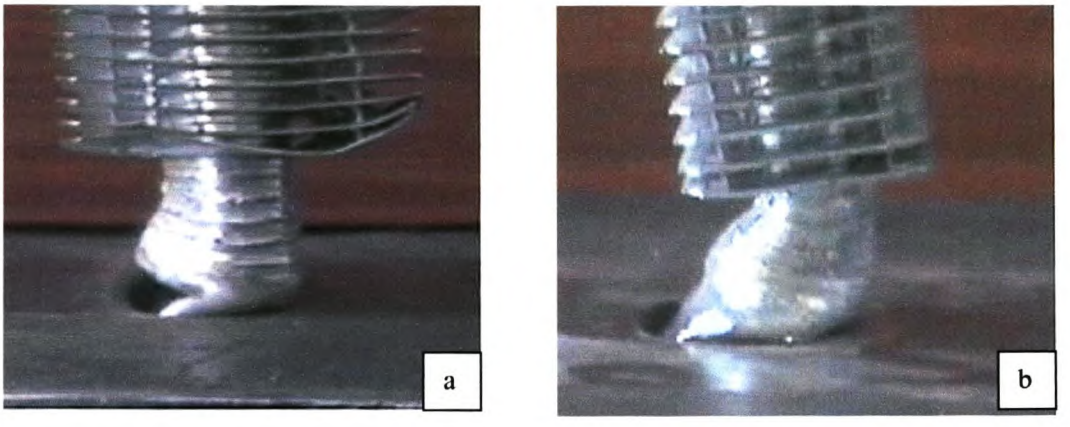

Figure 6.1.1. The deformation of the tube due to axial load. (a) A-tube and (b) F-tube.

2. Under these loading conditions, the efficiency of the welds of both the A- and the F-tube is found to be 103 % and 139 % respectively. Appendix B shows the calculations for the determination of these efficiencies. A weld efficiency greater than 100 % implies that the weld is able to withstand a minimum axial load that is greater than the minimum Tensile load $(A_t \times St)$ of the tube in question. Figure 6.1.2 below attest to this fact.

3. Whilst both tubes have permanently deformed under the action of the axial load, the weld has remained virtually intact. This implies that the strength of the weld is greater than that of the tube.

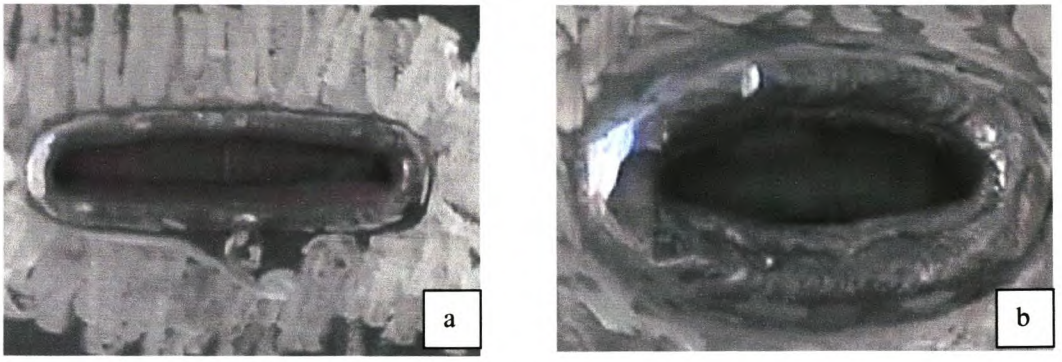

Figure 6.1.2. The weld of the tubes after the test. (a) the A-tube and (b) the F-tube.

4. Under ASME code's Section Viii, Division 1, the maximum allowable axial load on the weld of both the A-and the F-tubes is 20.89 kN and 14.55 kN respectively. These loads, when applied on the tubes, will ensure that the tube and weld are far from deformation and failure.

6.2 BENDING LOAD EXPERIMENT

The main objectives of these experiments are:

i) to determine the bending stress of the fin tube on the tube-sheet plate.

ii) to determine how the bending stress of the tube on the tube-sheet varies with the fin pitch of the tubes.

iii) to use this information, where necessary, in the Finite Element Modelling of the finned tubes.

Specimen preparation

- An elliptical fin tube is welded to the tube plate (300 mm x 300 mm) .
- Holes are drilled on the periphery of the tube plate to enable the mounting of the tube-to-tube-sheet assembly on the test rig.
- A mounting plate with two holes is placed on the other end of the tube. This plate allows for the ease of placing mass pieces in two planes.
- Using sandpaper, the positions where the strain gauges will be mounted are sanded away to remove rust and paint.
- These surfaces are then cleaned using a solvent (Acetone and acid) to remove traces of grease and oil.
- To dilute the acidity of these surfaces and also to give them a proper chemical affinity for the adhesives, a basic solution of Ammoniac is used. Dally and Riley **[16DA]** outlined the strain gauge adhesives and mounting methods for reliable experimental results.
- Four, 45° strain gauge rosettes of the type EA-06-060RZ-120 are then mounted on these surfaces using adhesive glue. Figure 6.2.1(a) below shows the position of these strain gauges.
- These strain gauges are then coupled to a scanner.

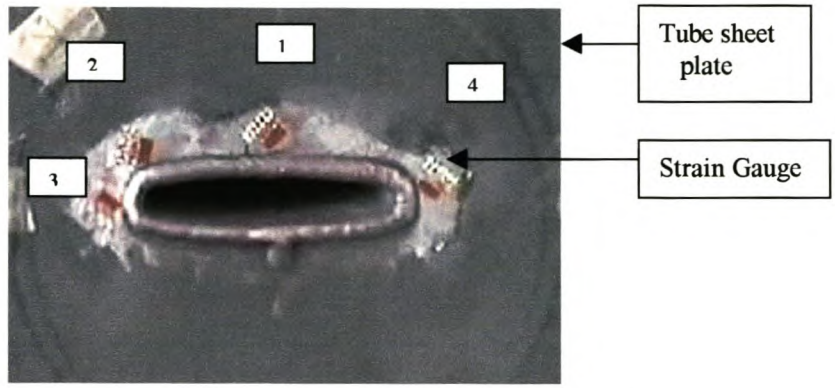

(a)

(b)

Figure 6.2.1. Strain gauge positions on the tube-to-tube-sheet assembly.
(a) Back view (b) Side view

Experimental procedure

- Two types of bending load tests are conducted. Figure 6.2.2 below schematically shows these tests.
- The tube-to-tube-sheet assembly is mounted on the pillar as shown in Appendix C.
- Different masses (2.82 kg; 5.09 kg; 7.36; 10.08 kg; 12.36 kg; 17.33 kg; and 19.61 kg) are hung on the mounting plate to subject the tube to a bending load in one plane.
- By hanging the masses from another hole in the mounting plate subjects the tube to a bending load at right angles to the minor axis of the ellipse as shown in figure 6.2.2 below.

- Each time a mass piece is hung, the strain readings are recorded on the scanner.
- This procedure is repeated for different tubes with different fin pitches viz. a 1.0 m long A-tube with a 4.3 mm and 2.5 mm fin pitch and a 0.690 m F-tube with a 3 mm fin pitch.

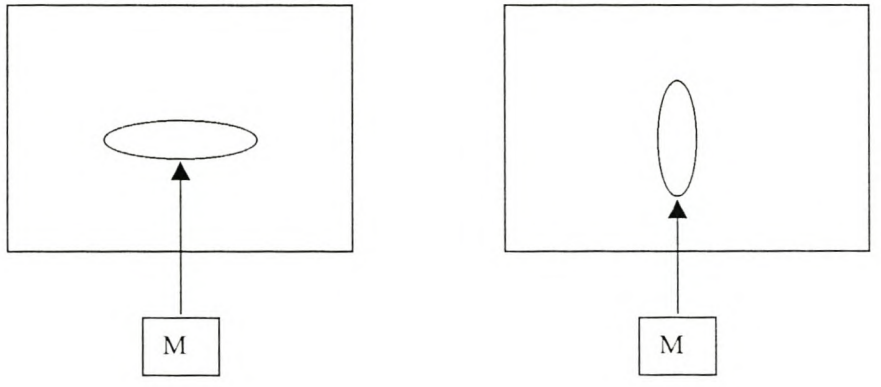

Figure 6.2.2. Two types of Bending Load tests. (a) Type 1, (b) Type 2.

- To establish the stress field from strain measurements at each gauge position the following equations are used:

$$\varepsilon_A = \varepsilon_{XX} Cos^2\theta_A + \varepsilon_{YY} Sin^2\theta_A + \gamma_{XY} Sin\theta_A Cos\theta_A$$

$$\varepsilon_B = \varepsilon_{XX} Cos^2\theta_B + \varepsilon_{YY} Sin^2\theta_B + \gamma_{XY} Sin\theta_B Cos\theta_B$$

$$\varepsilon_C = \varepsilon_{XX} Cos^2\theta_C + \varepsilon_{YY} Sin^2\theta_C + \gamma_{XY} Sin\theta_C Cos\theta_C \qquad (6.2a)$$

Where θ_A, θ_B *and* θ_C are the angles each gauge elements in the rosette makes with the x-axis and ε_A, ε_B *and* ε_C are strain measurements along θ_A, θ_B *and* θ_C respectively.

- Assuming a plane stress problem (the tube-sheet plate and the tube plate are fairly thin, being 16 mm and 1.6 mm thick respectively.), the stresses on the plate are calculated using the following equations:

$$\sigma_X = \frac{(\varepsilon_{XX} + \nu\varepsilon_{YY})E}{1-\nu^2} \qquad (6.2b)$$

$$\sigma_Y = \frac{(\varepsilon_{YY} + \nu\varepsilon_{XX})E}{1-\nu^2} \qquad (6.2c)$$

$$\tau_{XY} = \frac{\gamma_{XY} \times E}{2(1+\nu)} \qquad (6.2d)$$

Where σ_X, σ_Y *and* τ_{XY} are normal stresses and shear stress respectively.

- The principal stress at these gauge positions can be calculated directly from the strain measurements by using the following equations:

$$\sigma_1 = E\left[\frac{\varepsilon_A + \varepsilon_B}{2(1-\nu)} + \frac{1}{2(1+\nu)}\sqrt{(\varepsilon_A - \varepsilon_B)^2 + (2\varepsilon_B - \varepsilon_A - \varepsilon_C)^2}\right] \qquad (6.2e)$$

$$\sigma_2 = E\left[\frac{\varepsilon_A + \varepsilon_B}{2(1-\nu)} - \frac{1}{2(1+\nu)}\sqrt{(\varepsilon_A - \varepsilon_B)^2 + (2\varepsilon_B - \varepsilon_A - \varepsilon_C)^2}\right] \qquad (6.2f)$$

and the maximum shear stress is given by:

$$\tau_{max} = E\left[\frac{1}{2(1+\nu)}\sqrt{(\varepsilon_A - \varepsilon_B)^2 + (2\varepsilon_B - \varepsilon_A - \varepsilon_C)^2}\right] \qquad (6.2.g)$$

- A sample calculation for the determination of the Maximum Bending (σ) and Maximum Shear (τ_{max}) stress at each gauge position is shown in appendix D. These results are given in tabular form.

6.2.1 ANALYSIS AND DISCUSSION OF RESULTS

1. Under the above mentioned loading conditions, the maximum bending stress on the plate due to the bending of the A-tube (both with a 4.3 mm and with a 2.5 mm fin pitch) is found at gauge position 3 and 4. Table D.2.1 and D.2.2 in appendix D show these results. Figure 6.2.1 below shows a graphical representation of those results.

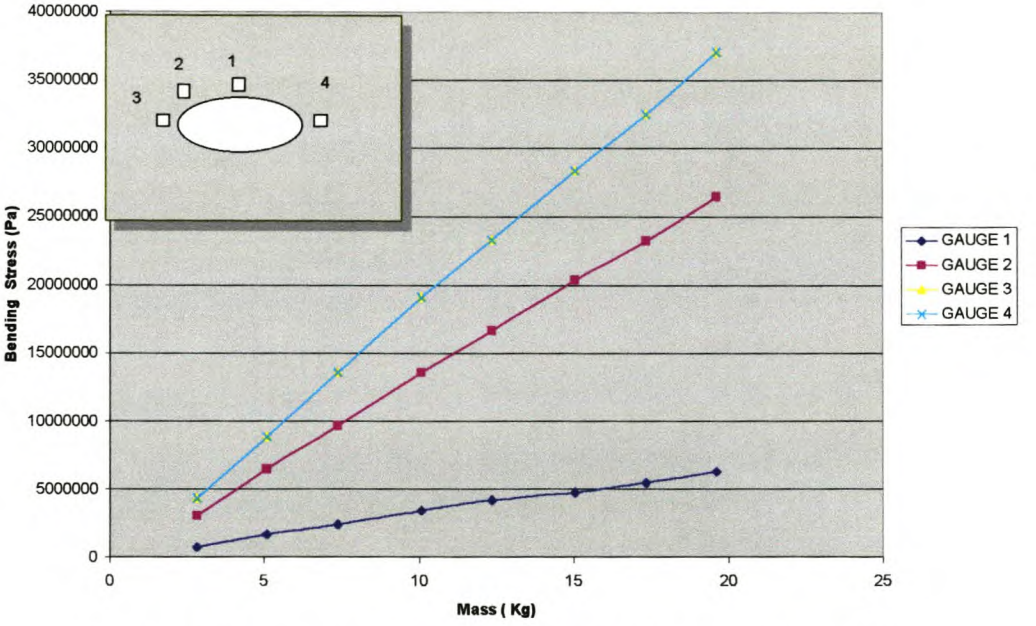

Figure 6.2.1 Maximum Bending Stress on the plate vs mass at each gauge position for the A-tube with a 4.3 mm fin pitch. Experiment type 1.

This maximum stress is attributed to the concentration of stress in the edge corners (along the major axis of the ellipse), and gauge 3 and 4 are placed in the closest proximity to these edge corners.

2. The F-tubes show a different stress distribution with a maximum bending stress occurring at gauge position 1 and 2 whilst the minimum occurs at gauge position 3 and 4. See figure 6.2.3 below.

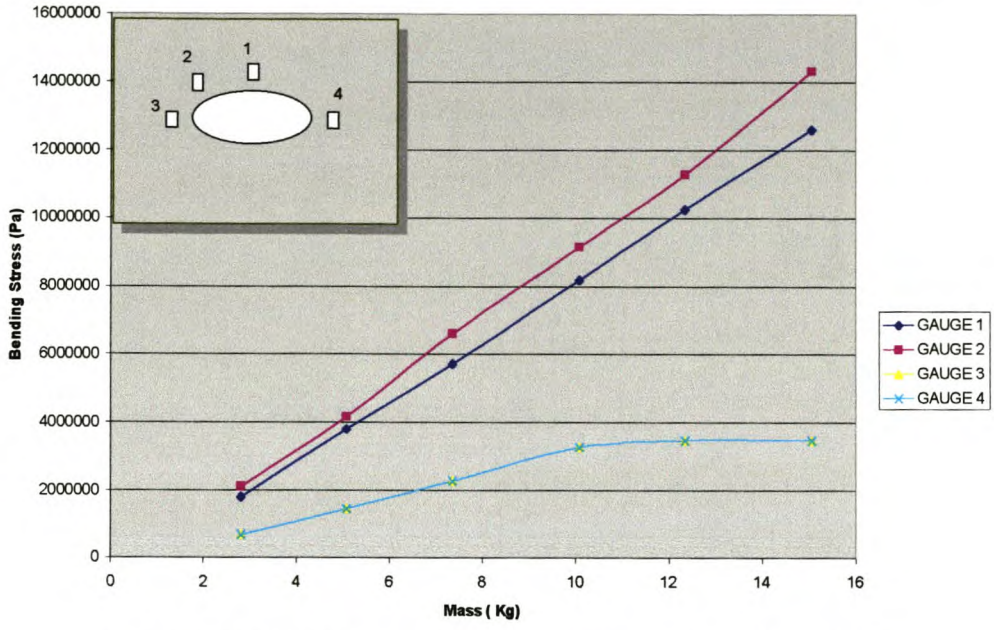

Figure 6.2.2 Max Bending Stress on the plate vs mass at each gauge position for the F-tube. Experiment type 1.

3. There is a significant difference in Bending stress between the A-tube in type 1 experiment and in type 2 experiment. Compare the data in table D.2.1 and D.2.4. The bending stress in type 1 experiment is higher than the bending stress in type 2 experiment because of their different resistances to bending or section modulus - I .

Table 6.2.3(a). Comparison of section properties of the tube.

Experiment type	Tube's bending stiffness	Principal stress @ gauge 4 Mass = 19.61 kg
1	$I_{XX} = 0.16 \times 10^{-7} m^4$	37.06 MPa
2	$I_{YY} = 0.233 \times 10^{-6} m^4$	7.19 MPa

4. In type 1 experiment there is a difference between the bending stress of the A-tube with a 4.3 mm fin pitch and that of the A-tube with a 2.5 mm fin pitch. Figure 6.2.3 below graphically shows this difference.

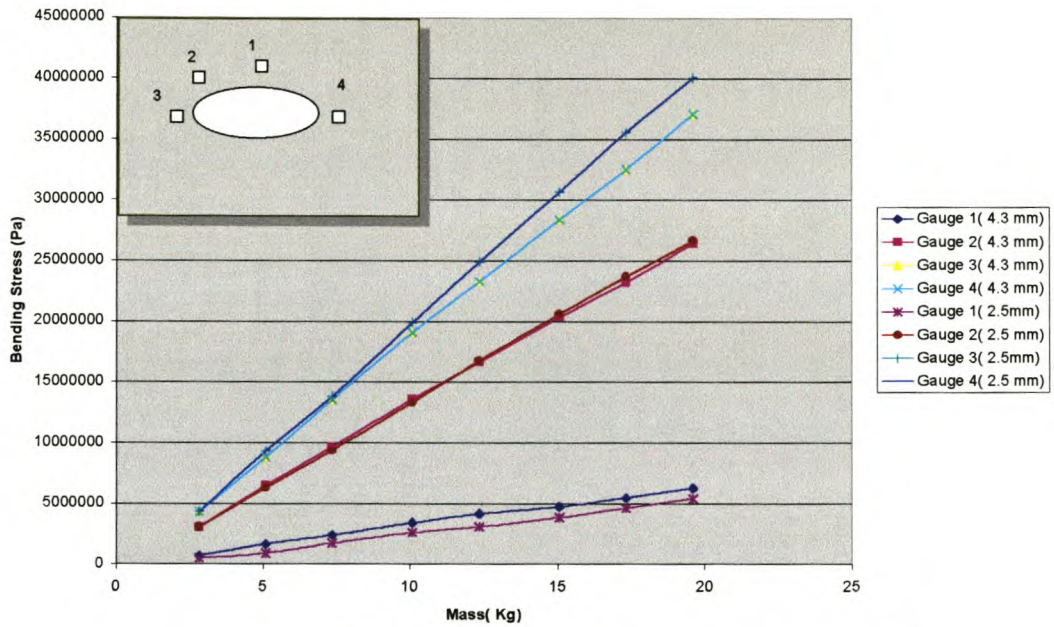

Figure 6.2.3 Vatiation of Bending Stress with fin pitch for A-tubes (Experiment type 1)

This difference is highly pronounced along the edge corners (gauge position 3 and 4). The resulting bending stress at these gauge positions for the A-tube with 4.3 mm fin pitch is between 2-3 MPa greater than that of the tube with a 2.5 mm fin pitch, see table D.2.1 and D.2.2. The mass difference of the tube-to-tube-sheet assembly, due to different fin pitches, can be attributed to this bending stress difference. Table 6.2.3(b) below shows the mass of the two tubes.

Table 6.2.3(b). Mass of the tube-to-tube sheet assembly

A-tube with a fin pitch of x mm	Mass of the assembly in kg
4.3	17.75
2.5	20.75

6.3 PRESSURE LOAD EXPERIMENT

The main aims and objectives of this experiment are:

i) to determine the resistance of the fin tubes to pressure load.

ii) to determine how the compressive stress of the tube on the tube-sheet varies with the fin pitch of the tubes.

iii) to use this information where necessary in the Finite Element Modelling of the finned tubes

Specimen preparation

- A steel cylinder 10 mm thick is welded on a 10 mm thick square plate (300 mm x 300 mm).
- Four 1.5 mm holes are drilled on the periphery of the cylinder.
- Soldering tags are glued below these holes, on the inner and the outer sides of the cylinder.
- Small copper wires are then used to connect the outer soldering tag to the inner tag.
- Cable wires from the strain gauges are connected directly to the inner soldering tags and the cable wires from the scanner are connected directly to the outer soldering tag.
- The cylinder is then placed on the back of the tube-sheet plate covering the strain gauges.
- To tighten this cover plate on to the tube-sheet plate, bolts and nuts are used.
- The other side of the fin tube is sealed off and a nozzle is placed to allow for the attachment to the pressure line. Figure 6.3(a) below shows a schematic drawing of a tube-to-tube-sheet assembly used for the pressure load experiment.

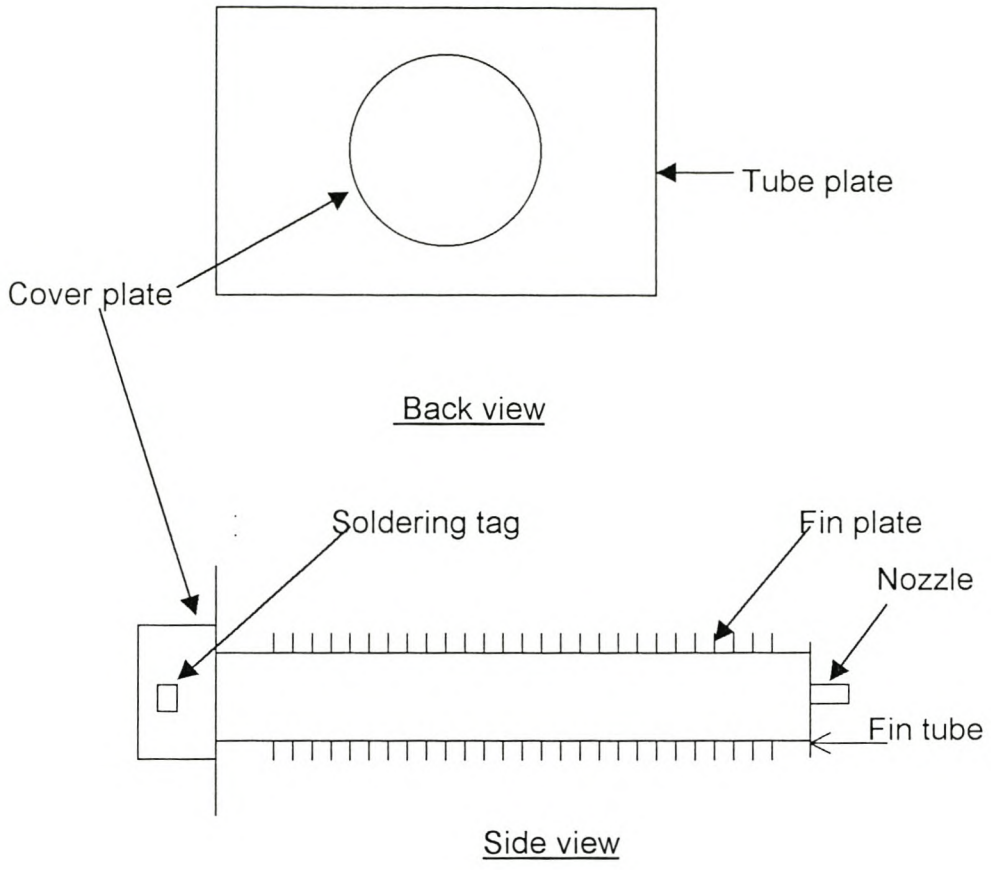

Figure 6.3(a). Tube-to-tube-sheet assembly with the cover plate for Pressure Load test.

Experimental procedure

- The tube-to-tube-sheet assembly is subjected to a pressure load.
- Pressure loads of the order 1 bar; 2 bar; 3 bar; 3.5 bar; 4 bar; 4.5 bar; 5 bar and 5.5 bar are used in this experiment.
- These pressure loads are below the design limits, it being:
  36.5 bar for the F-tubes with a 3.0 mm fin pitch
  11.7 bar for the A-tubes with a 2.5 mm fin pitch
  7.3 bar for the A-tubes with a 4.3 mm and 4.5 mm fin pitch
- Each time the tubes are pressurised the strain measurement are recorded.

- Using equation 6.2a to 6.2g, the compressive stress at each gauge position is determined.
- Figure 6.3(b) below shows a photographic image of the tube-to-tube-sheet assembly ready for this experiment.

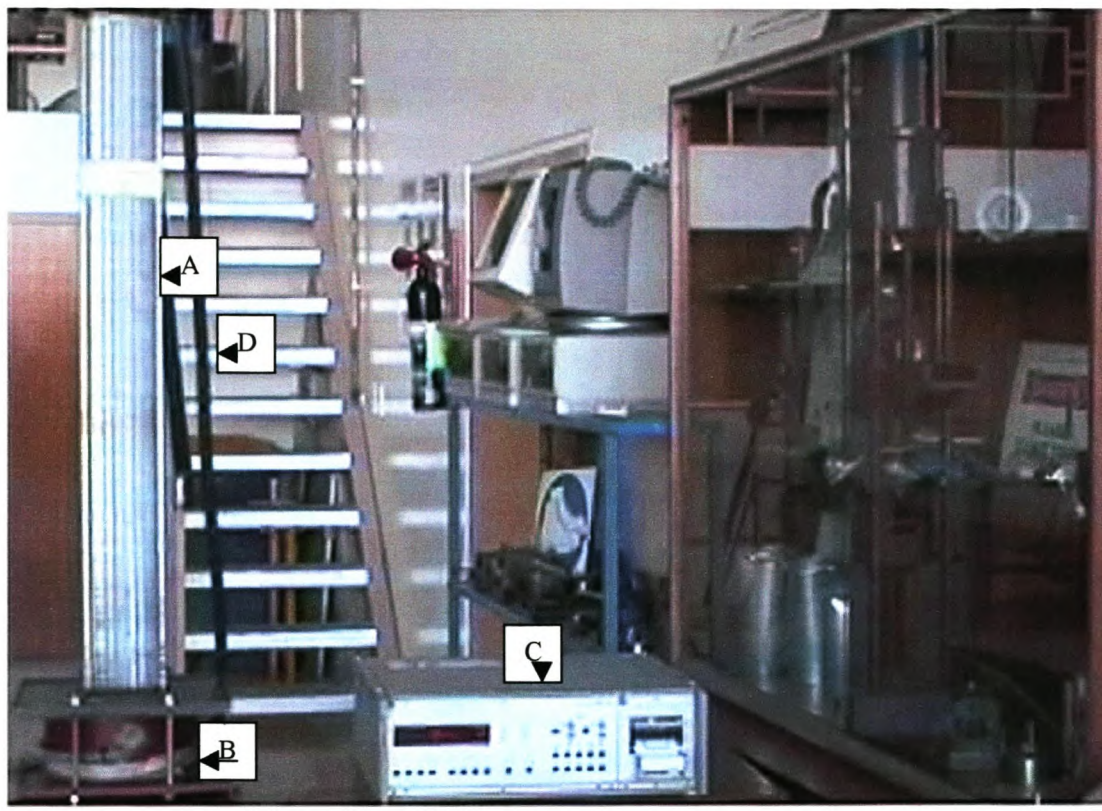

Figure 6.3(b). A Pressure Load experiment of a tube-to-tube-sheet assembly. (A) Fin tube, (B) Cover plate, (C) Scanner and (D) Pressure pipe.

6.3.1 ANALYSIS AND DISCUSION OF RESULTS

1. Under these loading conditions the maximum compressive stress on the tube-sheet plate is found at gauge position 3 and 4. These positions are along the major axis on the edge corners, and they have high stress concentrations. Figure 6.3.1 below shows the distribution of compressive stress around the weld.

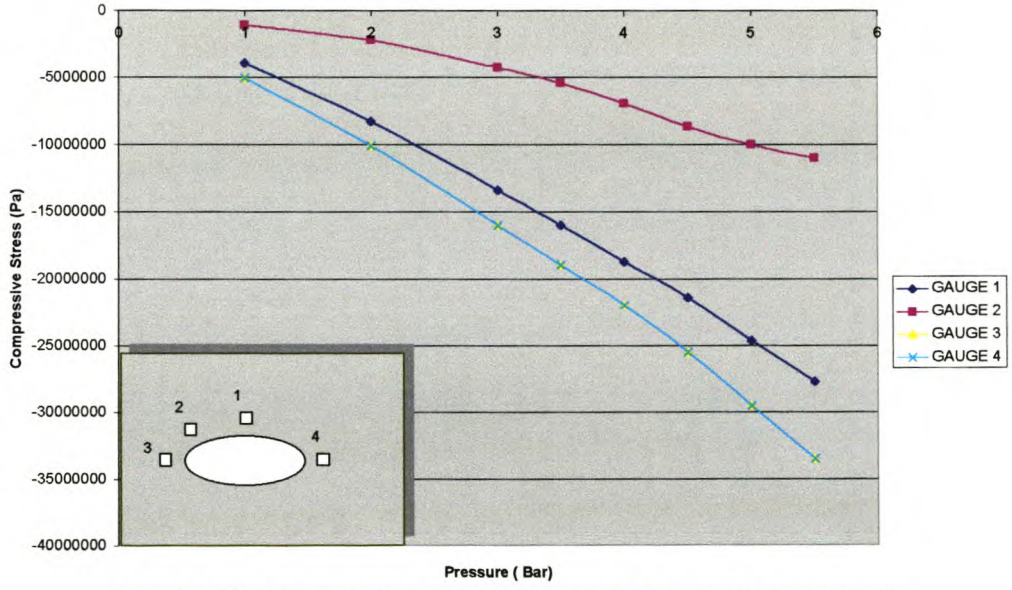

Figure 6.3.1 Max Compressive Stress vs Pressure at each gauge position for the A-tube with 4.3 mm fin pitch.

2. The minimum compressive stress is found at gauge position 2. The change in fin pitch has little or no effect at this gauge position. This is clear when comparing the compressive stress at gauge position 2 between the A-tube with a 4.3 mm and the A-tube with a 2.5 mm fin pitch, in table D.3.1 to D.3.3, in Appendix D.

3. The F-tubes has the same stress distribution as the A-tube. The compressive stress on the F-tube is lower than that on the A-tube under the same pressure load. Figure 6.3.2 below shows the distribution of stress on the F-tube as calculated from the strain gauge measurements.

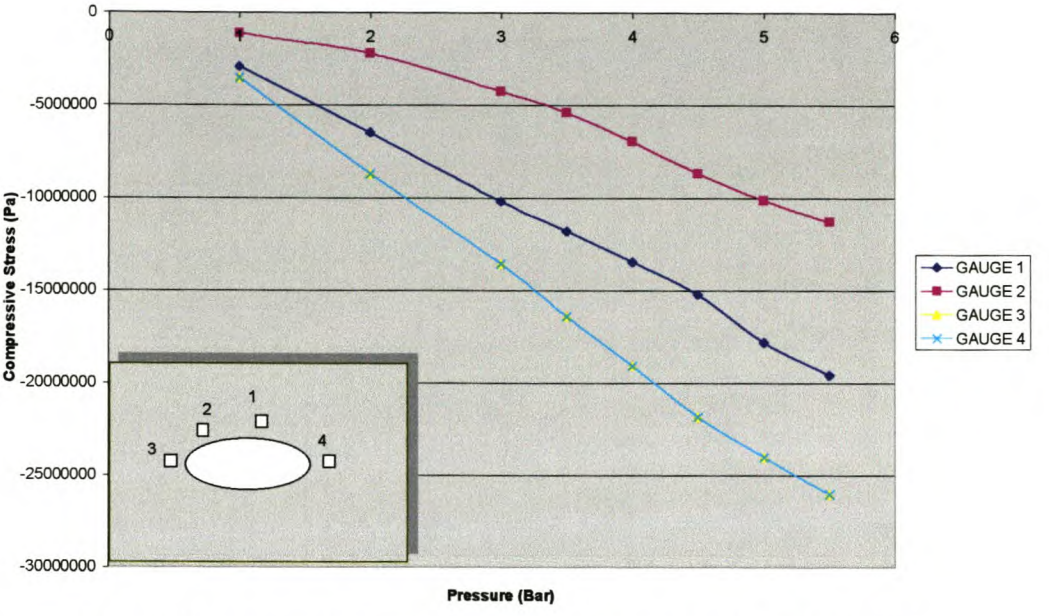

Figure 6.3.2 Max Compressive Stress vs Pressure at each gauge position for the F-tube with a 3.0 mm fin pitch.

4. F-tubes have a high resistance to internal pressure load when compare with A-tubes. This means that F-tubes can withstand higher internal pressure loads than A-tubes for the same deformation. This is evident in figure 6.3.1 and 6.3.2 above.

   This is due to the fact that the force, which is responsible for the deformation of the tube, is directly proportional to the internal area of the tube. This means that the smaller the area the smaller the force. Therefore, to cause the same deformation on the F-tube as on the A-tube, the internal pressure inside the F-tube must be increased.

5. The effect of the difference in fin pitch, on the resistance of the tube-sheet plate to a pressure load, is highly significant in areas of high stress concentration (gauge positions 3 and 4) .The effects of different fin pitches is significant at these positions as seen in figure 6.3.3 below.

The compressive stress on the A-tube with a 4.3 mm fin pitch is higher than that of a tube with a 2.5 mm fin pitch.

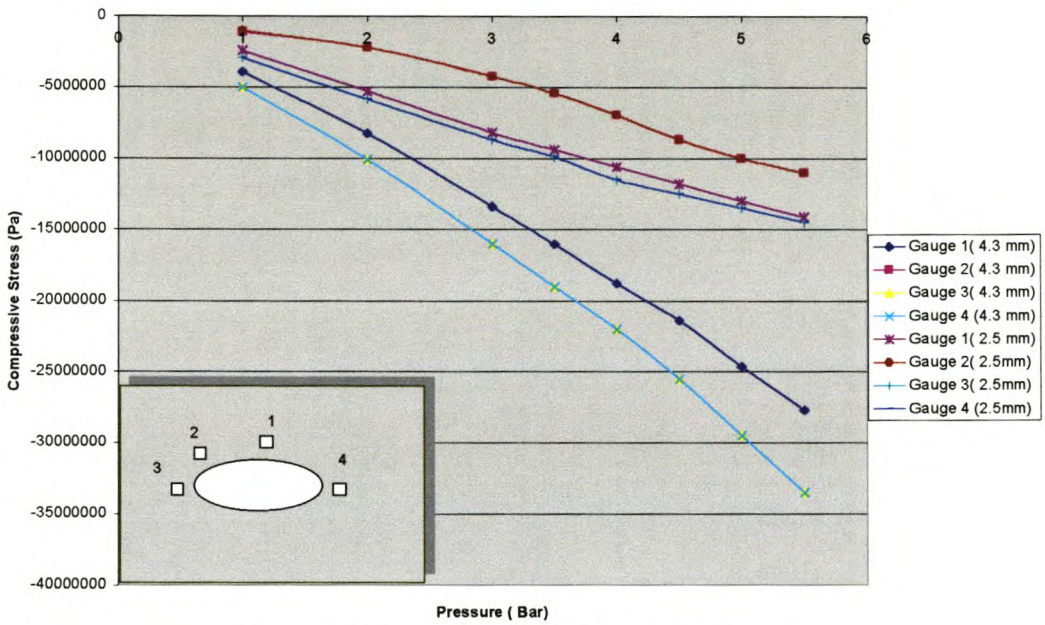

6.3.3 Variation of Compressive stress with fin pitch for A-tubes.

In structural mechanics, fin plates assist in the resistance of internal pressure. As a result it is only to be expected that the greater the number of fin plates the higher the resistance of the finned tube to internal pressure load. In other words, the smaller the fin pitch, the lower the compressive stress on the tube-sheet plate.

6.4 CONCLUSIONS

The following conclusions are drawn based on the discussion of results made during the experimental investigation:

Shear Load Experiment

1. A minimum axial load of 59.25 kN and 98.33 kN will cause the deformation and failure of both the F-tube and the A-tube respectively.
2. The efficiency of these welds are 103 % and 139 %, for the A and the F-tube respectively. These welds are very strong and can withstand an axial load higher than the one above.
3. For the safe operation of the tubes though, the maximum allowable axial load should be 20.89 kN and 14.55 kN for the A-and the F-tube respectively.

Bending Load Experiment

1. The maximum bending stress on the F-tube, as measured on the tube-sheet plate closest to the welds, is at the ends of the minor axis, whilst it is at the end of the major axis on the A-tube.
2. The tubes are able to resist higher bending loads when the load is applied parallel to the major axis.
3. Tubes of the same type but different fin pitches have different bending stresses, and the more the fins per metre (or the smaller the fin pitch), the higher the bending stress on the tube-sheet plate.

Pressure Load Experiments

1. The maximum compressive stress on the tube-sheet plate is found at the ends, along the major axis of the ellipse (gauge 3 and 4).
2. The F-tubes are able to withstand higher internal pressures than the A-tubes for the same number of fins.

3. Fin plates resist the volumetric expansion of the tube due to an internal pressure load. The higher the number of fins per length the greater is this resistance to volumetric expansion. Therefore stresses, due to an internal pressure inside the A-tube with a 4.3 mm fin pitch, are higher than stresses on the same type of tube but with a 2.5 mm fin pitch.

7. NUMERICAL INVESTIGATION

The main aim and objective of this numerical investigation is to model the tube-to-tube-sheet assembly, using a finite element program called NASTRAN. The finite element model together with the results and information obtained during the experimental investigation will be used to analyse the behaviour of the tube-to-tube-sheet assembly under certain loading conditions viz. bending and pressure load, and to test the pressure limits suggested by the manufacturer i.e. GEA Air Cooled Systems (Pty) Ltd.

Before the final modelling of the tube-to-tube-sheet assembly is done, a series of investigations will be conducted. These investigations are:

1. the effects of fins on the tube-sheet assembly by modelling two F-tubes i.e. the F-tube without fins and the F-tube with fins. Both these tubes will be subjected to a pressure load of 0.2 MPa and a bending moment (M_X) of 9.15 Nm at the free end.
2. the effects of pressure load on the tube-to-tube-sheet , when the fin pitch is changed, by modelling two A-tubes i.e. the A-tube with a 2.5 mm fin pitch and the A-tube with 4.3 mm fin pitch. These tubes will be subjected to a pressure of the same magnitudes as above.
3. to compare the difference in stress when an elliptical and a round tube with an equivalent hydraulic diameter d_e are subjected to an internal pressure load .

$$d_e = \frac{4 \times A_t}{P_W} \qquad 7.1$$

where :

A_{tc} = internal cross sectional flow area of an elliptical tube $\left[m^2\right]$

P_w = wetted perimeter of an elliptical tube $\left[m\right]$

The hydraulic diameter (d_e) is the diameter of a round tube that has the same flow pattern as in a tube of other geometry. In other words if in the analysis of Thermal

Flow and Heat Transfer a laminar flow pattern is establish in an elliptical tube at a certain Reynolds number (R_e) the same flow pattern can be achieved when a round tube with an equivalent diameter d_e is used, with all other factors remaining constant. The Reynolds number can be calculated from:

$$R_e = \frac{\rho \times V \times d_e}{\mu} \qquad 7.2$$

where:

ρ = density of the fluid flowing inside the tube $\left[kgm^{-3}\right]$

V = velocity of the fluid flowing inside the tube $\left[ms^{-1}\right]$

μ = dynamic viscosity of the fluid flowing inside the tube $\left[kgm^{-1}s^{-1}\right]$

Kröger **[17KR]** shows the use of the hydraulic diameter in his Analysis of Thermal Flow and Heat Exchanger Design and Performance.

Finally, the maximum pressure limits suggested by the manufacturer will be tested, and the following tubes will be subjected to an internal pressure load.

1. F-tube with a 3.0 mm fin pitch to a pressure load of 3.65 MPa
2. A-tube with a 2.5 mm fin pitch to a pressure load of 1.17 MPa
3. A-tube with a 4.3 mm fin pitch to a pressure load of 0.73 MPa

7.1 CREATING THE MODELS

All the models are created in the manner outlined here. The dimensions and technical drawings of the both the A- and F-tubes are given in figure E1-E3 in Appendix E. The models consist of a full tube-to-tube-tube-sheet assembly modelled using Nastran solid, plate and slide line elements.

7.1.1 THE F-TUBE MODEL

A 200×200 mm^2 tube-sheet is modelled using solid elements. These solid elements are made by extruding an artificial plate in the thickness directions. Four solid elements in the thickness direction are used for modelling this 16 mm thick steel plate. Solid elements are also used to model the tube, with two elements in the thickness direction being used for this 1.6 mm thick tube core. The length of the tube is 61 mm. The solid elements of the fin tube are 3 mm in length, a dimension dictated by the fin pitch .

Plate elements are used to model the fins and these fin plates are 3 mm apart. The thickness of the plate elements that are used to model the fin is 0.4 mm.

Slide lines are used around the contact points between the tube and tube-sheet plate. A 0.1 mm gap that exists between the tube and the tube-sheet plate allows for the placement of slide line elements around the periphery of both the tube and the plate. As a result the relative motion of the tube outside the slide line plane is ignored **[18MS]**.

7.1.2 THE A-TUBE MODEL

Except for the difference in size and material, the A-tube is modelled like the F-tube above. The length of the fin tube is 41 mm. The length of the solid ele-

ments that model the fin tube are dictated by the fin pitch of the tube to be modelled. A tube with a 4.3 mm fin pitch has solid elements with a 4.3 mm length in the z-direction and a tube with a 2.5 mm fin pitch has solid elements with a 2.5 mm length in the z-direction. The thickness of the plate elements that are used to model the fin is 0.49 mm. Table 7.1 below shows the different materials for both the A-and F-tubes.

In all of these models the weld at the back of the tube-sheet plate is given the same material strength as the tube-sheet plate. This is done because during the Shear Load Test the weld was found to have a strength higher than that of the tube. Appendix B contains the results of the Shear Load experiment.

7.1.3 THE ROUND TUBE MODEL

The model of the round tube is given the same material characteristic as the A-tube. The length of this fin tube is 41 mm. The solids elements that are used to model the tube are 2.5 mm long, and the fin plates of this model are placed at a fin pitch of 2.5 mm. The diameter of the tube is equivalent to the hydraulic diameter d_e of an elliptical tube. The calculations of the hydraulic diameter are given in Appendix F. This equivalent hydraulic diameter is used to establish a similar flow pattern that would exist inside a round tube as it exists inside an elliptical tube. In other words a round tube with a diameter d_e will have the same flow pattern as the elliptical tube with given dimensions in Appendix F. The geometry of the fin plate of the round tube is round unlike that of an elliptical tube which are rectangular.

Table 7.1 The Material Specifications of A-and F-tube.

Material	A-tube	F-tube
Tube material	ASTM A214	St 37 DIN 1629
Tube-sheet	BS1501-151-430A	BS1501-151-430A
Fin-material	Type T54 (T/A) [ISCOR specs]	EN 10139

7.2 DISCUSSION AND ANALYSIS OF FINITE ELEMENT MODEL RESULTS.

1. Figure 7.1 and 7.2 show the distribution of stress in the F-tube with fins, and without fins respectively, when subjected to an internal pressure load of 0.2 MPa. In these two models a maximum (Solid Equivalent) stress difference of 8.36 MPa exists, with the F-tube without fins registering a high of 21.24 MPa . As expected the deformation of the F-tube without fins is higher.

   Figure 7.3 and 7.2 shows the distribution of stress when F-tubes with fins and those without fins are subjected to a bending moment of 9.15 Nm respectively. In comparing the two models, one notices there is not much difference in the magnitudes of maximum (Solid Equivalent) stress. This observation agrees with the results of the Bending Load experiment of section 6.2.

2. In investigating the effects of variation of fin pitch with pressure, figure 7.5 and 7.6 show models of the A-tubes with a 4.3 mm fin pitch and the A-tubes with a 2.5 mm fin pitch subjected to an internal pressure load of 0.2 MPa, respectively. This variation of stress with the change in fin pitch is clearly significant on the tube core, especially at the points of contact of the tube core with the tube-sheet plate, along the major axis of an ellipse. This observation is also made in the Pressure Load experiment.

   A 4.3 mm fin pitched A-tube has less resistance to internal pressure load compared with the 2.5 mm fin pitch tube. This is due to the fact that the 4.3 mm fin pitch tube has less fins per unit length compared to a 2.5 mm fin pitch tube. Under the above internal pressure load, the maximum registered (Solid Equivalent) stress on the tube core with a 4.3 mm fin pitch is 89.25 MPa, whilst the A-tube with a 2.5 mm fin pitch registers a low of 72.97 MPa.

This observation agrees with the experimental results of the Pressure Load experiment of section 6.3, where the highest stress was found to occur on the A-tube with a 4.3 mm fin pitch.

3. When a round tube (whose diameter is equivalent to a hydraulic diameter of an elliptical tube) was model (figure 7.7) and the results, when subjected to an internal pressure, compared with those of the A-tube with a 2.5 mm fin pitch (figure 7.6), it was observed that the maximum (Solid Equivalent) stress on the round tube is lower.

   The difference in stress between the two tubes is due to the fact that the deformation of the tube is caused by a force and not by a pressure load, with the former being proportional to the internal area of the tube.

$$F \alpha A \qquad 7.3$$

   where:

   F = force that causes the deformation of the tube $[N]$

   A = internal area of the tube $[m^{-2}]$

   So, to cause the same deformation (on the round and elliptical tubes) the force on the round tube will have to be higher than that on an elliptical tube. This can be achieved ,*inter alia* , by increasing the internal pressure in the round tube.

   Therefore, keeping all else equal, the round tube (with a diameter equivalent to a hydraulic diameter of an elliptical tube) can withstand a higher pressure load than an elliptical tube. Using the same argument as above, it is true then to suggest that, keeping all else equal, the F-tubes carry higher internal pressure loads than A-tubes for the same deformation.

4. Figure 7.8 to 7.10 shows a complete model of a tube-to-tube-sheet assembly under the maximum design pressure load viz.
   a) F-tube with a 3.0 mm fin pitch to a pressure load of 3.65 MPa
   b) A-tube with a 2.5 mm fin pitch to a pressure load of 1.17 MPa
   c) A-tube with a 4.3 mm fin pitch to a pressure load of 0.73 MPa

   These tubes are able to withstand the maximum design pressure limits given by the manufacturer without any significant deformation or failure. This deformations being of the order 0.6 mm and 0.1 mm for the A-and the F-tube respectively.

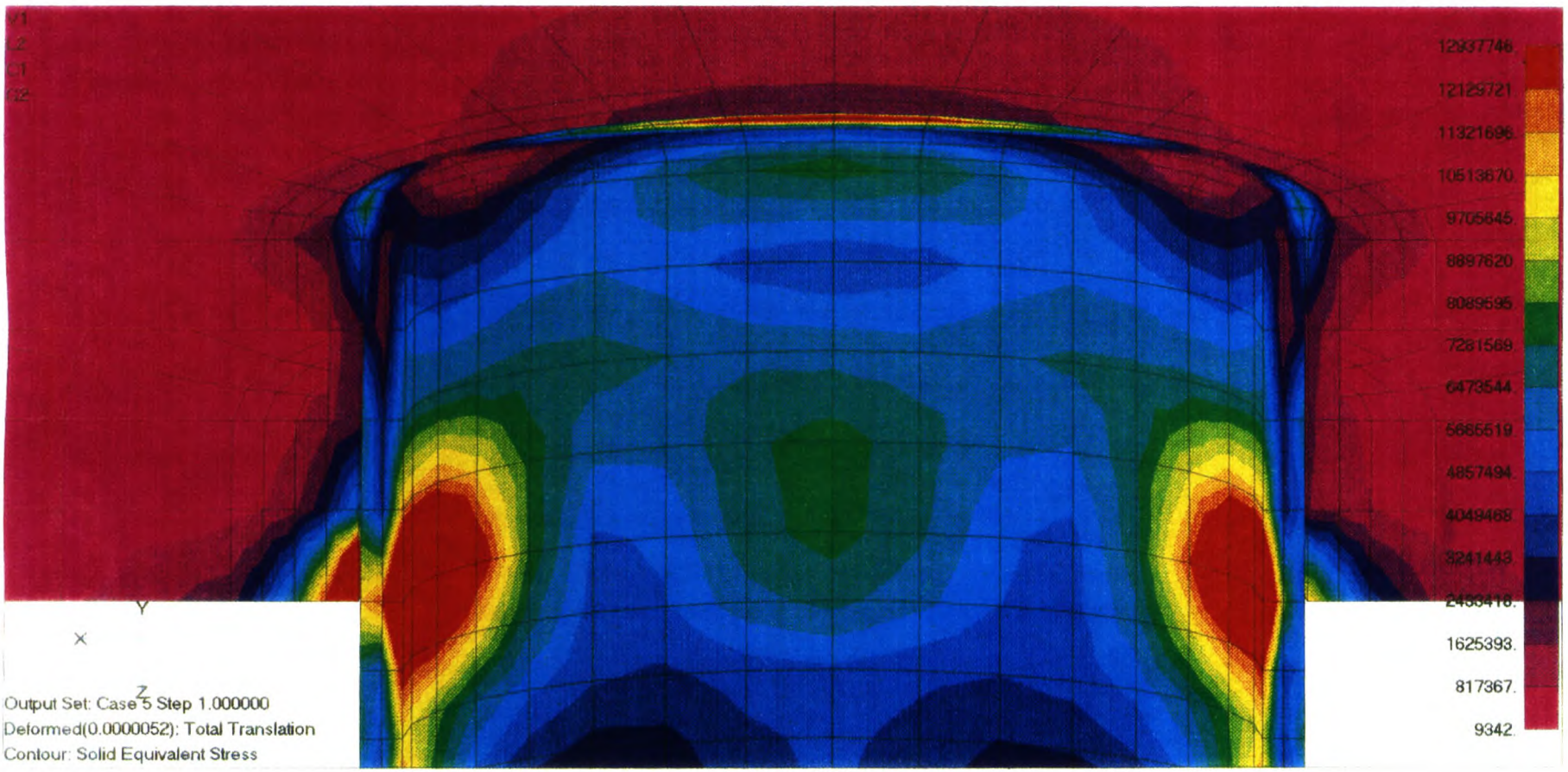

FIGURE 7.1. F-TUBE (WITH FINS) UNDER AN INTERNAL PRESSURE LOAD OF 0.2 MPa.

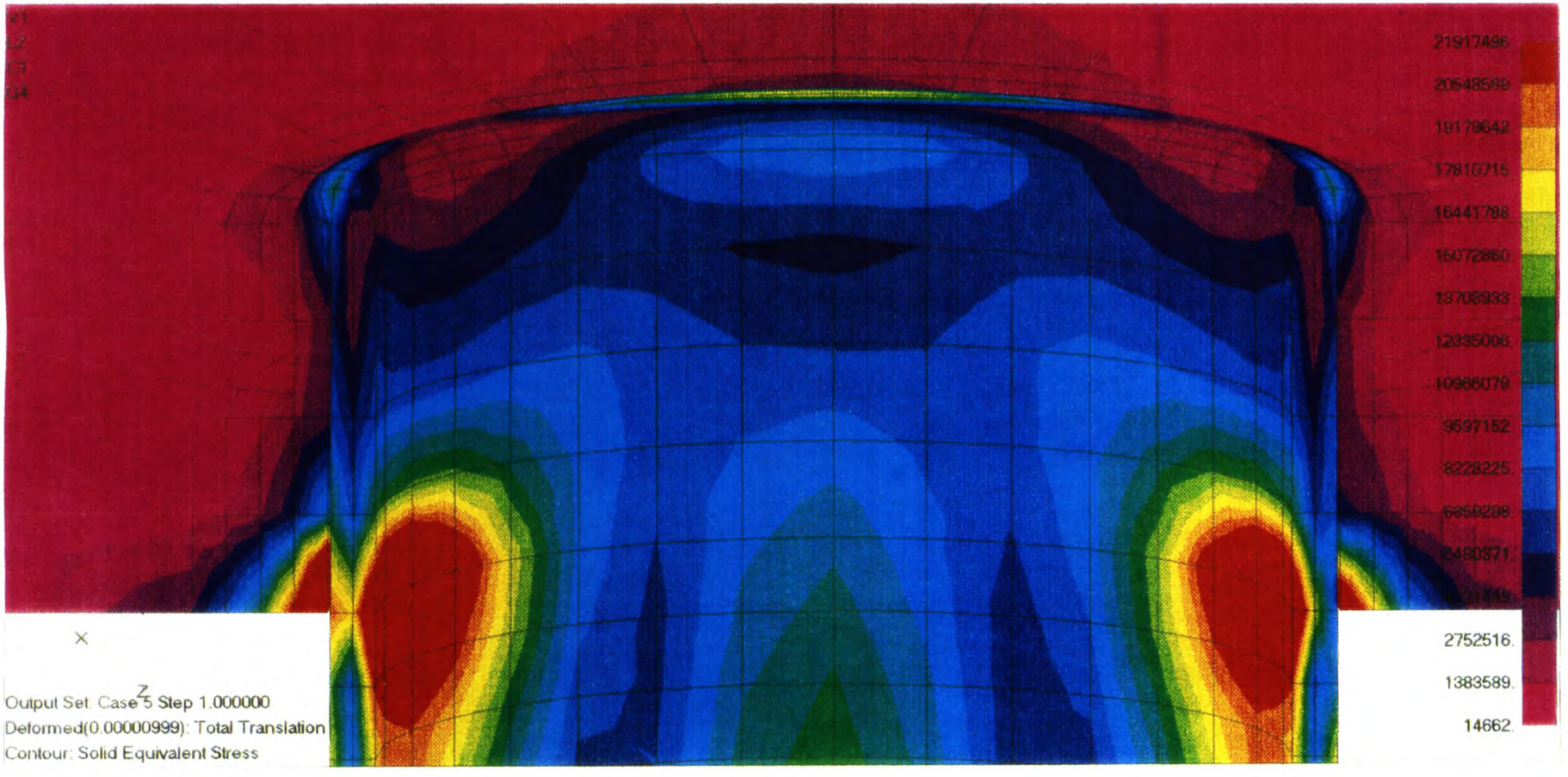

FIGURE 7.2. F-TUBE (WITHOUT FINS) UNDER AN INTERNAL PRESSURE LOAD OF 0.2 MPa.

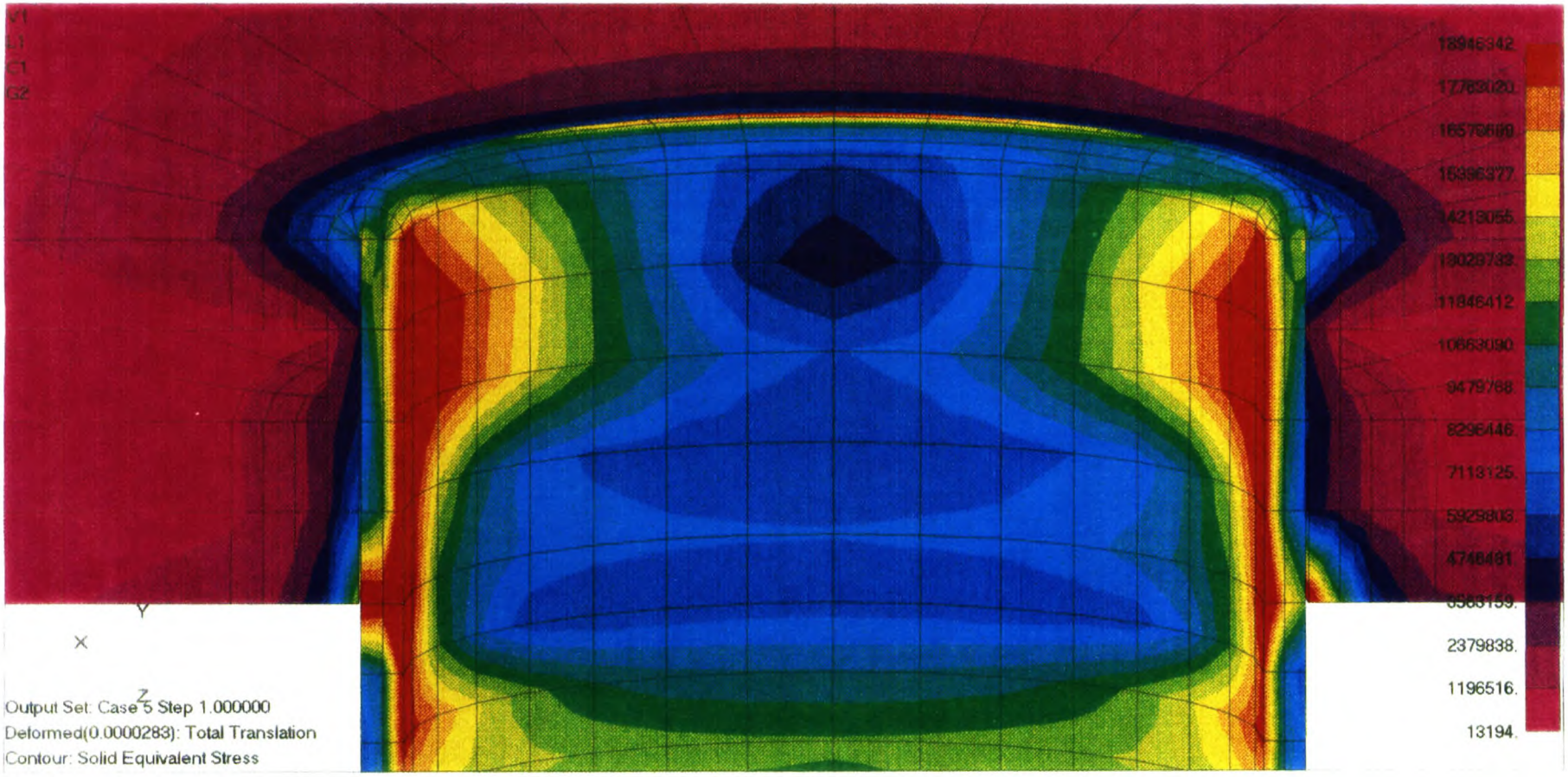

FIGURE 7.3. F-TUBE (WITH FINS) UNDER A BENDING MOMENT LOAD OF 9.15 Nm.

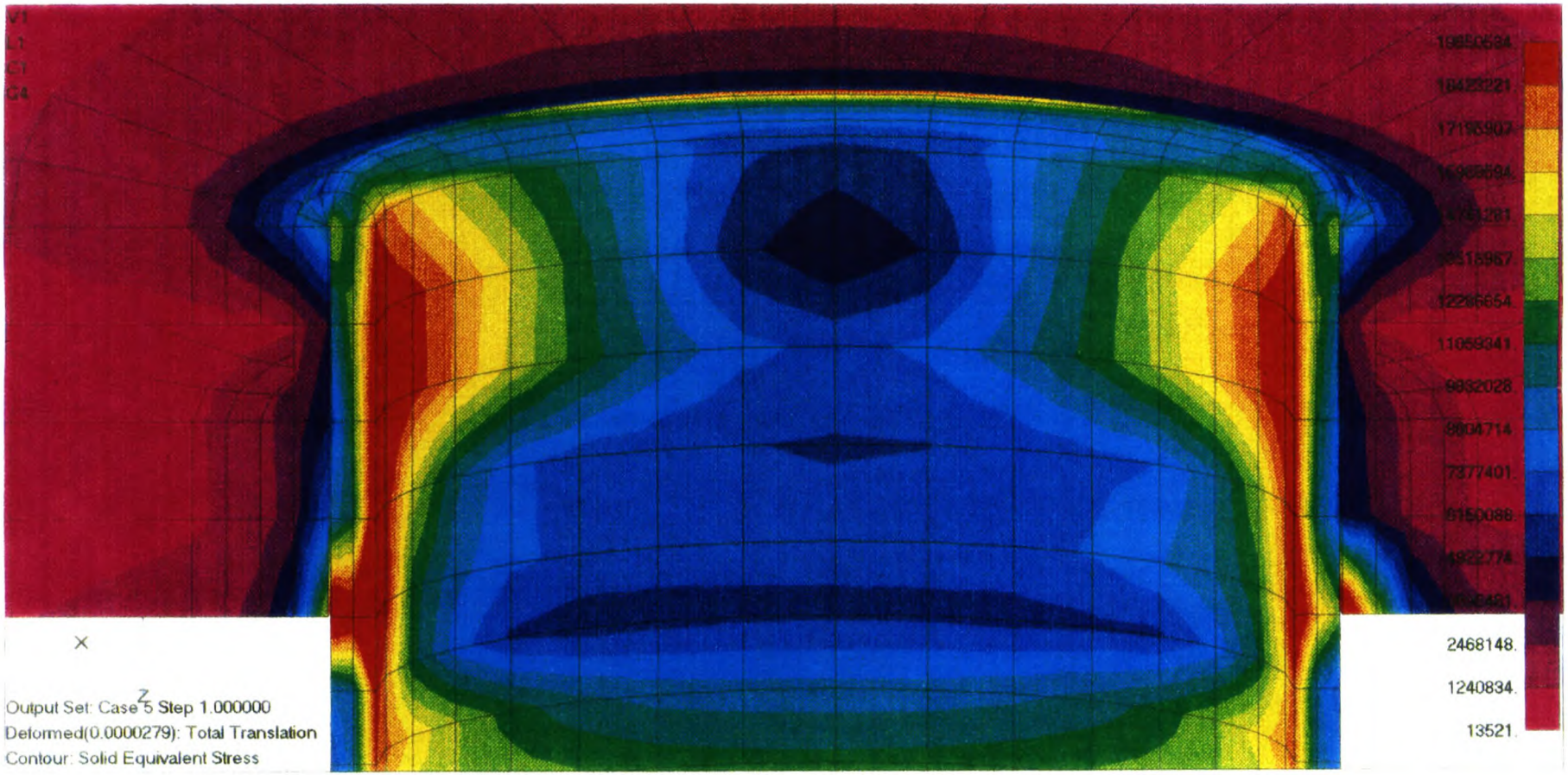

FIGURE 7.4. F-TUBE (WITHOUT FINS) UNDER A BENDING MOMENT LOAD OF 9.15 Nm.

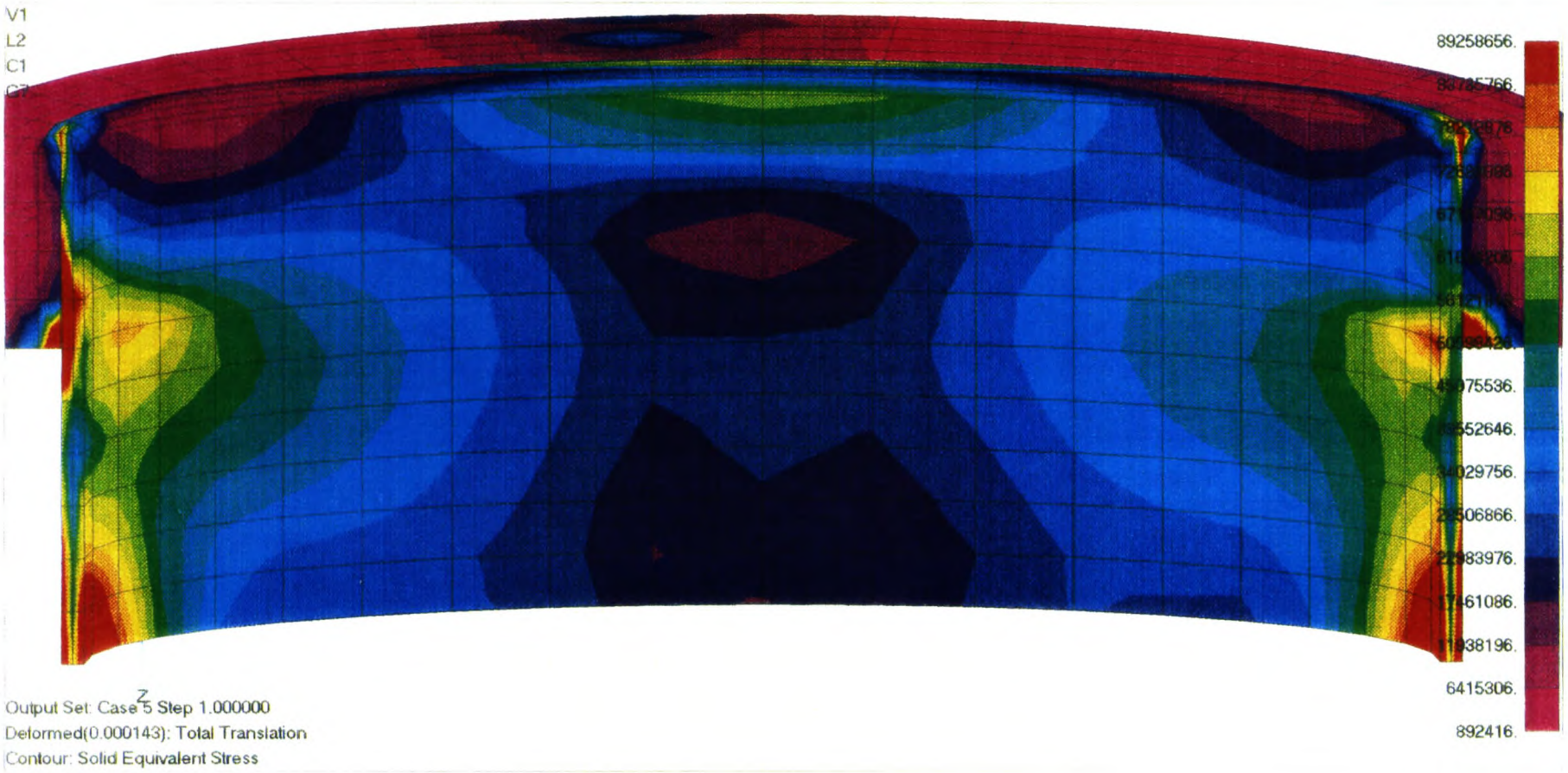

FIGURE 7.5. A-TUBE WITH A 4.3 MM FIN PITCH UNDER AN INTERNAL PRESSURE LOAD OF 0.2 MPa

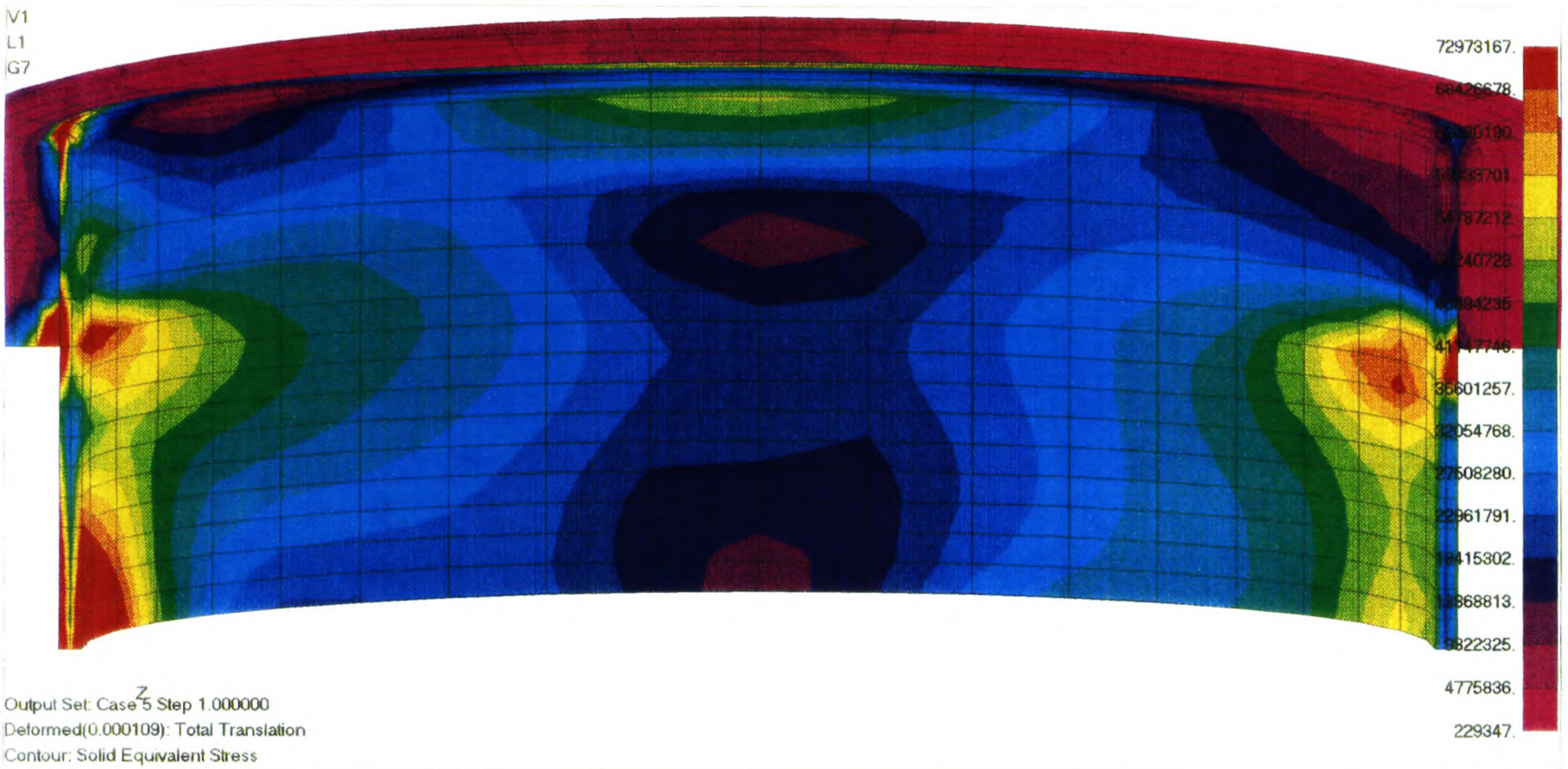

FIGURE 7.6. A-TUBE WITH A 2.5 MM FIN PITCH UNDER AN INTERNAL PRESSURE LOAD OF 0.2 MPa.

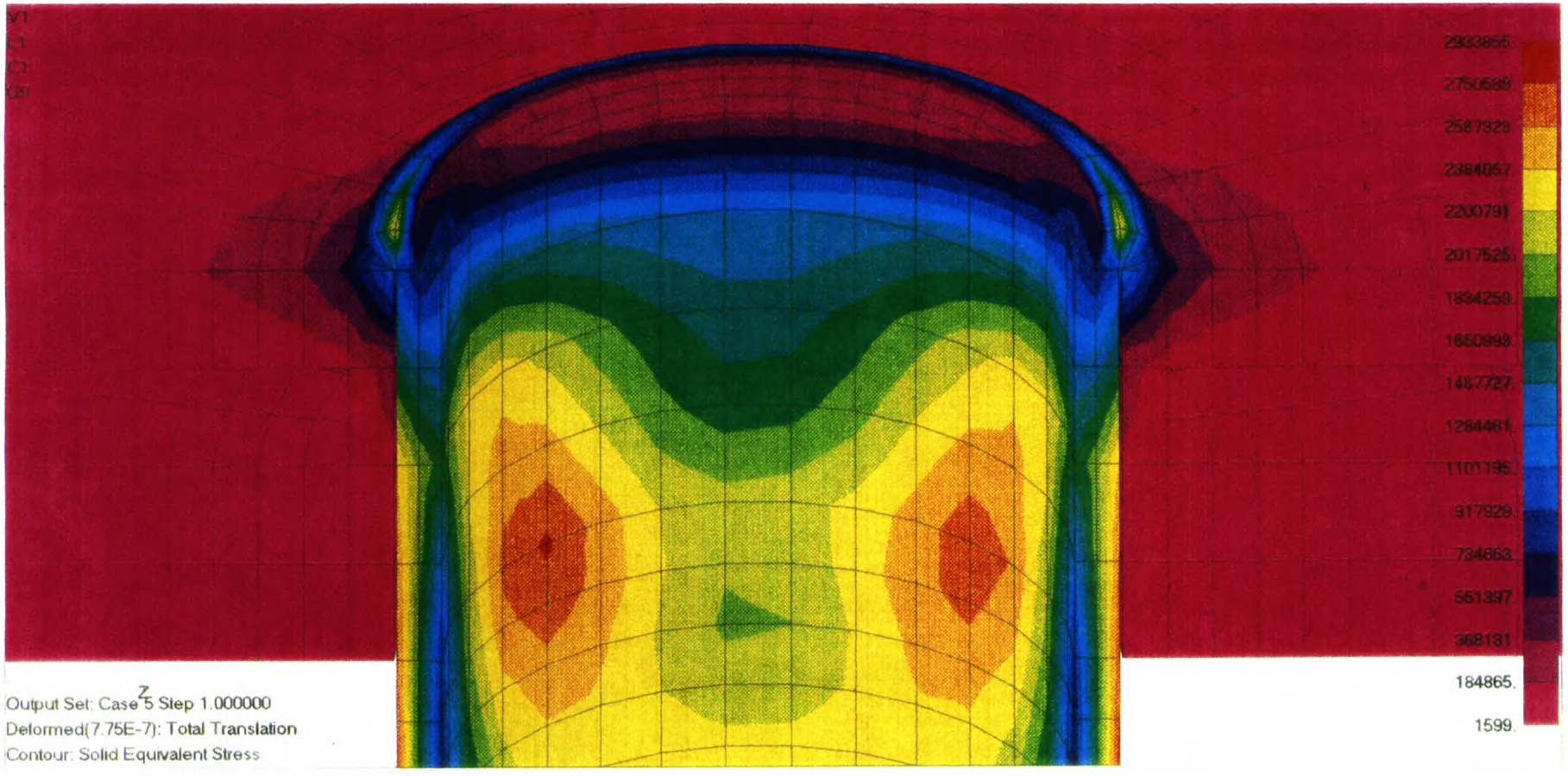

FIGURE 7.7. A ROUND TUBE WITH A FIN PITCH OF 2.5 MM UNDER AN INTERNAL PRESSURE LOAD OF 0.2 MPa.

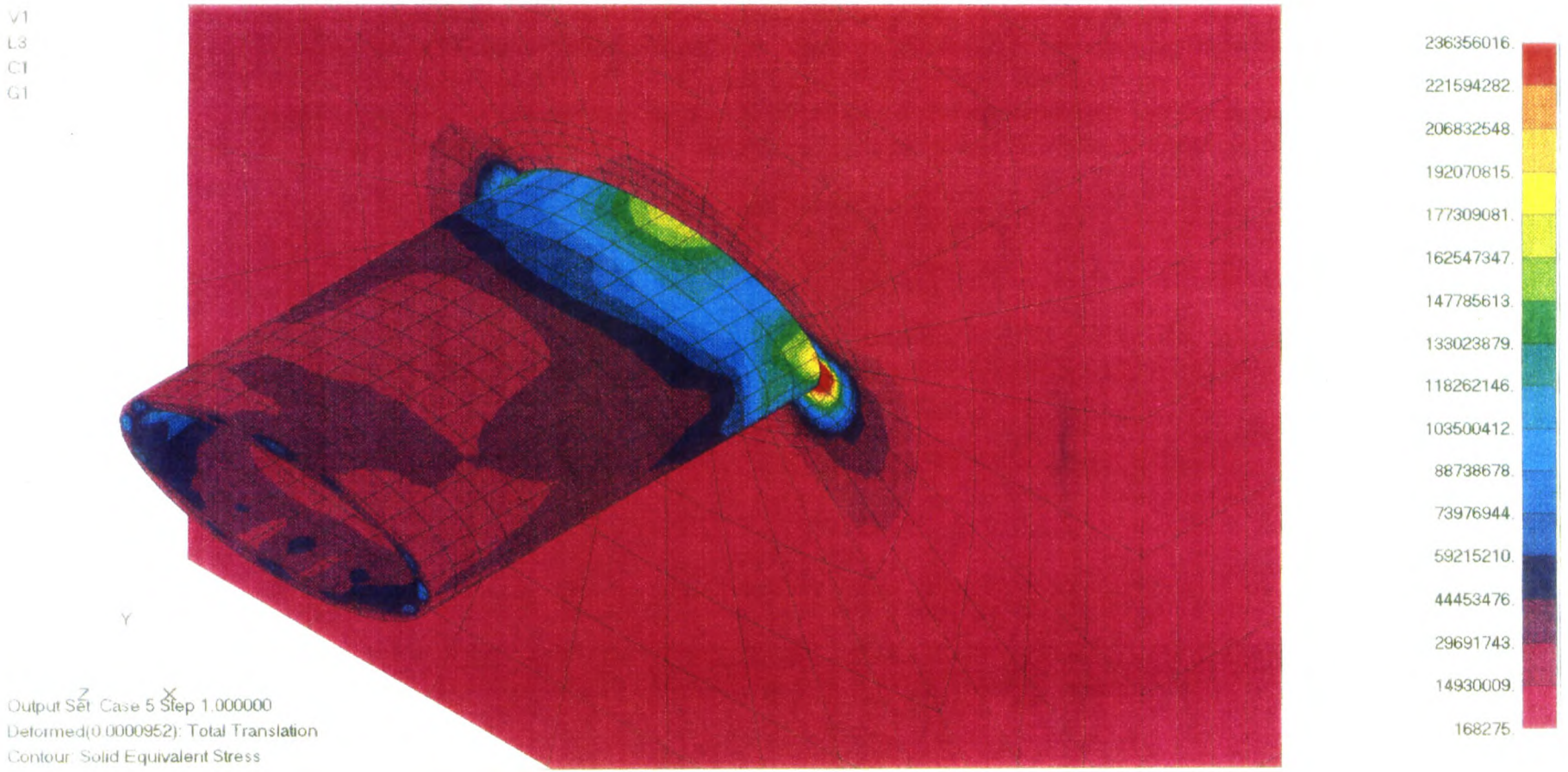

FIGURE 7.8. F-TUBE WITH A 2.5 MM FIN PITCH UNDER A DESIGN PRESSURE LIMIT OF 3.65 MPa.

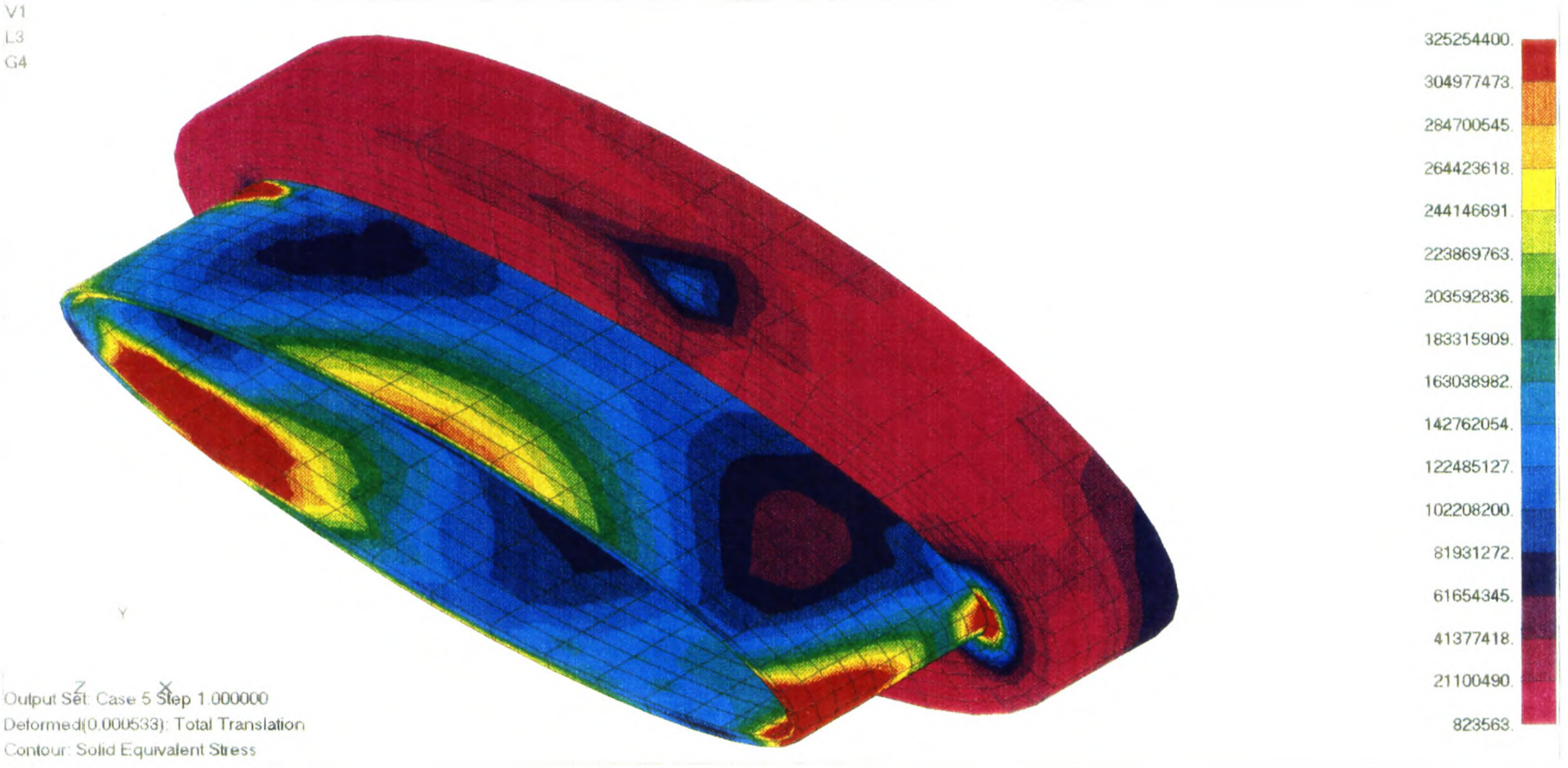

FIGURE 7.9. A-TUBE WITH 2.5 MM FIN PITCH UNDER A DESIGN PRESSURE LIMIT OF 1.17 MPa.

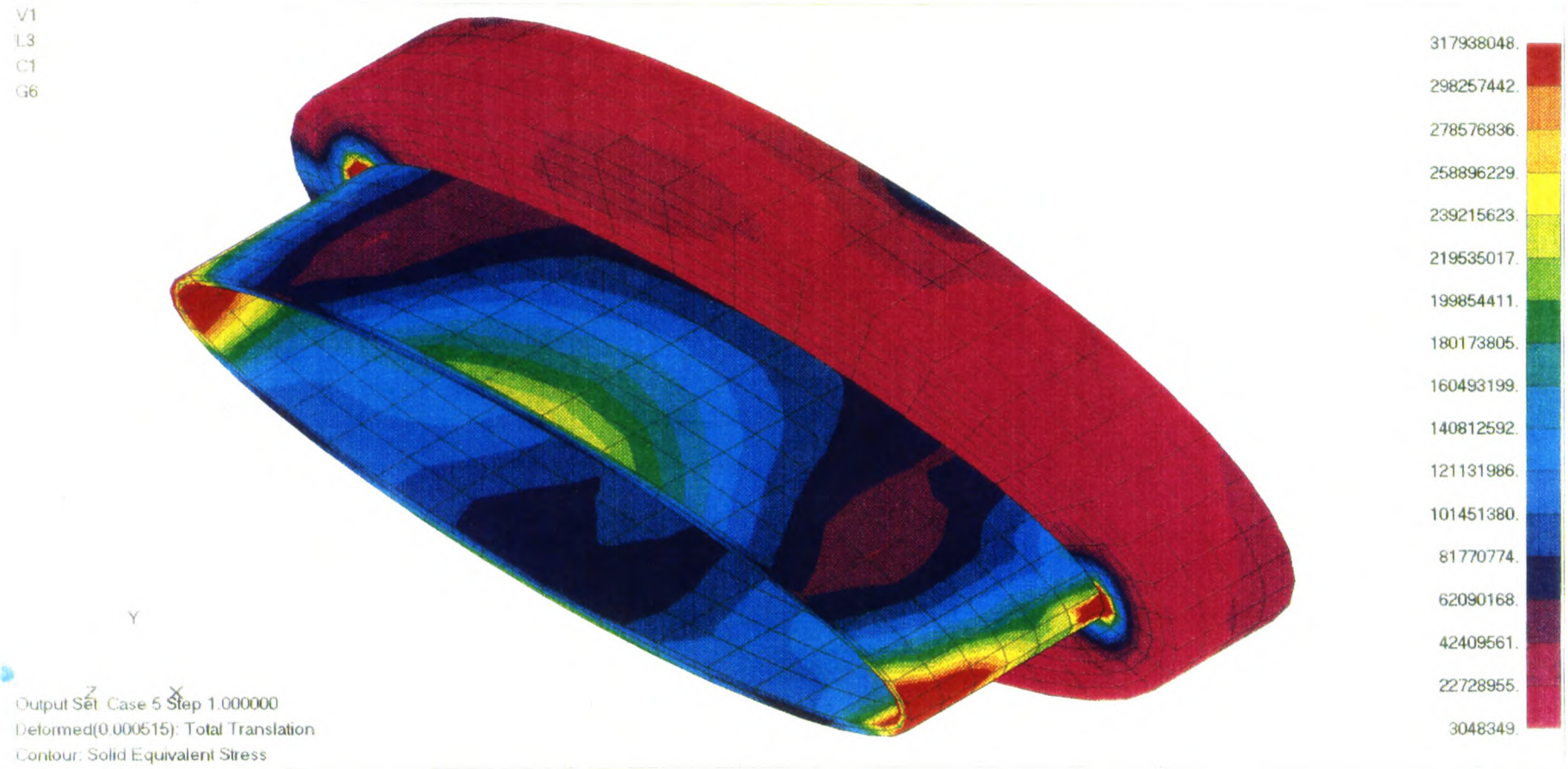

FIGURE 7.10. A-TUBE WITH A 4.3 MM FIN PITCH UNDER A DESIGN PRESSURE LIMIT OF 0.73 MPa.

7.3 CONCLUSIONS

Based on the discussion of the results, the following conclusions are drawn:

1. The effects of fins on the tube structure is to resist or decrease the volumetric expansion of the tube due to an internal pressure load. These same fins do not have any significant resistance to the bending of the tube, and a tube with fins and a tube without fins will experience more or less the same bending stress.
2. High stresses are concentrated on the tube core, especially along the major axis of the ellipse. These stresses increase in the direction from the minor to the major axis especially at the points of contact of the tube core with the tube sheet plate.
3. The fewer the number of fins per unit length the lesser the resistance to internal pressure load. The A-tube with a 4.3 mm fin pitch has less resistance to internal pressure load than a tube, of the same type, with a 2.5 mm fin pitch.
4. Round tubes whose diameter are equivalent to a hydraulic diameter of an elliptical tube can withstand more pressure load than the elliptical tubes from which they have been derived.
5. The maximum design pressure limits suggested by the manufacturer are correct and are absorbed by the tube without any failure. Therefore the maximum design pressure limits on the tubes are indeed:

Table 7.3. The maximum design pressure limits of the fin tubes

Tube type	Design pressure limit
F-tube with a 3.0 mm fin pitch	3.65 MPa
A-tube with a 2.5 mm fin pitch	1.17 MPa
A-tube with a 4.3 mm fin pitch	0.73 MPa

8. ANALYSIS OF THERMAL STRESSES AND EFFECTS OF VIBRATION ON THE TUBE BUNDLE

The objective of this finite element analysis is to investigate the effects of thermal load on the tube-sheet of the tube bundle. To successfully meet this objective the following finite element investigations will be made:

1. Investigate the distribution of thermal stress in a tube-sheet of the tube bundle when all the tubes are kept at maximum temperature of 120 °C, whilst the tube-sheet plates are kept at 20 °C . Under these loading conditions the thermal stress, when all the flanges of the tube bundle are pinned down, is compared with the thermal stress distribution, when only those flanges that are perpendicular to the tubes are pinned down.
2. A less conservative investigation is when there is a temperature gradient from one tube row to the next. In this investigation the first row (closest to the flanges) is kept at 120 °C whilst the second row is kept at 105 °C, the third at 95 °C and the fourth at 85 °C. Also here the same comparison as above is made.

In the analysis of vibration effects of the tube bundle, the objective is to find the natural frequency of the tube and their corresponding mode shapes. Also it is important to establish the frequency of the forcing function i.e. frequency of the fan that will induce vibration and to ensure that it does not come close to the natural frequency of the tube bundle.

8.1 CREATING THE MODEL

The tube bundle model is created using both plates and beam elements. Only half of the tube bundle is modelled because of the symmetry of the tube bundle. Figure G1 in Appendix G shows a heat exchanger bundle. A 240 mm x 235 mm x 250 mm box is modelled by plate elements. These plate elements are 16 mm thick. Axial symmetric constraints are applied where the 'cuts' are made. The flanges on which the constraints will be placed are also modelled using plate elements.

There are 4 rows of tubes and these tubes are modelled using beam elements. Each tube is modelled by 19 beam elements. There are 4 A-tubes in each row. Along each flange 9 equally spaced constraints are placed.

In the determination of the natural frequency of the tube, a 470 mm A-tube is modelled using 20 beam elements. These beam elements are modelled in a way that ensures that the mass of the tube and its contents (process fluid) are included.

In the structural dynamic analysis of the tube bundle, a complete tube bundle is modelled using plate elements. Modelling a 240 mm x 470 mm x 500 mm tube bundle as an axial symmetric structure, in structural dynamic analysis, will result in the omission of modes of vibration that are unsymmetrical **[14CO]**. This tube bundle is constrained on the flanges, that are modelled by plate elements, as in the analysis of thermal stresses.

8.2 DISCUSSION OF RESULTS

1. Figure 8.1 shows a distribution of stress due to a thermal load when all the tubes were placed at a constant temperature of 120 °C. This figure 8.1 shows a concentration of high thermal stresses in the first row i.e. the row that is closest to the flanges. This high thermal stress concentration is also evident in all other models (figure 8.2; 8.3; 8.4) and is due to the fact that the constraints on the flanges are close to this row. In other words the tubes in this row experience more resistance to their expansion, due to thermal load, than anywhere else in this tube bundle. More so is the tube in the corner right in the first row.

   When one removes the constraints on the flanges that are parallel to the tube, as shown in figure 8.2 and 8.4, the stress remain concentrated in the first row, but at higher order of magnitude than when there were constraints on all flanges (as in figure 8.1 and 8.3). This increase in thermal stress is due to the fact that the resistance to deformation of the plate is increased and is concentrated on only the flanges that are pinned down. In other words the deformation of the tube is increased when only the flanges that are perpendicular to the tube are pinned down. This is the premise of thermal stresses i.e. an increase in resistance to deformation results in an increase in thermal stress. Appendix G shows a sample calculation for the approximation of thermal stresses on the tube-sheet of the tube bundle.

2. Appendix H shows a sample calculation for the determination of natural frequency and mode shapes for a 470 mm A-tube clamped on both sides. These calculations agree with a finite element analysis and table 8.1 below shows these results.

Table 8.1. Natural frequency of the tube and the corresponding modes.

Modes	I.	II.	III.	IV.	V.
Freq.	(Hz)	(Hz)	(Hz)	(Hz)	(Hz)
FEM	323.53	891.81	1748.23	2889.50	4315.1
Calculation	323.50	892.34	1748.33	2890.58	4318.1

Figure 8.5 shows the first mode shape of the tube and other modes are shown in appendix H. Also shown in appendix H are the natural frequencies of the A-tube with a 2.5 mm fin pitch.

When the entire A- tube bundle is analysed, the natural frequency of the structure is reduced due to an increase in mass. Figure 8.6 shows the stress distribution on the bundle when it is vibrating at its fundamental frequency. Vibration at this frequency results in the concentration of stress along the edge corner and on the plates that are on the sides that are perpendicular to the tubes. The frequency of the subsequent modes of vibration remain relatively constant as seen in table 8.2 below, but the stress varies with each mode as seen in figure 8.7

Table 8.2. Natural frequency of the tube bundle for each mode of vibration.

Modes	I.	II.	III.	IV.	V.
Freq. (Hz)	286.52	286.52	286.52	286.52	286.52

The most likely source of vibration is the fan. To ensure that the fan does not induce vibration to the structure (tube bundle), the frequency, ω, of the forcing function $F = F_o \cos(\omega t)$ must not be close to the natural frequency of the tube bundle for each mode. If the fan has N number of blades, then frequencies that contribute to the total forcing function are those that are multiples of the number of blades **[21BR]**. If for example the fan has four blades then the forcing function will have a frequency of 4ω, 8ω, 12ω, ..., etc.

Also according to API standards **[22AP]** it is important that the natural frequency of the fan not to be within 20 % of the blade pass frequency. Where the blade pass frequency is equal to the number of blades times the angular speed of the fan.

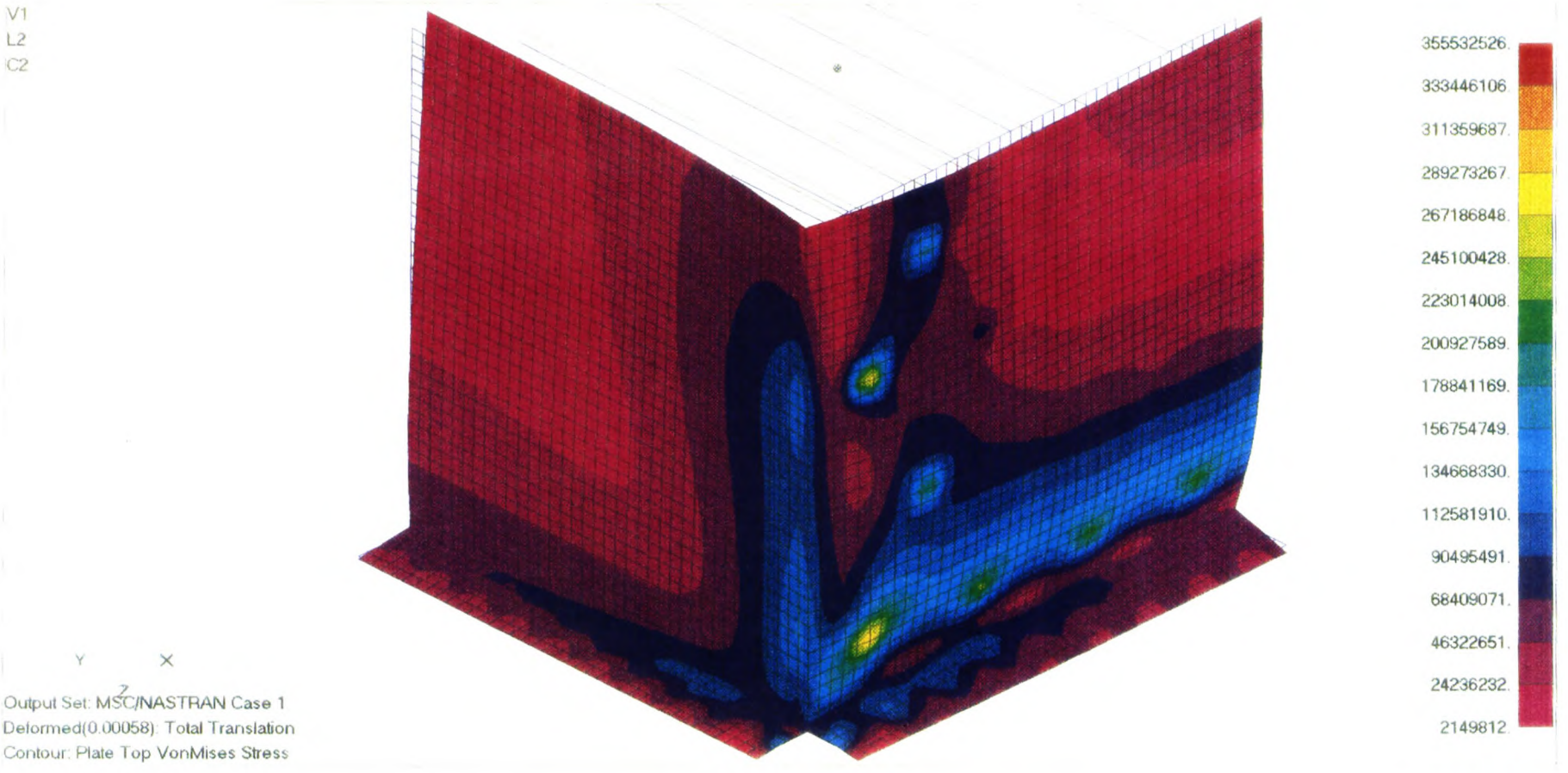

FIGURE 8.1. THERMAL STRESS DISTRIBUTION WHEN THE TUBE BUNDLE IS FIXED ALL AROUND.

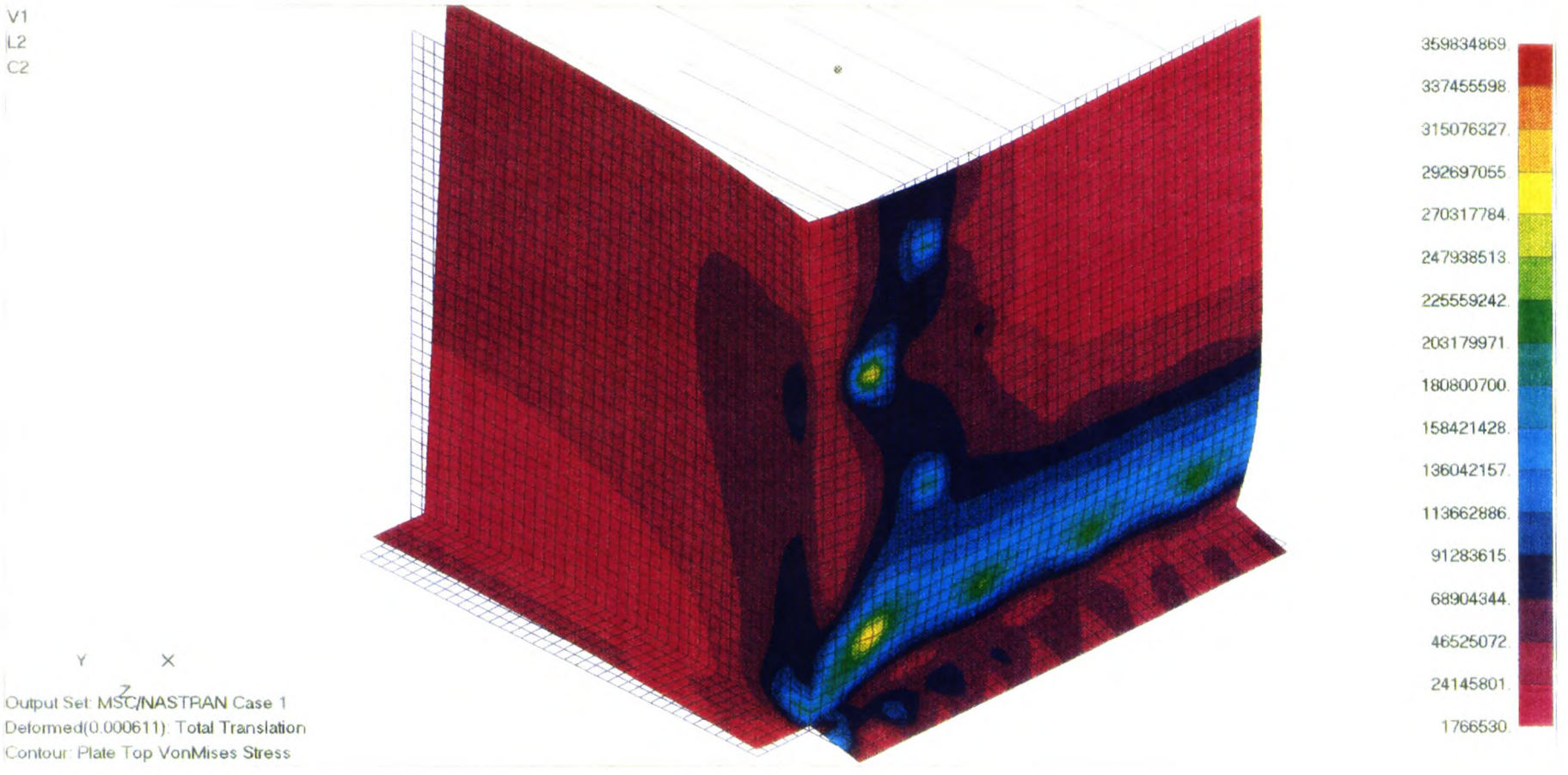

FIGURE 8.2. THERMAL STRESS DISTRIBUTION WHEN ONLY THE SIDES PERPENDICULAR TO THE TUBES ARE FIXED.

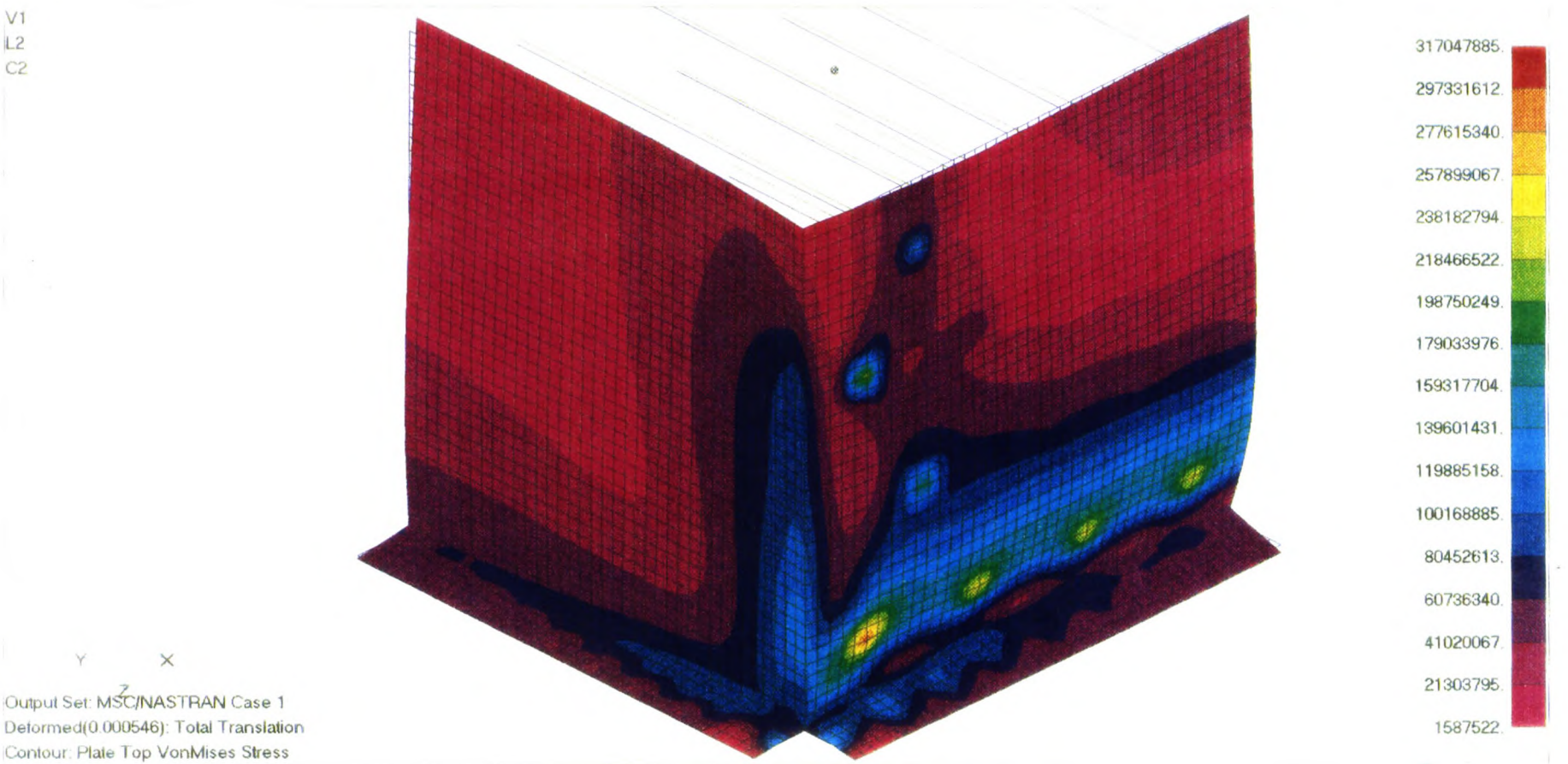

FIGURE 8.3. THERMAL STRESS DISTRIBUTION WHEN THE TUBE BUNDLE IS FIXED ALL AROUND.

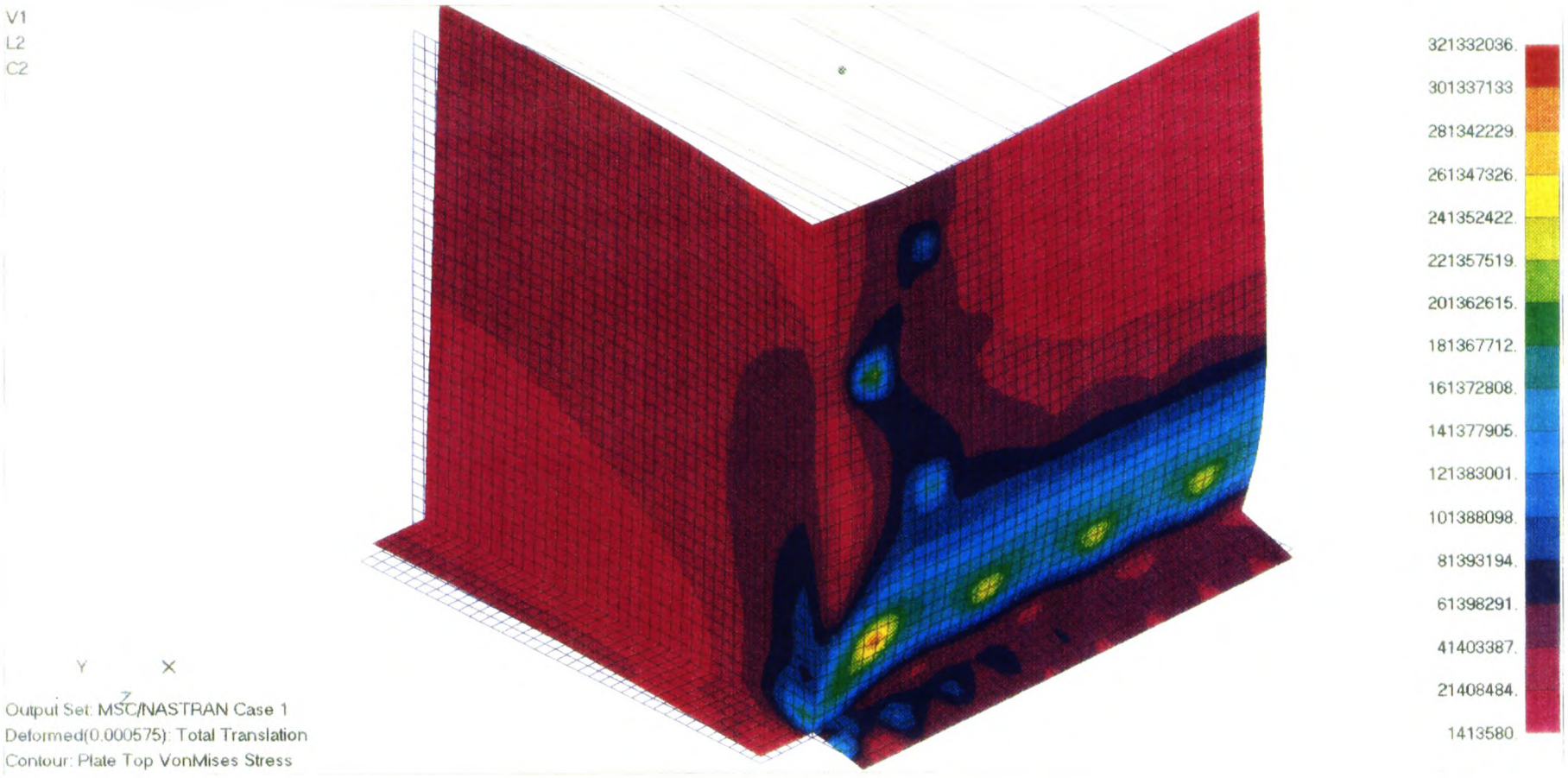

FIGURE 8.4. THERMAL STRESS DISTRIBUTION WHEN ONLY THE SIDES THAT ARE PERPENDICULAR TO THE TUBES ARE FIXED.

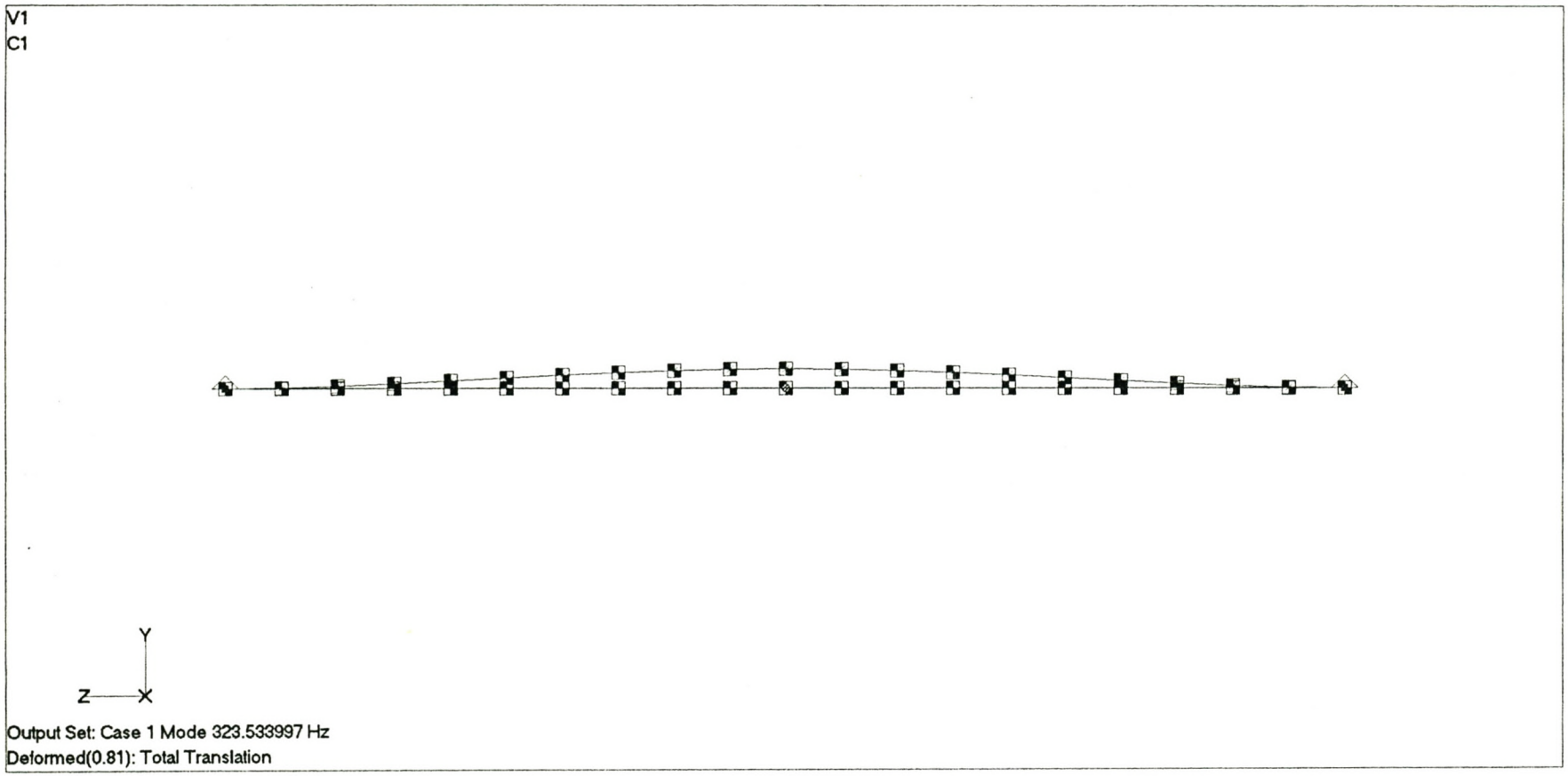

FIGURE 8.5. STRUCTURAL DYNAMIC ANALYSIS FOR THE FIRST MODE OF VIBRATION.

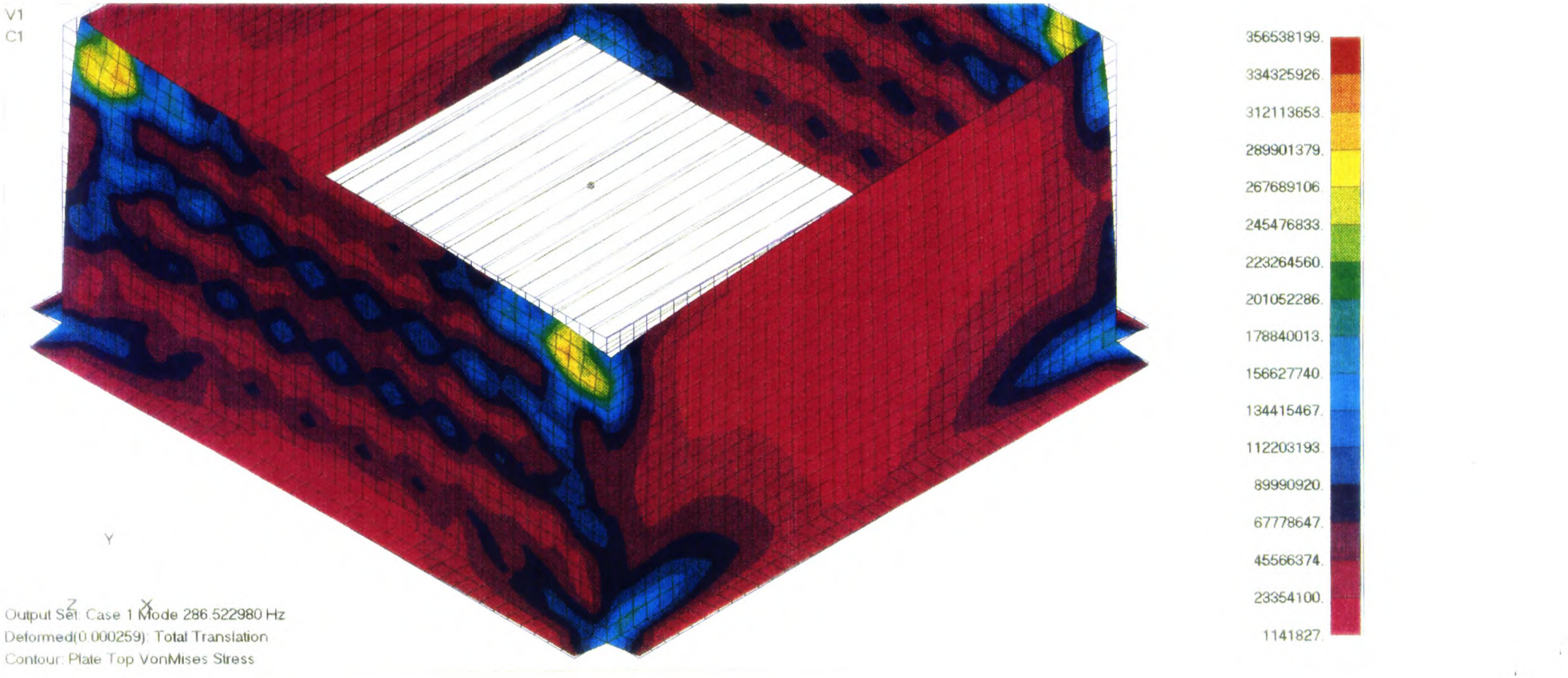

FIGURE 8.6. STRESS DISTRIBUTION ON THE BUNDLE WHEN VIBRATING WITH THE FUNDAMENTAL FREQUENCY.

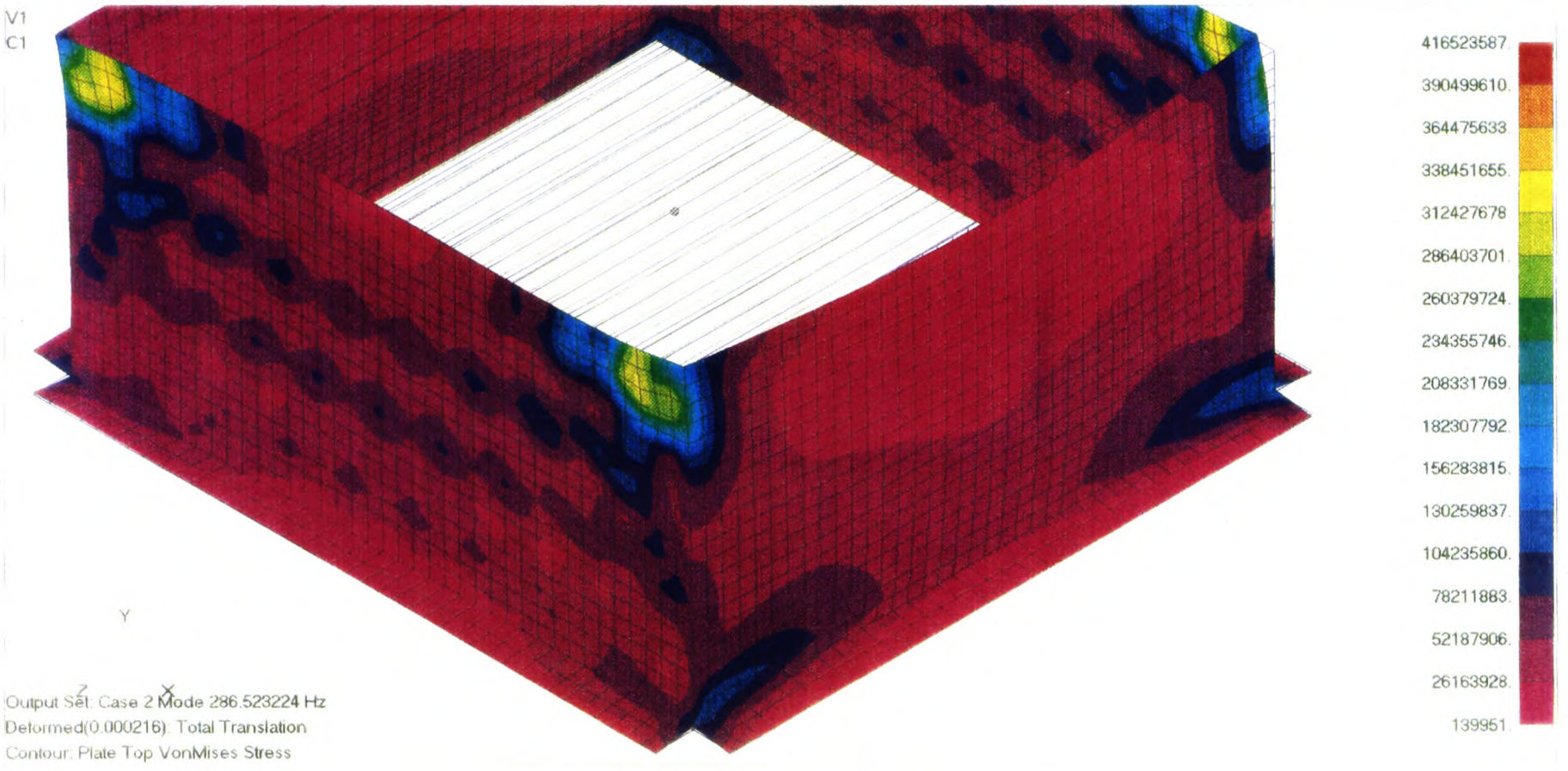

FIGURE 8.7. STRESS DISTRIBUTION ON THE BUNDLE WHEN VIBRATING WITH THE SECOND MODAL FREQUENCY

8.3 CONCLUSIONS

Based on the discussions of the results the following conclusions are drawn:

1. Thermal stresses on the tube bundle are highly concentrated on the first row i.e. the row that is closest to the flanges or to the constraints. These thermal stresses are reduced when there is a temperature gradient between each row (as is the case in real life).

   The first tube in the first row (counting from either side) experiences more thermal stresses than any other tube anywhere in the bundle. Constraining the tube bundle on only sides that are perpendicular to the tube length, increases the thermal stress on the tube bundle.

2. In the design of tube bundle structures care must be taken not to induce vibration. Having decided on the type of fan to be used, it is important that the frequency of the forcing function, , not to be close to the natural frequency of the tube bundle.

   For rigid structures like tube bundle, the natural frequency for each mode of vibration will remain constant but the stress induced varies with each modal frequency. Stresses induced by vibration (especially during resonance) are concentrated along edge corners and on the plates that are parallel to the tube length. Note also that these stress values have no meaning, and only their relative magnitude in relation to each mode of vibration should be considered.

   It is important that the fan itself remain stable and no vibration should be induced by its rotation.

9. RECOMMENDATIONS

Based on the conclusions drawn from Experimental and Numerical Investigations, the following recommendations are made:

1. A minimum axial load 59.25 kN and 98.33 kN must not be subjected to F-tubes and A-tubes respectively.
2. The maximum allowable axial load (according to ASME codes')on the tubes must be 12.67 kN and 20.89 kN for the F- and the A-tubes respectively.
3. The maximum internal pressures that the tubes should be subjected to are:
   - F-tube with a 3.0 mm fin pitch – 3.65 MPa
   - A-tube with a 2.5 mm fin pitch – 1.17 MPa
   - A-tube with a 4.3 mm fin pitch – 0.73 MPa
4. In cases where the expected internal pressure are going to be high, the use of round tubes or the F-tubes must be considered.
5. The tube bundle must be pinned (bolted) down on all sides and not only on the sides that are perpendicular to the tube length.
6. Provision for the expansion of the tube must always be made, both for the volumetric expansion due to internal pressure loads and the longitudinal expansion due to thermal loads.
7. The fan must always be checked for stability and should not induce vibrations. Always ensure that the natural frequency of the tube bundle structure is not equal to for each mode of vibration. In case where some form of vibration is experienced, structural dampers must be used.

10. REFERENCES

[1WH] :White, Frank M," *Viscous Fluid Flow, Second edition.*", McGraw-Hill, New York, 1991.

[2GE] :Gerlach, C. R., Dodge, F.T., "An Engineering Approach to Flow Induced Vibration.", *"Flow Induced Vibration in Heat Exchangers."* ASME Technical Committee on Unfired Heat Transfer Equipment, pp 88 New York, 1979.

[3NE] :Nelms, H.A., "An Engineering Approach to Flow Induced Vibration.", "*Flow Induced Vibration: A Problem in the Design of Heat Exchangers for Nuclear Service.*", Design Council, British Standard Institute, Oxford University Press,1979.

[4OS] :Osborne, W.C., "*The Selection and Use Of Fans.*"

[5ER] :Erskine, J.B., Hensman N., "Vibration and Noise in Pumps, Fans and Compressors.", "*Vibration Induced by Pump Instability and Surging.*"

[6WA] :Walker, G.,"*Industrial Heat exchangers: A Working Guide.*" ,Hemisphere, Washington D.C.,1982.

[7SP] :Spencer, J., Tooth, A.S., "*Pressure Vessel Design : Concepts and Principles.*", Spon, London,1994.

[8TI :Timoshenko, S.P., Goodier, J.N., "*Theory of Elasticity, Third Edition.*" McGraw-Hill, New York1970.

[9HA] :Harvey, John F., "*Theory and Design of Modern Pressure Vessels, Second Edition..*", Van Nostrand Reinhold, New York,1974.

[10YO] :Yokell, Stanley, "*A Working Guide to Shell and Tube Heat Exchangers.*" McGraw-Hill, New York, 1990.

[11AS] :ASME Code's Appendix A Section Viii, Division 1,"*Basis for Establishing Allowable Loads for Tube-to-tube-sheet joints.*" , ASME, July 1998.

[12GO] :Goodier J.N., Schoessow G.J, "*The Holding Power and Hydraulic Tightness of Expanded Tubes: Analysis of Stress and Deformation.*", Trans., ASME, July 1943.

[13HU] :Huebner K.H., Thorton A.E., "*Finite Elements for Engineers, Second*

Edition..", John Wiley and Sons, New York,1982.

[14CO] :Cook, R.D., Malkus, D.S., Plesha, M.E., "*Concepts and Application of Finite Element Analysis, Third Edition* ." John Wiley and Sons, New York, 1989.

[15Gè] :Gèrdin, M., Rixen, D., "*Mechanical Vibrations , Theory and Application to Structural Dynamic.*" John Wiley and Sons, New York, 1994.

[16DA] :Dally, J.W., Riley, W.F., "*Experimental Stress Analysis, Second Edition.*", McGraw-Hill, New York,1978.

[17KR] :Kröger, D.G., "*Air Cooled Heat Exchangers and Cooling Towers, Thermal Flow Performance and Design.*" Stellenbosch University, Stellenbosch, 1998.

[18 MS] :MSC/ Nastran for Windows, Version 2.1, Vol. 1 and Vol. 2.

[19ÇE] :Çengel, Y.A., Boles, M.A., "*Thermodynamics an Engineering Approach, Second Edition* ", McGraw-Hill, New York, 1994.

[20CH] :Church , Austin H., "*Mechanical Vibrations, Second Edition.*", John Wiley and Sons, New York, 1964.

[21BR] :Bramwell, A.R.S., "Helicopter Dynamics.", Anorld London, 1976.

[22AP] :API Standard 661, "*Air Cooled Heat Exchangers for General Refinery Service, Third Edition.*", American Petroleum Institute, Washington,1992.

APPENDIX A

Figure A.1 Apparatus used in the Shear Load Experiment. A) Tube-to-tube-sheet assembly B)Tensile machine, C) Data processor

APPENDIX B

CALCULATIONS FOR THE DETERMINATION OF THE JOINT EFFICIENCY AND THE MAXIMUM ALLOWABLE LOAD.

Table B.1. Material specifications of the core tube of the A and F-tubes at room temperature.

Material Specs.	Tube Type	Min. Tensile Strength	Min. Yield Strength	Max. Allowable Stress
		$St\ (MPa)$	$Sy\ (MPa)$	$Sa\ (MPa)$
ASME'S (SA214)	A	324	179	69
DIN 1626 (St 37)	F	362	235	86

From the three Shear Load tests conducted the load (L_{test}) that caused failure is:

Table B.2. Results of the Shear Load test.

Test no.	L_{test} (kN)	deviation (s) from the mean
1	98.36	0.025
2	98.36	0.025
3	98.31	0.025

Figure B.1 graphically illustrates the Force vs. Displacement curve of the A-tube during the experiment.

Where $S^2 = (x_i - \bar{x})^2$ B.1

From ASME code's Section Viii ,Division 1, the load (L_{test}) to be used must be 2 X S.

L_{test} = 98.33 kN

Table B.3 The dimension of the F-and A-tubes.

Tube Type	Major axis	Minor axis	Thickness	Crss. Area
	a (mm)	b (mm)	t (mm)	A_t (mm)^2
A-tube	50	10	1.6	293.5
F-tube	18	7	1.6	117.6

Where $A_t = \pi \times a \times b$ B.2

Calculation for the joint efficiency (fr_{test}) for the A-tube.

$$fr_{test} = \frac{L_{test}}{St \times A_t} \quad \text{B.3}$$

$$= \frac{98.33 \times 10^3}{324 \times 10^6 \times 293.5 \times 10^{-6}}$$

= 103 %.

This means that the weld can withstand more than the minimum Tensile Load of the A-tube (95.09 kN) before failure occurs.

If the smallest load to cause failure of the weld is 98. 33 kN and the efficiency of the weld is 103 %, then the maximum allowable load ($L_{\max}$) under ASME code [SEC VIII D1 NMA APP A,1998] can be calculated as follows:

Calculation for the maximum allowable load (L_{max}) for the A-tube.

$$L_{max} = A_t \times S_a \times fr_{test} \qquad \text{B.4}$$

$$= 293.5 \times 10^{-6} \times 69 \times 10^{6} \times 1.03$$

$$= 20.86 \times 10^{3} N$$

=20.86 kN

For the safe operation of the A-tube the maximum allowable axial load (L_{max}) on the weld under ASME codes is 20.86 kN.

Calculation for the joint efficiency (fr_{test}) for the F-tubes.

Table B.4. Results of the Shear Load test.

Test no.	L_{test} (kN)	Standard deviation (s)
1	59.23	0.02
2	59.27	0.02

Figure B.2 show a Force vs. Displacement curve for the F-tube.
Using the mean value of L_{test} to calculate the efficiency of the weld.

L_{test} = 59.25 kN

$$fr_{test} = \frac{L_{test}}{St \times A_t} \qquad \text{B.3}$$

$$= \frac{59.25 \times 10^{3}}{362 \times 10^{6} \times 117.6 \times 10^{-6}}$$

= 139 %.

This means that the weld is able to withstand a load 39 % more than the minimum Tensile Load (42.57 kN) of the F-tube before failure occurs.

If the smallest load to cause failure in the weld is 59.25 kN and the efficiency of the welds 139 %, then the maximum allowable load ($L_{\max}$) by ASME code [SEC VIII D1 NMA APP A,1998] can be calculated as follows:

Calculation for the maximum allowable load($L_{\max}$) for the F-tubes

$$L_{\max} = A_t \times S_a \times fr_{test} \qquad \text{B.4}$$

$$= 117.6 \times 10^{-6} \times 86 \times 10^{6} \times 1.39$$

$$= 14.55 \times 10^{3} N$$

$$= 14.55 \text{ kN}$$

For the safe operation of the F-tubes, the maximum allowable axial load ($L_{\max}$) on the weld under ASME code [SEC VIII D1 NMA APP A,1998] is 14.55 kN.

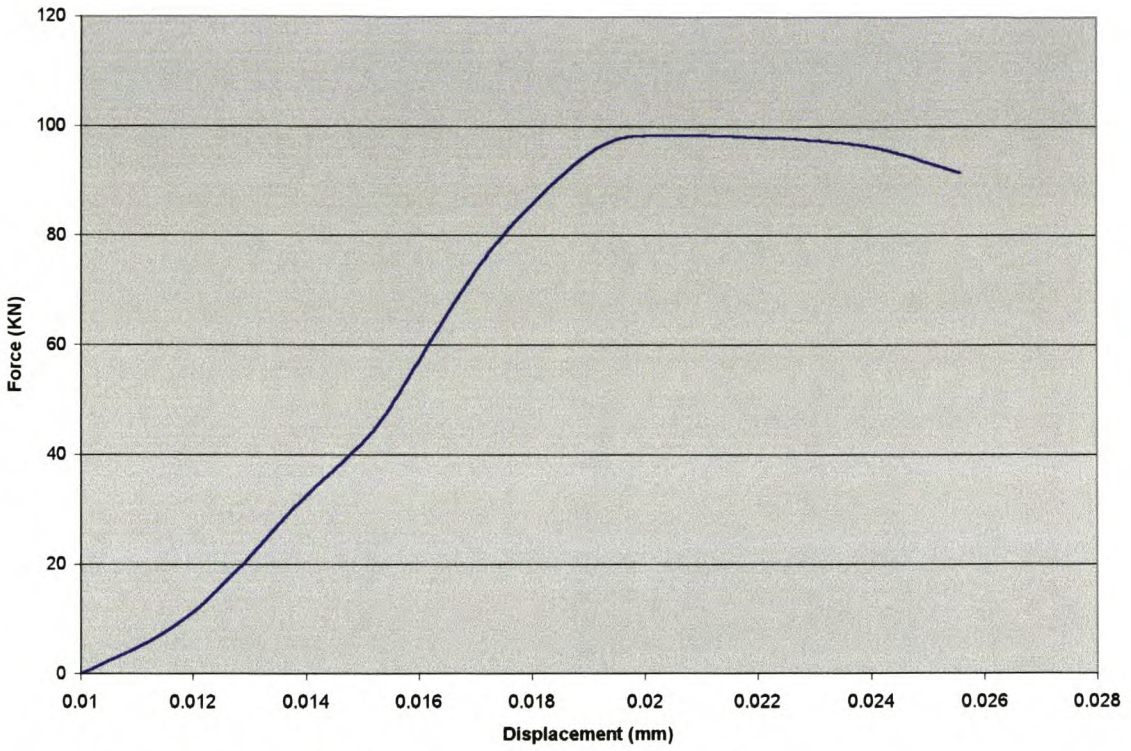

Figure B.1. Results of the Shear Load Test conducted on the A-tube

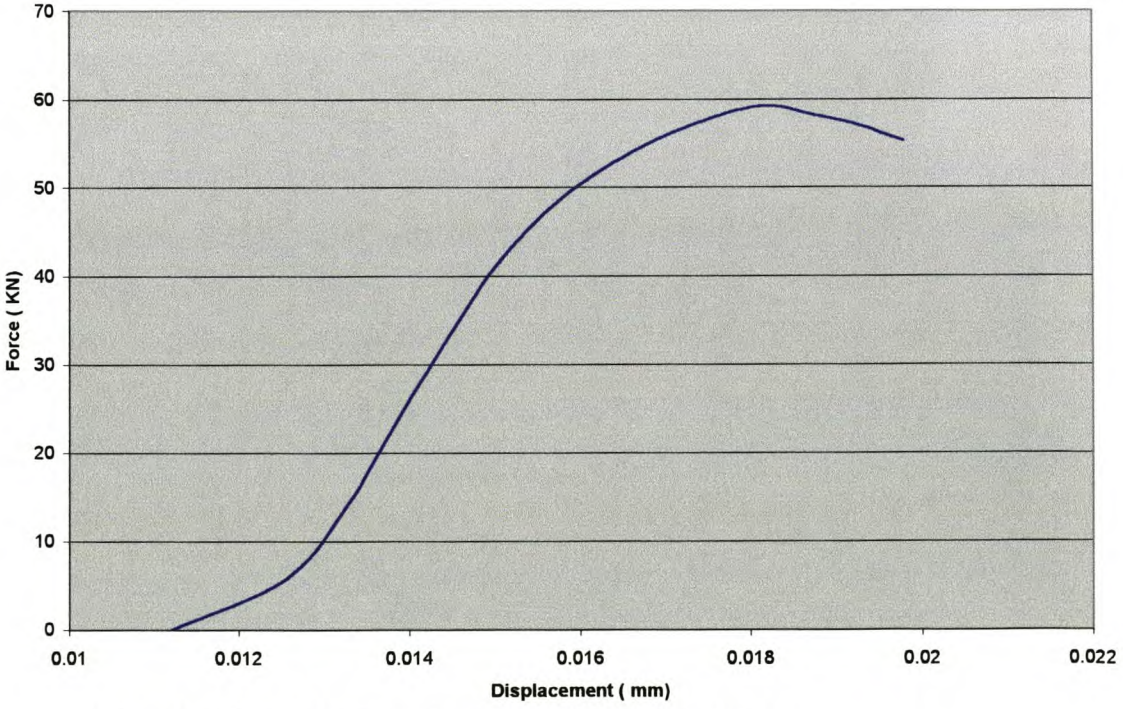

Figure B.2. Results of the Shear Load Test conducted on the F-tube

APPENDIX C

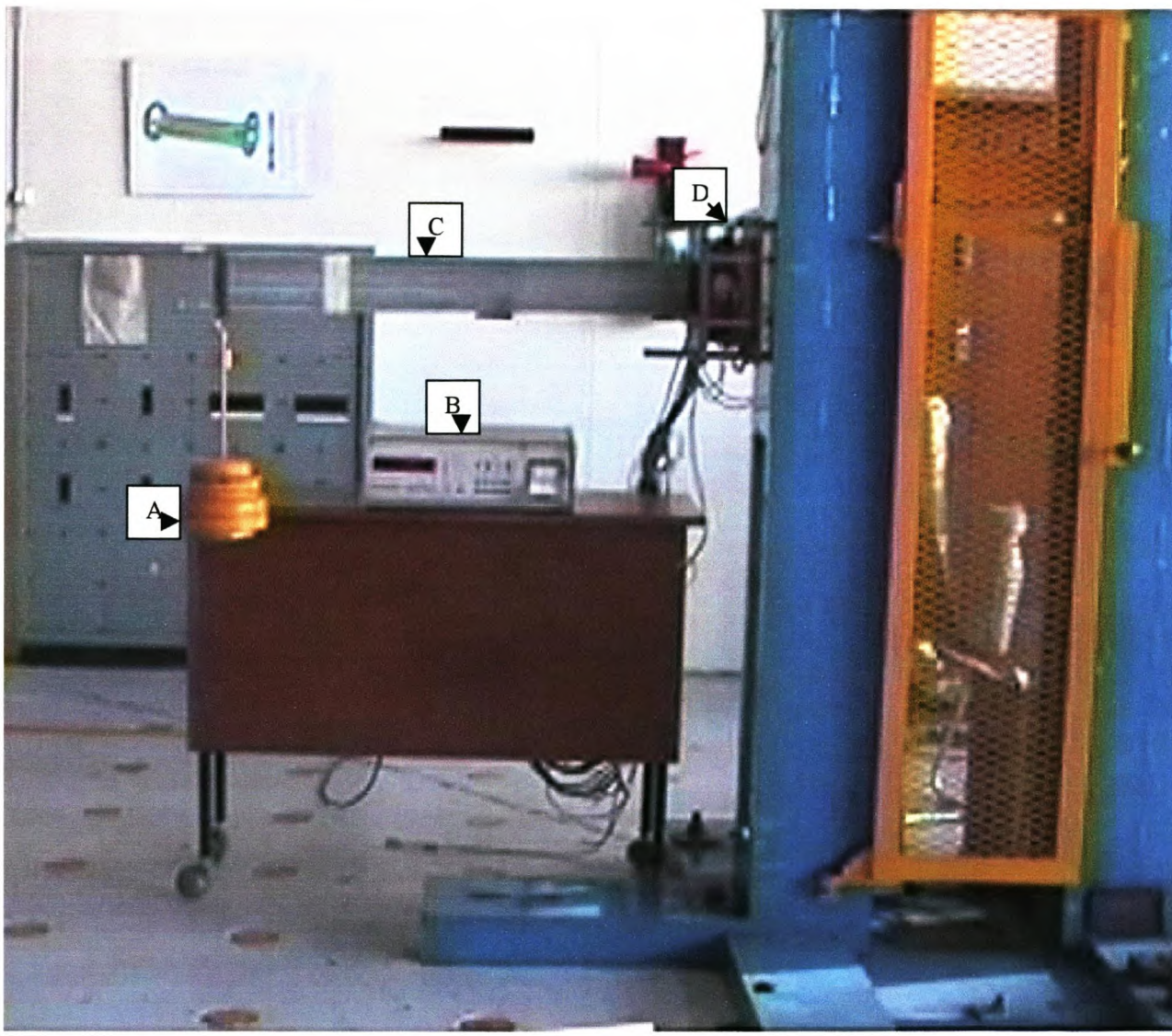

Figure C.1 Apparatus used in the Bending Load Test. (A) Weights, (B) Scanner, (C) Fin tube and (D) Cover plate

APPENDIX D

CALCULATION FOR THE DETERMINATION OF STRESS AT EACH GAUGE POSITION

A three element strain rosette is used. This rosette employs gauges placed at 0º, 45º and 90º positions. These strain gauges are placed at the back of the tube-sheet plate at position shown below.

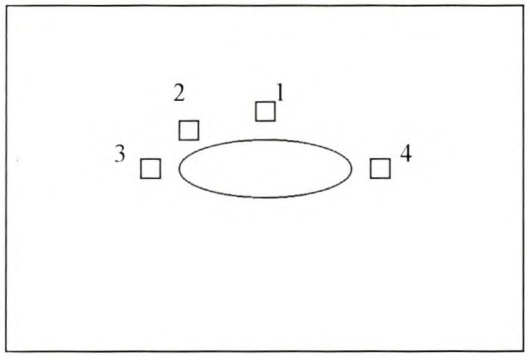

Figure D.1 Tube-sheet plate with strain gauges.

The strain gauge readings are recorded for the bending load placed on the tube. To illustrate the procedure used to calculate the principal stresses, the data for strain gauge 1 at a bending load of 147.7 Nm is used. The length of the tube is 1.0 m.

Test no. :1 Experiment : Bending load Gauge factor: 2.05

Experiment type : 1 Gauge type :EA-06-060RZ-120

Tube type : AE436D with a 4.3 mm fin pitch

Mass (kg)	Strain reading	angle of alignment
15.06	$\varepsilon_A = 64 \times 10^{-6}$	$\theta_A = 0^\circ$
	$\varepsilon_B = -23 \times 10^{-6}$	$\theta_B = 45^\circ$
	$\varepsilon_C = -133 \times 10^{-6}$	$\varepsilon_C = 90^\circ$

The strain field at this gauge position is determined from:

$$\varepsilon_A = \varepsilon_{XX} Cos^2\theta_A + \varepsilon_{YY} Sin^2\theta_A + \gamma_{XY} Sin\theta_A Cos\theta_A \qquad \text{D.1a}$$

$$\varepsilon_B = \varepsilon_{XX} Cos^2\theta_B + \varepsilon_{YY} Sin^2\theta_B + \gamma_{XY} Sin\theta_B Cos\theta_B \qquad \text{D.1b}$$

$$\varepsilon_C = \varepsilon_{XX} Cos^2\theta_C + \varepsilon_{YY} Sin^2\theta_C + \gamma_{XY} Sin\theta_C Cos\theta_C \qquad \text{D.1c}$$

Substitute these values in the above equations and simultaneously solve for:

ε_{XX} , ε_{YY} and γ_{XY} .

The solution for the strain field at this gauge position is:

$$\varepsilon_{XX} = 64 \times 10^{-6}$$

$$\varepsilon_{YY} = -133 \times 10^{-6}$$

$$\gamma_{XY} = 23 \times 10^{-6}$$

Because of the thickness of the tube-sheet plate (16 mm), the determination of the stress at any point on the plate can be done by assuming a plane stress problem, i.e. $\sigma_Z, \tau_{XZ} and \tau_{YZ} = 0$. From this assumption the stress distribution at any point on the plate can be determined from the following equation.

$$\sigma_X = \frac{(\varepsilon_{XX} + \nu\varepsilon_{YY})E}{1-\nu^2} \qquad \text{D.2a}$$

$$\sigma_Y = \frac{(\varepsilon_{YY} + \nu\varepsilon_{XX})E}{1-\nu^2} \qquad \text{D.2b}$$

$$\tau_{XY} = \frac{\gamma_{XY} E}{2(1+\nu)} \qquad \text{D.2c}$$

Substituting in the above equations $E = 206 \times 10^9 \ Nm^{-2}$ and $\nu = 0.33$. The resulting stress components are:

$$\sigma_X = 4.69MPa$$
$$\sigma_Y = -25.86MPa$$
$$\tau_{XY} = 1.78MPa$$

The principal stresses at this gauge position can be obtained directly from the strain readings.

$$\sigma_1 = E\left[\frac{\varepsilon_A + \varepsilon_C}{2(1-\nu)} + \frac{1}{2(1+\nu)}\sqrt{(\varepsilon_A - \varepsilon_C)^2 + (2\varepsilon_B - \varepsilon_A - \varepsilon_C)^2}\right] \qquad \text{D.3a}$$

$$\sigma_1 = 206 \times 10^3\left[\frac{64-133}{2(1-0.33)} + \frac{1}{2(1+0.33)}\sqrt{(64+133)^2 + (-2\times 23 - 64 + 133)^2}\right]$$

$$\sigma_1 = 4.75MPa$$

$$\sigma_2 = E\left[\frac{\varepsilon_A + \varepsilon_C}{2(1-\nu)} - \frac{1}{2(1+\nu)}\sqrt{(\varepsilon_A - \varepsilon_C)^2 + (2\varepsilon_B - \varepsilon_A - \varepsilon_C)^2}\right] \qquad \text{D.3b}$$

$$\sigma_2 = 206 \times 10^3\left[\frac{64-133}{2(1-0.33)} - \frac{1}{2(1+0.33)}\sqrt{(64+133)^2 + (-2\times 23 - 64 + 133)^2}\right]$$

$$\sigma_2 = -25.97MPa$$

and the maximum shear stress is given by:

$$\tau_{\max 1} = E\left[\frac{1}{2(1+\nu)}\sqrt{(\varepsilon_A - \varepsilon_C)^2 + (2\varepsilon_B - \varepsilon_A - \varepsilon_C)^2}\right] \qquad \text{D.3c}$$

$$\tau_{\max} = 206 \times 10^3\left[\frac{1}{2(1+0.33)}\sqrt{(64+133)^2 + (-2\times 23 - 64 + 133)^2}\right]$$

$\tau_{max} = 15.36MPa$

The table below shows some of the strain readings obtained during the conduction of this experiment.

Table D.1 The Strain reading ($\times 10^{-6}\, m$)at each gauge position.

TEST NO.:8			EXPERIMENT: Bending load				DATE:10 June 99		
			EXPERIMENT TYPE : 1				Gauge factor :2.05		
			TUBE TYPE: AE436D with a 4.3 mm fin pitch				Gauge type:EA-06-060RZ-120		
			strain readings						
mass(kg)	Gauge	2.815	5.09	7.36	10.08	12.355	15.055	17.33	19.61
channel	position								
0	1	9	20	30	43	53	64	73	84
1	1	-3	-7	-11	-15	-18	-23	-27	-30
2	1	-18	-39	-60	-86	-107	-133	-154	-174
3	2	9	19	29	40	49	60	68	78
4	2	17	36	54	77	95	117	134	152
5	2	-8	-16	-26	-37	-47	-60	-69	-78
6	3	-1	-1	-2	-3	-5	-7	-9	-9
7	3	27	56	86	121	149	181	208	236
8	3	2	4	7	9	10	12	13	16
9	4	13	27	41	58	72	87	99	113
10	4	-21	-44	-68	-97	-120	-150	-174	-196
11	4	-10	-23	-35	-50	-64	-79	-91	-102

The results of the Bending and Pressure Load experiment are tabulated below.

Tabular presentation of the Maximum Bending and Shear stress on the tube-sheet plate due to bending of the finned tube in Experiment Type 1.

Table D.2.1 Maximum stress on the plate at each gauge position.

TUBE TYPE : AE436D with a 4.3mm fin pitch

MASS	MAX BENDING STRESS (MPa)				MAX SHEAR STRESS (MPa)			
(kg)	GAUGE 1	GAUGE 2	GAUGE 3	GAUGE 4	GAUGE 1	GAUGE 2	GAUGE 3	GAUGE 4
2.82	0.72	3.03	4.32	4.32	2.10	2.87	4.11	4.11
5.09	1.66	6.45	8.82	8.82	4.59	5.99	8.45	8.45
7.36	2.39	9.64	13.56	13.56	7.00	9.18	12.95	12.95
10.08	3.43	13.59	19.10	19.10	10.04	13.13	18.30	18.30
12.36	4.17	16.66	23.32	23.32	12.47	16.35	22.72	22.72
15.06	4.75	20.37	28.39	28.39	15.36	20.37	27.69	27.69
17.33	5.45	23.22	32.52	32.52	17.84	23.38	31.95	31.95
19.61	6.28	26.46	37.10	37.10	20.12	26.46	36.06	36.06

Table D.2.2 Maximum stress on the plate at each gauge position.

TUBE TYPE : AE510D with a 2.5 mm fin pitch.

MASS	MAX BENDING STRESS (MPa)				MAX SHEAR STRESS(MPa)			
(kg)	GAUGE 1	GAUGE 2	GAUGE 3	GAUGE 4	GAUGE 1	GAUGE 2	GAUGE 3	GAUGE 4
2.82	0.48	3.06	4.34	4.34	2.02	2.60	3.14	3.14
5.09	0.88	6.31	9.32	9.32	4.42	5.70	6.65	6.65
7.36	1.73	9.36	13.82	13.82	6.94	8.75	10.11	10.11
10.08	2.59	13.35	19.89	19.89	9.64	12.43	14.29	14.29
12.36	3.08	16.76	24.93	24.93	12.61	15.38	17.76	17.76
15.06	3.85	20.61	30.67	30.67	15.49	18.91	22.31	22.31
17.33	4.62	23.71	35.56	35.56	18.01	21.86	25.87	25.87
19.61	5.38	26.65	40.08	40.08	20.54	24.95	29.68	29.68

Table D.2.3 Maximum stress on the plate at each gauge position.

TUBE TYPE : F-tube with a 3.0 mm fin pitch

MASS	MAX BENDING STRESS (MPa)				MAX SHEAR (MPa)			
(kg)	GAUGE 1	GAUGE 2	GAUGE 3	GAUGE 4	GAUGE 1	GAUGE 2	GAUGE 3	GAUGE 4
2.82	1.79	2.10	0.68	0.68	2.56	2.56	1.87	1.87
5.09	3.79	4.15	1.45	1.45	5.33	5.22	4.06	4.06
7.36	5.71	6.59	2.27	2.27	8.32	7.98	6.26	6.26
10.08	8.18	9.15	3.27	3.27	11.87	11.45	8.65	8.65
12.36	10.26	11.29	3.46	3.46	14.57	14.21	10.88	10.88
15.06	12.61	14.33	3.46	3.46	17.99	17.56	13.28	13.28

Tabular presentation of the Maximum Bending and Shear stress on the tube sheet plate due to the bending of the finned tube in Experiment Type 2

Table D.2.4 Maximum Stress on the plate at each gauge position.

TUBE TYPE: AE436D with a 4.3 mm fin pitch.

MASS	MAX BENDING STRESS (MPa)				MAX SHEAR STRESS(MPa)			
(kg)	GAUGE 1	GAUGE 2	GAUGE 3	GAUGE 4	GAUGE 1	GAUGE 2	GAUGE 3	GAUGE 4
2.82	0.35	-0.01	0.74	0.89	0.35	0.45	0.49	0.73
5.09	0.74	-0.40	1.49	2.29	0.59	0.83	1.18	1.52
7.36	0.83	-0.83	1.51	2.92	0.83	1.32	1.81	2.30
10.08	1.07	-1.20	2.65	3.95	1.22	1.87	2.60	3.18
12.36	1.56	-1.38	3.34	4.74	1.71	2.46	3.09	3.97
15.06	1.80	-1.87	3.46	5.62	2.11	3.05	3.83	4.85
17.33	1.69	-2.56	4.04	6.46	2.30	3.44	4.41	5.53
19.61	1.93	-3.10	4.53	7.19	2.69	3.97	5.15	6.42

Table D.2.5 Maximum Stress on the plate at each gauge position.

TUBE TYPE : AE510D with a 2.5 mm fin pitch.

MASS	MAX BENDING STRESS (MPa)				MAX SHEAR STRESS(MPa)			
(kg)	GAUGE 1	GAUGE 2	GAUGE 3	GAUGE 4	GAUGE 1	GAUGE 2	GAUGE 3	GAUGE 4
2.82	0.24	-0.27	0.74	1.27	0.39	0.35	0.31	0.35
5.09	3.94	-0.72	1.49	2.18	0.86	0.67	0.64	0.64
7.36	0.88	-1.30	1.51	3.25	1.34	1.01	1.03	7.90
10.08	1.73	-1.57	2.65	4.78	2.04	1.35	1.40	1.10
12.36	2.19	-2.01	3.34	5.71	2.50	1.68	1.82	1.40
15.06	2.98	-2.59	3.46	7.27	3.29	2.02	2.28	1.73
17.33	3.59	-2.64	4.04	8.49	3.90	2.43	2.70	2.04
19.61	4.29	-2.92	4.53	9.79	4.45	2.77	3.01	2.26

Table D.2.6 Maximum Stress on the plate at each gauge position.

TUBE TYPE : F-tube with a 3.0 mm fin. pitch

MASS	MAX BENDING STRESS (MPa)				MAX SHEARS STRESS (MPa)			
(kg)	GAUGE1	GAUGE2	GAUGE 3	GAUGE4	GAUGE 1	GAUGE 2	GAUGE 3	GAUGE 4
2.82	1.23	1.79	0.74	-0.98	0.77	0.56	2.45	0.56
5.09	2.61	3.97	1.49	-1.73	1.54	1.35	7.90	0.88
7.36	3.99	5.99	1.51	-2.96	2.30	1.84	1.10	1.04
10.08	5.44	8.17	2.65	-4.52	3.29	2.63	1.56	1.32
12.36	6.58	10.14	3.34	-0.55	4.28	3.22	2.02	1.37
15.06	8.19	12.37	3.46	-6.78	5.27	3.91	2.50	1.67

Tabular presentation of the Compressive stress on the tube-sheet due to a pressure load.

TableD.3.1 Maximum Compressive Stress on the plate at each gauge position .

TUBE TYPE : AE436 with a 4.3mm fin pitch.

PRESS.	COMPRESSIVE STRESS (MPa)			
(Bar)	GAUGE 1	GAUGE 2	GAUGE 3	GAUGE 4
1.0	-3.93	-1.10	-5.01	-5.01
2.0	-8.27	-2.21	-10.10	-10.10
3.0	-13.94	-4.24	-16.00	-16.00
3.5	-16.22	-5.40	-19.00	-19.00
4.0	-18.76	-6.95	-22.00	-22.00
4.5	-21.33	-8.67	-25.50	-25.50
5.0	-24.64	-10.00	-29.50	-29.50
5.5	-27.70	-11.00	-33.50	-33.50

Table D.3.2 Maximum Compressive Stress on the plate at each gauge position

TUBE TYPE : AE510 with a 2.5mm fin pitch

PRESS.	COMPRESSIVE STRESS (MPa)			
(Bar)	GAUGE 1	GAUGE 2	GAUGE 3	GAUGE 4
1.0	-2.43	-1.01	-2.92	-2.92
2.0	-5.30	-2.21	-5.87	-5.87
3.0	-8.20	-4.24	-8.70	-8.70
3.5	-9.40	-5.40	-9.89	-9.89
4.0	-10.60	-6.95	-11.50	-11.50
4.5	-11.80	-8.67	-12.50	-12.50
5.0	-13.00	-10.00	-13.50	-13.50
5.5	-14.10	-11.00	-14.50	-14.50

Table D.3.3 Maximum Compressive Stress on the plate at each gauge position.

TUBE TYPE : F-tube with a 3.0 mm fin pitch

PRESS.	COMPRESSIVE STRESS(MPa)			
(Bar)	GAUGE 1	GAUGE 2	GAUGE 3	GAUGE 4
1	-2.90	-1.10	-3.50	-3.50
2	-6.46	-2.21	-8.70	-8.70
3	-10.19	-4.24	-13.57	-13.57
3.5	-11.79	-5.40	-16.42	-16.42
4	-13.47	-6.95	-19.08	-19.08
4.5	-15.23	-8.67	-21.83	-21.83
5	-17.80	-10.14	-24.02	-24.02
5.5	-19.57	-11.30	-26.02	-26.02

APPENDIX E

THE TECHNICAL DRAWING OF BOTH THE F AND A-TUBES.

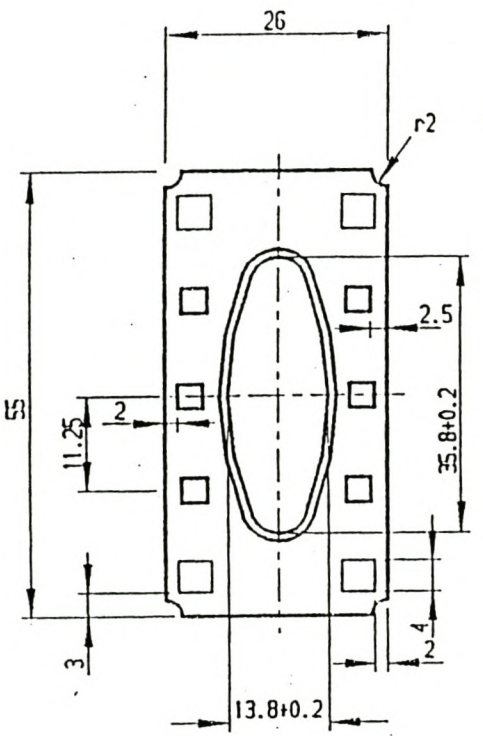

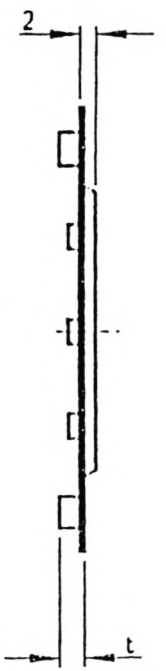

Total fin thickness = zinc layer + fin strip
= 0.4 mm

fin strip / thickness =0.23 mm

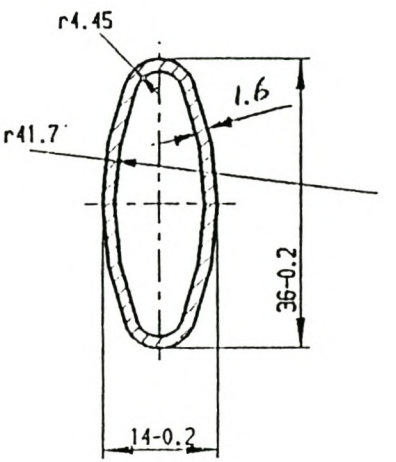

Figure E.1. Detailed drawing of the F-tube.

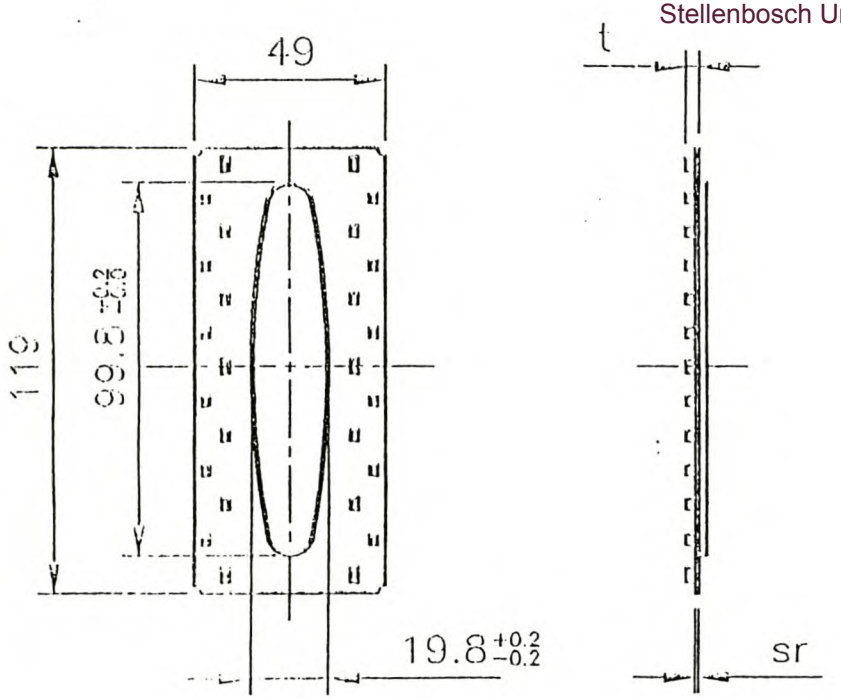

FIN DETAIL

Total fin thickness = zinc layer + fin strip
= 0.49 mm

fin strip / thickness =0.23 mm

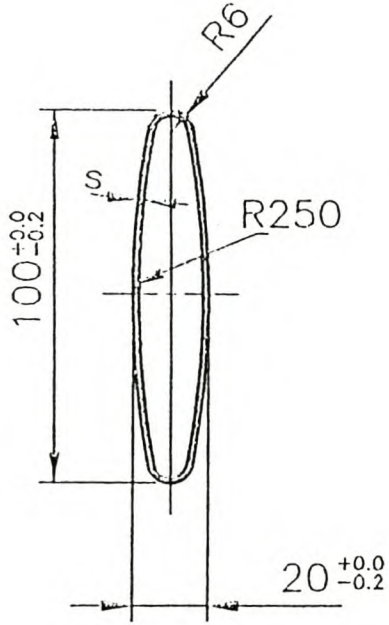

TUBE SECTION

REV.	DATE	NAME	REMARKS	DATE	CHCK.	APP.
2						
1						

	DATE	NAME	GEA O/No.
DRWN.	8.4.99	E.K.	CLIENT:
CHCK.			
APP.			

Manufacturer: AIRCOOLED SYSTEMS (Pty.) LTD. R.S.A. (Reg. No. 70/01564/07)

TITLE: FIN TYPE 510

SCALE: A4 | GEA No. | REV ()

CLIENT No.

Figure E.2. Detailed drawing of the A-tube with a 2.5 mm fin pitch.

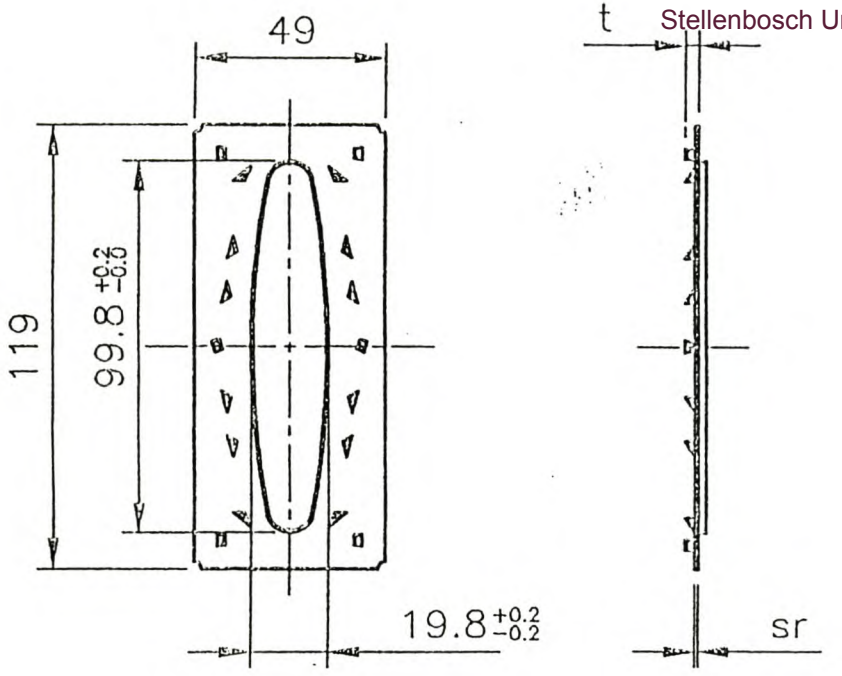

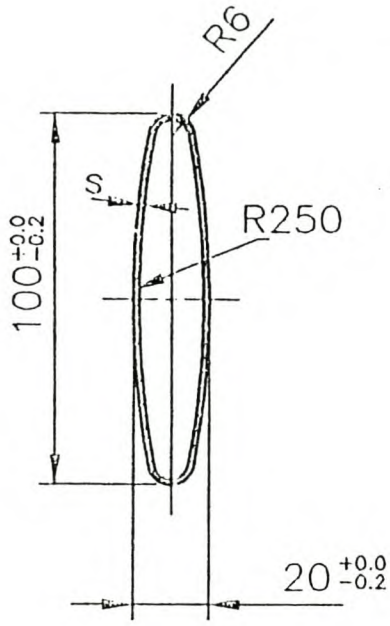

TUBE SECTION

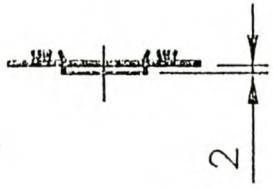

FIN DETAIL

Total fin thickness = zinc layer + fin strip
= 0.49 mm

fin strip / thickness =0.23 mm

REV.	DATE	NAME	REMARKS	DATE	CHCK.	APP.
2						
1						
	DATE	NAME	GEA O/No.			
DRWN.	8.4.99	E.K.	CLIENT:			
CHCK.						
APP.						

Manufacturer: GEA (Pty.) Ltd. Reg. No. 71/03812/07

TITLE: FIN TYPE 906 D

SCALE: A4 | GEA No. | CLIENT No. | REV ()

Figure E.3. Detailed drawing of the A-tube with a 4.5 mm or 4.3 mm pitch.

APPENDIX F

CALCULATIONS FOR A HYDRAULIC DIAMETER (d_e) OF THE A-TUBE

The dimensions of the A-tubes are given in appendix E. Figure F.1 below shows a detailed cross sectional area of an elliptical finned tube viz. A-tube. To successfully quantify the hydraulic diameter (d_e), one needs to calculate the inside cross sectional flow area (A_{tc}) and the wetted perimeter (P_w).

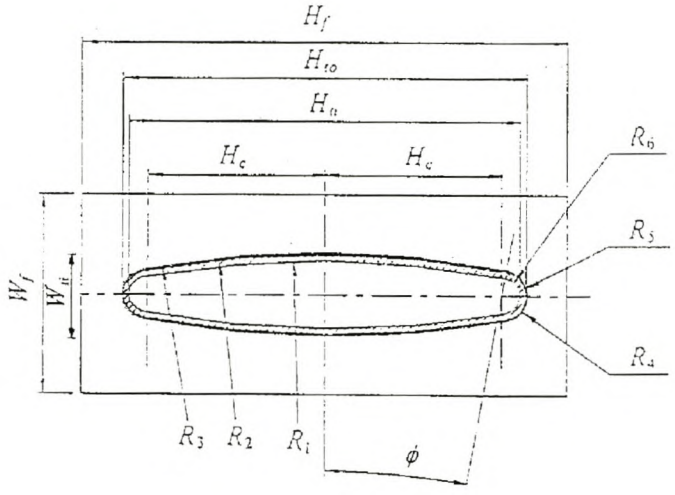

Figure F.1. Detailed drawing of the A-tube.

Tube geometry

Outside tube height	H_{to} = 100 mm
Inside tube height	H_{ti} = 98.26 mm
Fin Height	H_f = 119.0 mm
Tube height	H_c = 42.33 mm
Fin width	W_f = 49.0 mm
Inside tube width	W_{ti} = 20.0 mm

Radius 1 R_1 = 248.4 mm

Radius 2 R_2 = 250 mm

Radius 3 R_3 = 250.14 mm

Radius 4 R_4 = 6.14 mm

Radius 5 R_5 = 6 .0 mm

Radius 6 R_6 = 4.4 mm

Calculations for the inside cross sectional flow area (A_{tc}).

$$A_{tc} = 2 \times \left[\left(\frac{\phi}{360} \right) \times 2\Pi R_1^{\,2} - \frac{1}{2} \times H_c \left(R_2 - \frac{W_{ti}}{2} \right) \right] + 2 \times \left[\left(\frac{90 - \phi}{360} \right) \times 2\Pi R_6^{\,2} \right] \qquad \text{F.1}$$

where :

$$\phi = \arctan\left(\frac{H_c}{R_2 - 0.5W_{ti}} \right) \qquad \text{F.2}$$

$$= \arctan\left(\frac{42.33}{250 - 10} \right)$$

$$= 10.00°$$

substituting equation F.2 back into equation F.1

$$A_{tc} = 2 \times \left[\left(\frac{10}{360} \right) \times 2\Pi \times 248.4^2 - \frac{1}{2} \times 42.33(250 - 10) \right] + 2 \times \left[\left(\frac{90 - 10}{360} \right) \times 2\Pi \times 4.4^2 \right]$$

$$= 1273.91 \ mm^2$$

$$= 1273.91 \times 10^{-6} m^2$$

Calculations for the wetted perimeter (P_w).

$$P_w = 4 \times \left[\left(\frac{\phi}{360} \right) \times 2\Pi R_1 \right] + 4 \times \left[\left(\frac{90 - \phi}{360} \right) \times 2\Pi R_6 \right] \qquad \text{F.3}$$

$$= 4 \times \left[\left(\frac{10}{360} \right) \times 2\Pi \times 248.4 \right] + 4 \times \left[\left(\frac{90-10}{360} \right) \times 2\Pi \times 4.4 \right]$$

$= 197.99\ mm$

$= 197.99 \times 10^{-3}\ m$

Calculations for the hydraulic diameter (d_e).

The diameter of a round tube that has the same hydraulic diameter as an elliptical finned tube with the dimensions given above can be calculated as follows:

$$d_e = \frac{4 \times A_{tc}}{P_w} \qquad \text{F.4}$$

$$= \frac{4 \times 1273.91 \times 10^{-6}}{197.99 \times 10^{-3}}$$

$= 25.74 \times 10^{-3}\ m$

APPENDIX G

CALCULATIONS FOR THE DETERMINATION OF THERMAL STRESSES ON A TUBE BUNDLE.

The following is a sample calculation to determine the stresses induced by a thermal load on the tube, to a tube-sheet plate. The dimensions of the tube bundle are given below in figure G1. This bundle has the same dimension as the tube bundle that Kröger **[17KR]** uses in evaluation of performance characteristics of extended finned tubes.

Tube information:

Tube length	L_t = 470 mm
Number of tube rows	n_{tr} = 4
Number of tubes	n_t = 32
Mass of the A-tube	m_t =3.248 kg
Tube temperature	T_t =120 ºC

Tube-sheet plate information

Plate Volume	V_p = 0.745 x 10^{-3} m^{-3}
Plate thickness	t_p = 16 mm
Plate temperature	T_p = 20 ºC
Plate density	ρ_p = 7840 kg/m^{-3}

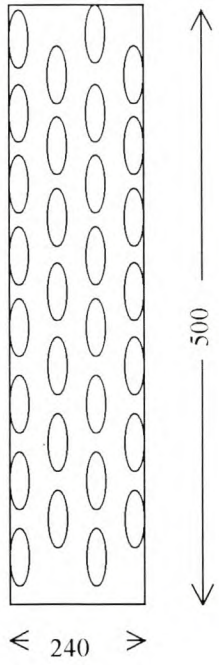

Figure G1. Heat exchanger bundle

The thermal stress on the tube-sheet plate can be obtained by first determining the average temperature of the tube bundle.

Calculation of the average temperature of the tube bundle.

By considering the First Law of Thermodynamics i.e. the change in internal energy in a system is equal to the heat and work done on that

system **[19ÇE]**. Expressed mathematically this gives:

$$Q - W = \Delta U = \Delta U_{tubes} + \Delta U_{plates} \qquad \text{G.1}$$

where:

$$\Delta U = mC_v\left(T_f - T_i\right) \qquad \text{G.2}$$

where:

Q = heat added to the system which is zero $[kJ]$

W = work done on the system which is zero $[kJ]$

ΔU = change in internal energy $[kJ]$

m = mass of the plate or the tubes $[kg]$

Cv = specific heat at constant volume $\left[kJ\left(kg\ ^{\circ}C\right)^{-1}\right.$

T_f = average or final temperature $[^{\circ}C]$

T_i = average or final temperature $[^{\circ}C]$

ρ = density $[kgm^{-3}]$

$$\therefore \quad mC_v\left(T_f - T_i\right)\Big|_{tubes} + mC_v\left(T_f - T_i\right)\Big|_{plates} = 0 \qquad \text{G.3}$$

C_v of the plate and of the tubes are almost equal and therefore can be ignored. This sample calculation is for a plate whose temperature is at 20 °C and tubes at 120 °C. Equation G.3 can be simplified further to give:

$$V_t \times \rho_t C_v\left(T_f - T_t\right)\Big|_{tubes} + V_P \times \rho_P C_v\left(T_f - T_p\right)\Big|_{plates} = 0 \qquad \text{G.4}$$

Further simplification gives:

$$n_t \times m_t\left(T_f - T_t\right)\Big|_{tubes} + V_P \times \rho_t\left(T_f - T_p\right)\Big|_{plates} = 0$$

$$32 \times 3.248 \times \left(T_f - 120\right) + 0.745 \times 10^{-2} \times 7840\left(T_f - 20\right) = 0$$

$$103.936 \times \left(T_f - 120\right) + 58.408\left(T_f - 20\right) = 0$$

$$T_f = 84\,^{\circ}C$$

The thermal stress on the plate can be calculated as follows:

Calculation of thermal stress

$$\sigma = \frac{\alpha \times E \times T_f}{1 - \nu} \qquad \text{G.5}$$

where:

σ = thermal stress $[MPa]$

α = coefficient of thermal expansion $[^{\circ}C^{-1}]$

E = Young's modulus $[GNm^{-2}]$

ν = Poisson's ratio

substituting $\sigma = 10.8 \times 10^{-6}\ ^{\circ}C$; $E = 206\ GNm^{-2}$ and $\nu = 0.33$

$$\sigma = \frac{10.8 \times 10^{-6} \times 206 \times 10^{9} \times 84}{1 - 0.33}$$

$\sigma = 278.93\ MPa$.

So the thermal stress on the plate is of the order 278.9 MPa.

APPENDIX H

CALCULATION OF THE NATURAL FREQUENCY AND THE MODE SHAPES OF THE TUBE .

In the analysis of the tubes response to excitation one can treat the tube as if it is rigidly clamped at each end as shown in figure H.1 below.

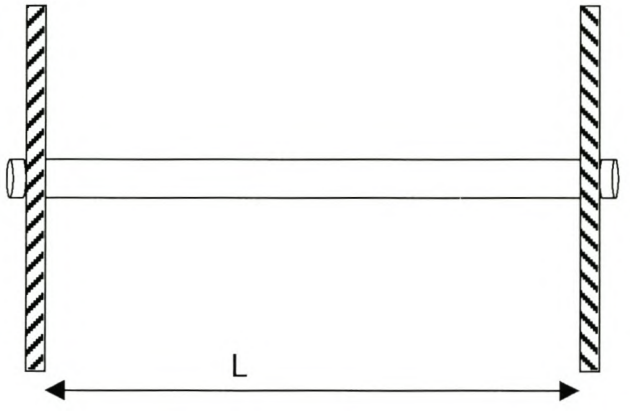

Figure H.1. Tube clamped on both sides.

To calculate the natural frequency of the tube the following equation is used:

$$f_{tn} = C_n \times \sqrt{\frac{gEI}{WL^4}} \qquad \text{H.1}$$

where:

C_n = constant for each mode

g = Gravitational acceleration $\left[9.81\, ms^{-2}\right]$

E = Young's modulus $\left[Nm^{-2}\right]$

I = moment of inertia $\left[m^{-4}\right]$

W = weight of the tube and its contents per unit length $\left[Nm^{-1}\right]$

L = Length $\left[m\right]$

Substituting the following constants , which are applicable to the A-tubes with a 4.3 mm fin pitch in equation H.1, gives:

$E = 206 \times 10^9\ Nm^{-2}$, $I = 0.16 \times 10^{-7}\ m^{-4}$, $L = 0.470\ m$ and $W = 80.23\ Nm^{-1}$

$$f_{tn} = C_n \times \sqrt{\frac{9.81 \times 206 \times 10^9 \times 0.16 \times 10^{-7}}{80.23 \times (0.47)^4}}$$

$$= 90.87 \times C_n\ Hz$$

Church **[20BR]** shows the mathematical derivation of equation H.1 and subsequently the values of C_n. Using the values of C_n given in table H.1 below, the natural frequency of the tube clamped at both ends can be determined for each mode of vibration.

Table H.1. Natural frequency of the tube for the first five modes of vibration.

Modes	I.	II.	III.	IV.	V.
C_n	3.56	9.82	19.24	31.81	47.52
Freq. (Hz) A-tube 4.3 m	323.50	892.34	1748.33	2890.58	4318.14
Freq. (Hz) A-tube 2.5 m	275.23	759.20	1487.48	2459.28	3673.85
Freq. (Hz) F-tube 3.0 m	116.68	321.84	630.58	1042.54	1557.43

The weight per unit length of 470 mm A-tube with a 2.5 mm fin pitch and a 470 mm F-tube with a 3.0 mm fin pitch are 110.86 Nm^{-1} and 77.11 Nm^{-1} respectively. Figure H.2 to H.6 shows the results of the structural dynamic analysis for the first 5 modes of vibration of the A-tube with a 4.3 mm fin pitch.

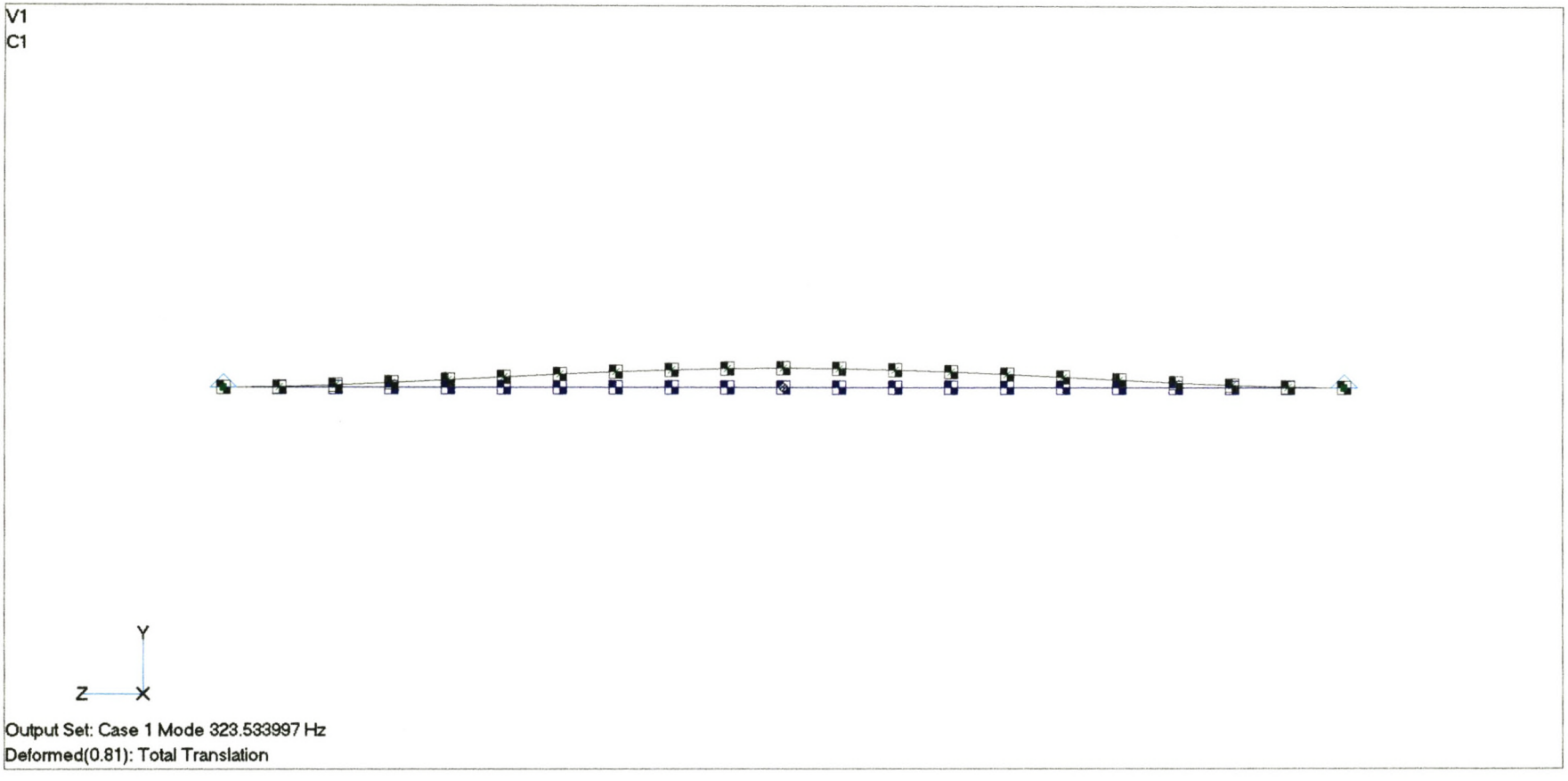

FIGURE H.2. STRUCTURAL DYNAMIC ANALYSIS FOR THE FIRST MODE OF VIBRATION.

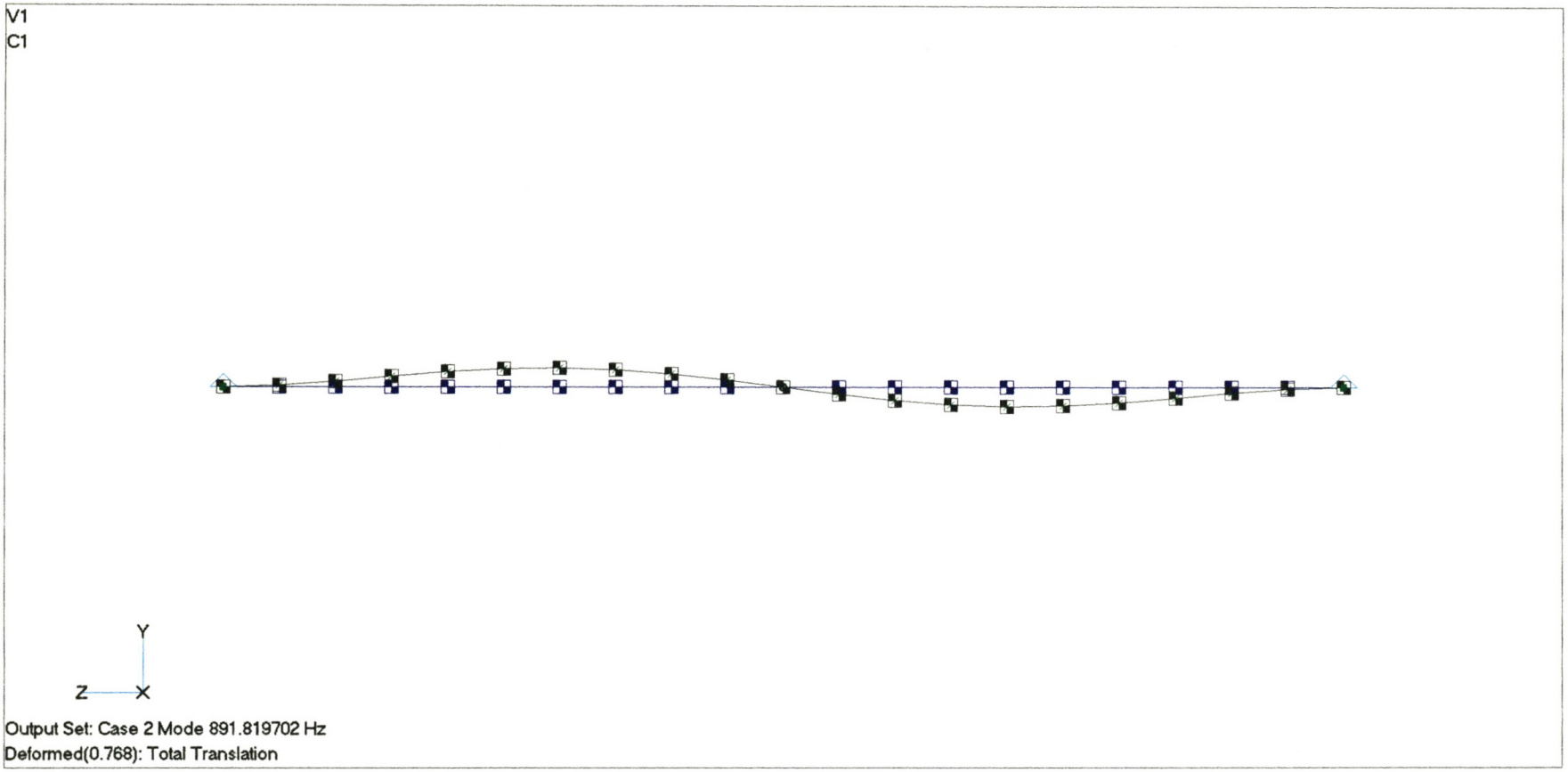

FIGURE H.3. STRUCTURAL DYNAMIC ANALYSIS FOR THE SECOND MODE OF VIBRATION.

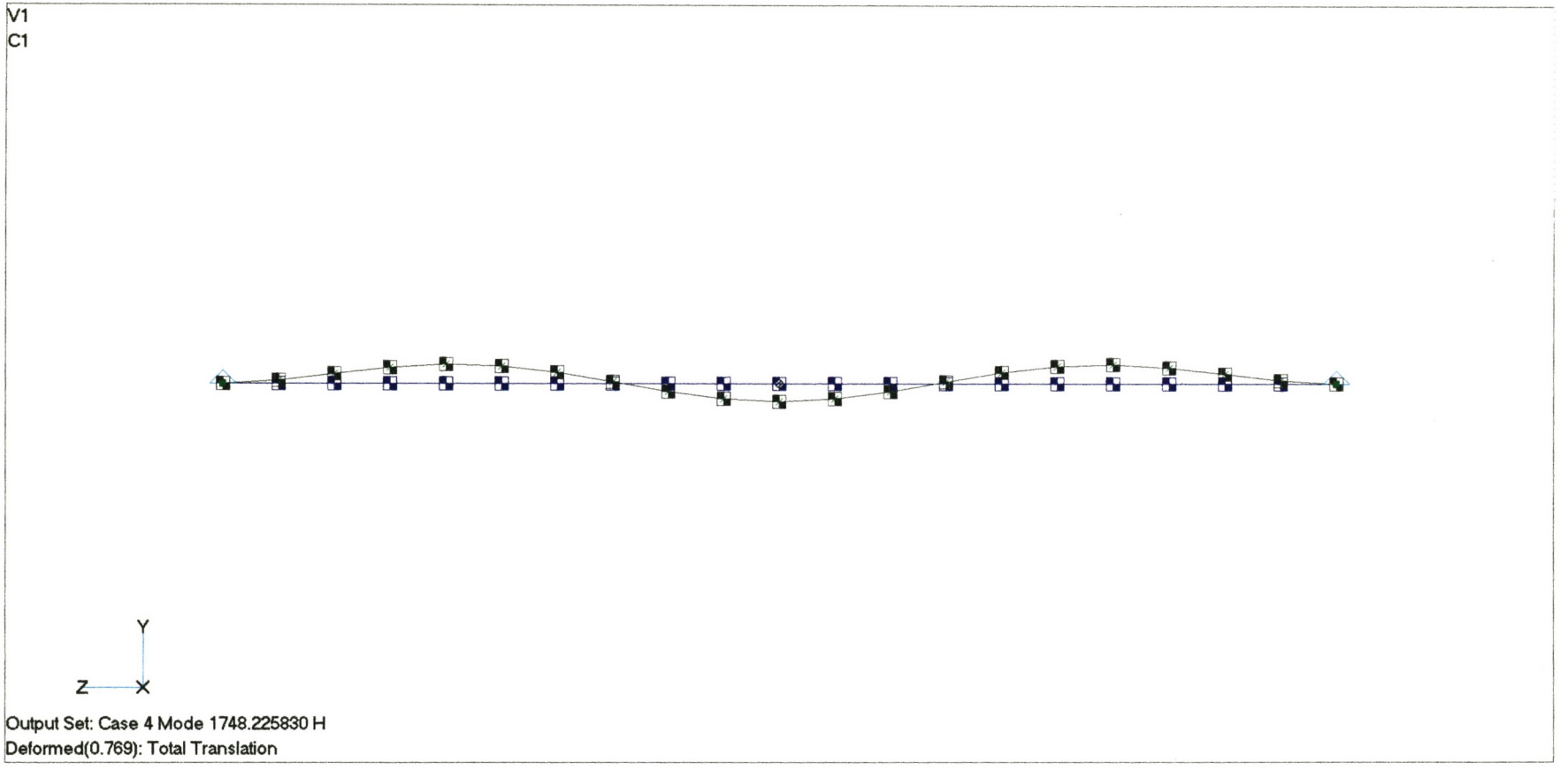

FIGURE H.4. STRUCTURAL DYNAMIC ANALYSIS FOR THE THIRD MODE OF VIBRATION.

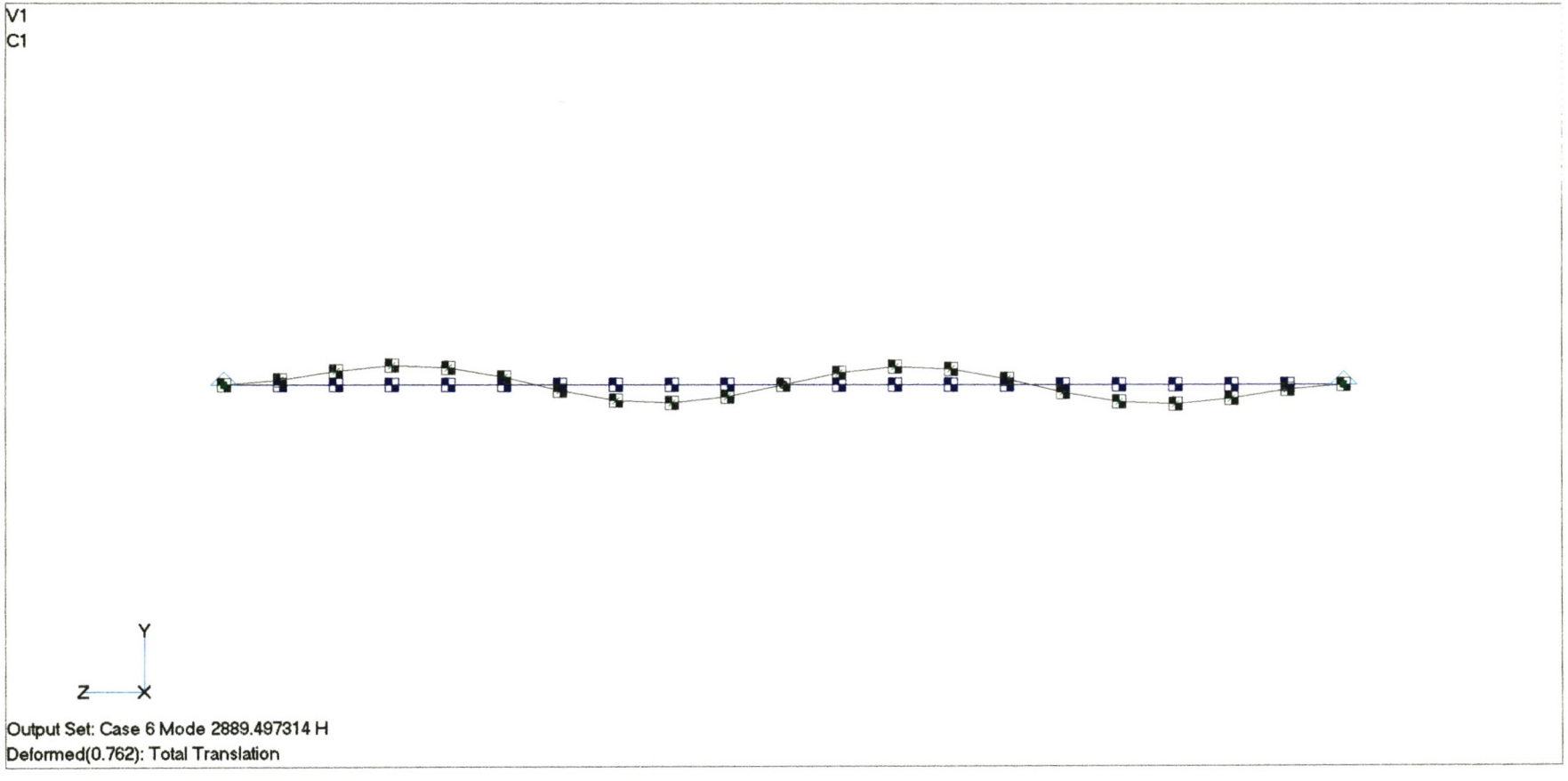

FIGURE H.5. STRUCTURAL DYNAMIC ANALYSIS FOR THE FOURTH MODE OF VIBRATION.

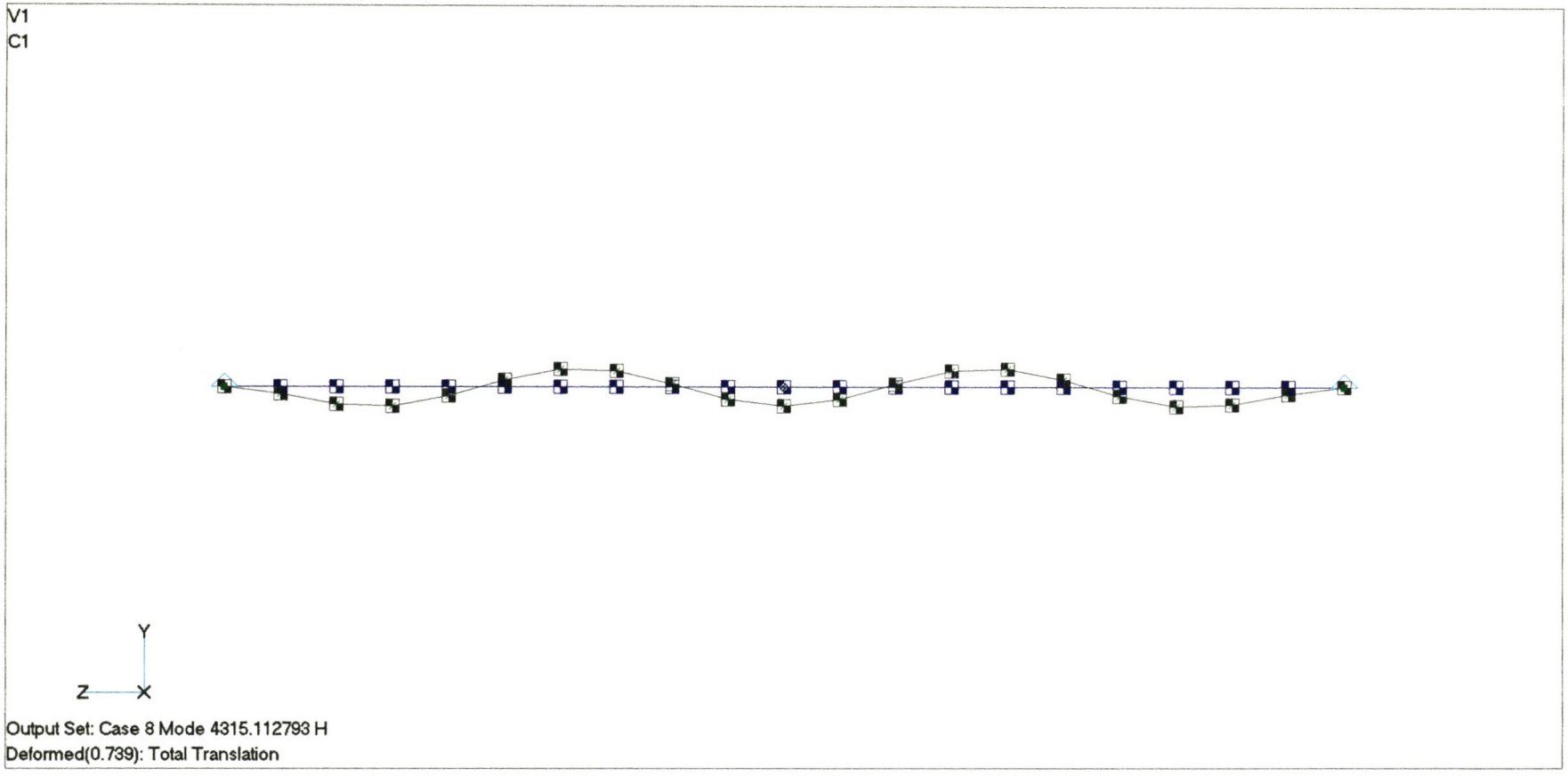

FIGURE H.6. STRUCTURAL DYNAMIC ANALYSIS FOR THE FIFTH MODE OF VIBRATION.